Thermo-Structural Analysis of a Rocket Engine Thrust Chamber

Chethan Madhu Suryavanshi

SUPERVISED BY

Dr. Jose Ignacio Rojas Gregorio

Dr. Luca d' Agostino

Universitat Politècnica de Catalunya

&

University of Pisa

Master in Aerospace Science & Technology

December 2018

This Page Intentionally Left Blank

Thermo-Structural Analysis of a Rocket Engine Thrust Chamber

BY

Chethan Madhu Suryavanshi

DIPLOMA THESIS FOR DEGREE

Master in Aerospace Science and Technology

AT

Universitat Politècnica de Catalunya & University of Pisa

SUPERVISED BY:

Dr. Jose Ignacio Rojas Gregorio

Dr. Luca d' Agostino

Department of Aerospace Science and Engineering

Dedicated to my family and my inspiration
« Dr B.R Ambedkar »

ABSTRACT

The rocket engine market today presents several new trends that will substantially change the current technological scenario. Apart from the imminent applications to the mega constellations and the advancement of electric propulsion, some aspects such as environmental protection require a conceptual redefinition of rocket propulsion systems with chemical propellants. One of the best technological options to contribute to the protection of the environment and personnel is to use "green" propellants to replace current toxic and / or ecologically harmful propellants.

Thermal and mechanical loads represent the most stringent operating limits for liquid propellant rocket combustion devices (chamber, injectors, expansion nozzle). This report describes the two-dimensional model developed for the evaluation of the temperature distribution across the wall of the thrust chamber and the extension of a typical rocket motor.

In the model the thrust chamber and the nozzle extension are divided into several stations using ANSYS APDL 16.0 and are subjected to a steady state and a transient analysis to study the characteristics of heat transfer and to understand the thermal response and structural of the model.

The results obtained help to study the thermo-structural feasibility and to identify the most critical operating conditions and their impact on the design of the combustion devices of rocket engines with chemical propellants.

The analysis developed in this paper includes the selection of the most suitable materials and the subsequent modeling of the rocket thrust chamber and the nozzle extension using the ANSYS APDL 16.0 software and the SolidWorks software. Loads and constraints on the structure are applied after the combination of the thermal and structural models.

Key words: Rocket Propulsion, Liquid Propellant Rocket Engines, Structural Analysis, Thermal Analysis, R-4D.

ACKNOWLEDGEMENTS

I owe my gratitude to my supervisor Dr Luca d' Agostino, Department of Aerospace Engineering who offered invaluable assistance, guidance and support throughout my completion of master thesis at the University of Pisa. Deepest thanks to Eng. Riccardo Simi and Dr Mario Rosario Chiarelli, Department of Aerospace Engineering, without whose knowledge and assistance this thesis would not have been successful. I would like to thank Dr. Jose Ignacio Rojas Gregorio, Dept. of Physics - Division of Aerospace Engineering, for providing guidance and support throughout my master thesis. Their constant support in term of technical and scientific has laid an immense foundation for my master thesis.

I am very thankful to my mother, father and brother for always believing in me and allowing me to realize my potential. All the support I got from them over the years was the greatest gift anyone has ever given to me. I would like to thank sincerely to my friends and colleagues Guru, Abhilash, Ankit, Akash, Prasenjit, Siddharth, Basavaraj, David, Naveen, Arjun and Gabriel from bottom of my heart for constant support, love and encouragement.

Very special thanks to my girlfriend Ivette Fernandez for her support and assistance throughout thesis. She encouraged and inspired me which has given me a lot of courage and energy to complete my master thesis.

A special thanks to Universitat Politecnica de Catalunya for providing me an opportunity to pursue my master thesis in University of Pisa, Italy.

"Life should be great rather than long"

Dr B.R.Ambedkar.

.

MOTIVATION

Rocket engines' thrust chambers operate at high temperatures and pressures. From a structural point of view, this is fundamental for two reasons. Some properties of the material, such as yield strength, are negatively affected by an increase in temperature. The second reason is that during transient operation (startup and shutdowns) there may be strong temperature gradients which produce strong stresses in the chamber wall material. The thermo-structural analysis allows to estimate these two effects.

The success of the Apollo mission and the lunar missions have attracted great attention. In particular, the rocket propellant engines used in these missions have aroused much interest because they made the mission possible and operated accordingly. The R-4D engine, used as reference in this work is a liquid propellant rocket engine produced by Marquardt, which is now part of Aerojet Rocketdyne. This engine is used for attitude control, for docking maneuvers and in general for those missions requiring small or moderate spacecraft velocity changes. The R-4D engine uses radiative and film cooling and have the option to shutoff when the heat flux to the combustion devices it's too high. Heat removal plays an important role in rocket engines, since the temperature field affects the structure. The combustion temperature depends on the propellants used, which influence the thrust and performance of the liquid propellant rocket engine and represent a key parameter in rocket engines.

To study the structural behavior of the thrust chamber it is necessary to perform a 2D axisymmetric analysis which is a quick and reliable way to obtain representative results for the preliminary design and for the verification of more elaborate numerical simulations.

Table of contents

List of Figures

List of tables

1 Introduction

Liquid rocket engines (LPRs) are currently the most used space propulsion system and the workhorse of the space launcher industry [1]. In 2013 most of the orbital launches were equipped with LPR engine system in their early stages. For the same calendar year, the overall market size of the global launcher industry was estimated at $ 5.4 billion [2].

Liquid propellant propulsion systems include one or more rocket engines the tanks for storing the propellants(s) and the feed system to combustion chamber. Most of the rocket engines currently in use a bipropellant configuration where the fuel and the oxidizer are stored in separate tanks [3]. Liquid propellant rocket engines include the following main subsystems: the thrust chamber, the propellant control system, the feed system (pressurized or through a turbopump) to feed the propellants from the tanks to the thrust chamber, the driving system (gas generator, pre-burner and turbine) for operating the propellant feed turbopumps, the electric and pneumatic control systems, the thrust vector control system and the measuring and assembly devices. The control system is particularly helpful during engine start-ups and shutdown, as well as to effect changes in propellant flow and therefore in thrust [3].

Any liquid rocket engine will be designed to meet specific mission requirements, which are generally established according to the intended application (I e anti-aircraft missile, space launcher stage propulsion, flight control and orbital maneuvering etc.) taking into account of the launch site, the minimum life in orbit, the number of specimens to be made, and so on. These requirements often affect the engine mass, costs and safety precautions. The aforementioned mission requirements and their definition result in the requirements of the liquid propellant rocket engine, which include the specification of the thrust profile, the minimum specific impulse, the re-start capability, the use of acceptable propellants, and the limitations of the mass and dimensions of the propulsion system. Engine requirements such as thrust, chamber pressure, oxidizer/fuel mixing ratio, total engine mass, throat diameter and nozzle expansion ratio must be selected in the most appropriate manner for the realization of a specific mission [3]

Many engine parameters can be chosen based on experience and design studies involving subsystem changes. For example, the fuel system can be customized according to requirements, the engine components can be assembled according to the required dimensions, the engine cycle, the thrust modulation and the thrust vector control system modifications can be modified on the basis to mission requirements. Typically, at least two or more preliminary projects are developed to compare them, eliminate any problems, improve the performance of the propulsion system and define its most appropriate design for the mission under consideration. [3].

So far, many liquid rocket engines have been studied, designed and built on the basis of different specifications, in which the thrust level varies from 0.044 N to 7.7 MN. The flow of propellants must be contro lled appropriately because some engines need a single start, while smaller engines for attitude control may require more than 150000 restarts [3].

Liquid propellant rocket engines are classified into engines for primary and auxiliary propulsion based on the thrust delivered and the function performed. The increase in the payload corresponds to the increase in the thrust required at launch. The auxiliary propulsion system performs functions that require less thrust, such as control of the spacecraft trajectory and attitude. The main features of engines for primary and auxiliary propulsion are listed in the following table [3].

Purpose	***Boost propulsion system***	***Auxiliary propulsion system***
Job	Gives momentous velocity to propel a vehicle along their path.	Trajectory correction, maneuvers, attitude control.
Operation	The large missile, booster stage, the upper stage of the launch vehicle.	Satellites, spacecraft, space assignation, antiballistic missile.
Impulse	High	Low
Number of thrust chambers per engine	Generally, 1 but frequently 2,3 or 4 will be equipped.	It ranges from 4 to 24.
Thrust level	High; 4500-7,900,000 N	Small;0.001 - 4500N.
Feed system	Turbopump type.	Pressurized feed system.
Cooling Method.	Propellant cooled	Radiation cooled.
Propellants	Cryogenic and storable liquid.	Storable liquids, monopropellants
Chamber Pressure	2.4-21 MPa	0.14-2.1 MPa
Time to reach full thrust.	It takes several s.	Very fast like 0.004-0.080 s
Lifespan in space	From several hours till months.	Up to 15years

Table 1.1 Exemplary characteristic of two different Liquid propellant rocket engine [1].

The thrust chamber is equipped with the main injector and nozzle where the liquid propellants are injected, atomized, mixed, ignited and burnt until a practically complete combustion is attained [4]. The gaseous products of combustion are accelerated and released at supersonic speeds through a convergent-divergent nozzle to obtain the thrust. The feed system transfers the propellants from the tanks to the combustion chamber through the supply lines, the valves and possibly the turbopumps [4]. The combustion reaction generates gas at high pressures and temperatures, and therefore need be strong enough to withstand mechanical and thermal loads without structural damage. Due to the high temperature of the gases and the consequent thermal flow

towards the walls of the thrust chamber, the liquid propellant rocket engines must be cooled appropriately.

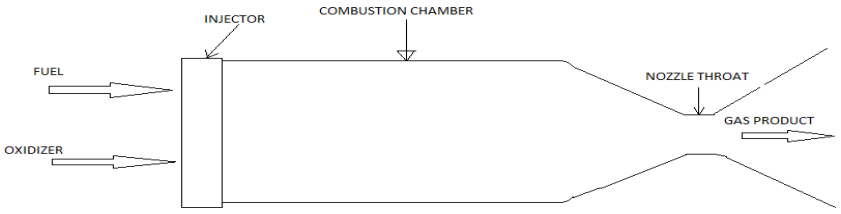

Figure 1.1 Typical liquid Rocket engine combustion chamber

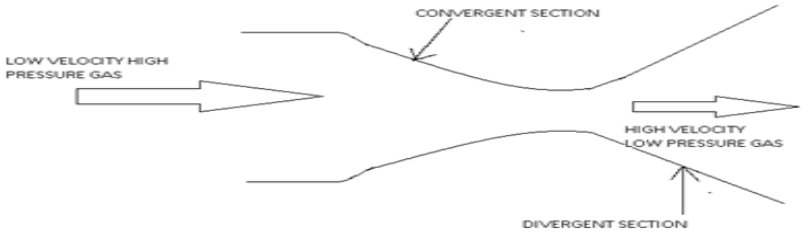

Figure 1.2 Typical Liquid rocket engine nozzle section

1.1 Characteristic of liquid rocket engine

The main disciplines underlying the operation of liquid propellant rocket engines are essentially mechanics, thermodynamics, chemistry and fluid dynamics. The propulsion is obtained when a force is applied to a vehicle, accelerating it and / or keeping it at a given speed against a resistive force.

1.1.1 Specific impulse (I_s)

As for automotive engines, even for a rocket engine it is necessary to evaluate the level of its propulsive performance. The main parameter that measures the performance of a rocket engine is the specific impulse. A rocket propulsion system generates thrust by using a certain flow of propellants. The specific impulse (I_s) is defined as.

$$I_s = \frac{F}{\dot{m} g_0} \tag{1.1}$$

where *F* is thrust, $\dot{m}$ is mass flow of the propellants and $g_0$is gravitational acceleration constant (with an average value at the earth's sea level of 9.8 m/s²). This equation provides the specific impulse in seconds (s) both in S.I. and British unit, for any rocket propulsion system. On the earth's surface the product $\dot{m} g_0$is the weight flow rate of propellant *W*.

Why it is so important to calculate specific impulse of liquid propellant rocket engine?

If the value of the propellant flow rate is known, the specific impulse provides an easy way to calculate rocket thrust.

If we consider two different engines with different specific impulses, the motor with a higher specific impulse will be more efficient from the propulsive point of view as it produces more thrust for the same amount of propellant. So, the specific impulse quantifies the propulsive efficiency of the engine.

The knowledge of the specific impulse helps to define in advance the characteristics of an engine and the flow rate of propellants to be used for developing the required thrust. [5].

It is essential to specify whether the specific impulse refers exclusively to the thrust chamber or to the entire propulsion system. In fact, if we consider, for example, propulsion systems powered by turbopumps, the overall specific impulse must also take into account the propellant used to power the turbines without generating propulsive thrust [5]

$$(I_{sp})tc = \frac{F}{\dot{w}} \qquad \textbf{(1.2)}$$

1.1.2 Thrust

The thrust of a liquid propellant rocket engine is also an important performance parameter, capable of modifying the momentum (mass-velocity product) of the vehicle to which it is applied. In rocket propulsion systems the thrust is generated by action-reaction of the engine on the propellant expelled from the nozzle (as for example in the case of the recoil of a firearm), and is expressed as a function of the variation of the momentum of the vehicle by the equation:[1].

$$F = \frac{d(mv_2)}{dt} = \frac{W}{g_\circ} v_2 \qquad \textbf{(1.3)}$$

Here the gas velocity at the outlet of the nozzle is considered constant, uniform and purely axial. However, this equation provides the total propulsive force only when the gas pressure at the outlet of the nozzle is equal to the ambient pressure. In general, the pressure of the surrounding atmosphere provides an additional component to the thrust.

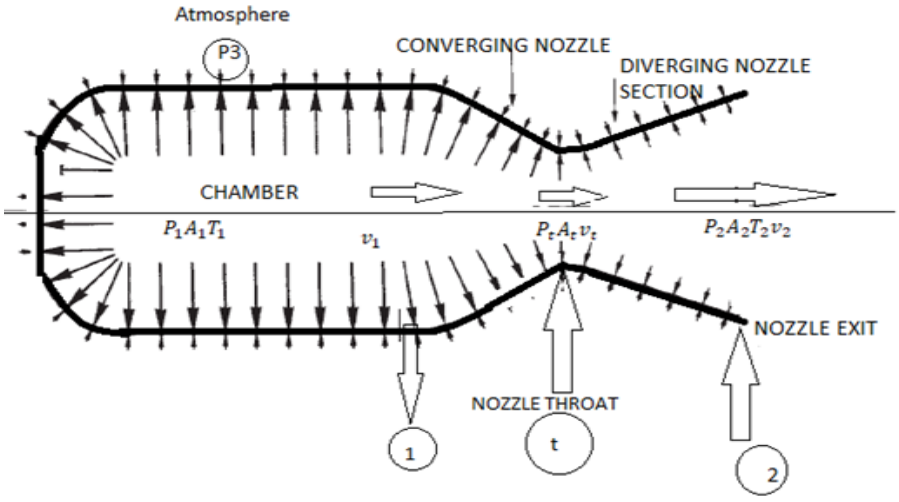

Figure 1.3 Simplified thrust chamber external and internal uniform pressure acting on inside and outside surface of thrust chamber

Figure 1.3 illustrates the operation of a simplified thrust chamber in which the different pressures acting on the outer and inner surfaces of the chamber generate the thrust of the rocket motor. The length and direction of the arrows acting on the two surfaces indicate the magnitude of the pressure forces. The thrust can be obtained by integrating the pressure forces components in the direction of the nozzle axis. On the other hand, the radially acting pressure forces mechanically load the chamber walls but do not contribute to the axial thrust [3]

In atmospheric flight the ambient pressure changes with the altitude, modifying the difference between the atmospheric pressure P3 and the pressure of the propellant gas P2. As mentioned previously, the length and direction of the arrows indicate a change in pressure forces. The gas pressure on the wall of the chamber and on the inner wall of the nozzle is not constant. The internal pressure is high in the chamber, so it is indicated with P1 arrows of high length and decreases steadily in the nozzle until it reaches the outlet pressure P2. The ambient pressure P3 is instead constant. The center line and the horizontal arrow represent the relative speed, while the subscript inside the circle indicates the station in which the quantities are evaluated, such as area *A*, speed *v,* temperature *T* and pressure *p* [2][1]. For a stationary-running engine in a homogeneous atmosphere the total thrust can be expressed as

$$F = \dot{m}v_2 + (P_2 - P_3)\mathrm{A}_2 \qquad \textbf{(1.4)}$$

In equation 1.4 the first term is known as moment thrust, which results from the mass flow of the propellant and its discharge speed, and the second term indicates the pressure thrust, given by the exit area of the nozzle *A* multiplied by for the difference between the exhaust gas pressure and the ambient pressure (P_2 may differ from P_3 only in the supersonic nozzle discharge). The pressure thrust is positive or negative depending on whether the gas pressure at the nozzle outlet is higher or lower than the ambient pressure, respectively. If the atmospheric pressure is equal to the pressure of the gas at the outlet of the nozzle, the pressure term is zero and the thrust is the same as in equation 1.4. Therefore, in space where $P_3 = 0$ the pressure thrust becomes maximum and is expressed by equation 1.5

$$F = \dot{m}v_2 + P_2A_2 \qquad \textbf{(1.5)}$$

Equation 1.4 shows that the thrust is independent of the flight speed but increases with the altitude inside the atmosphere due to the decrease of the ambient pressure, reaching a maximum in vacuum. The change in thrust with respect to the vacuum thrust is expressed by Equation 1.6 [1][2].

$$F = F_{opt} + P_1A_\mathrm{t}\left(\frac{P_2}{P_1} - \frac{P_3}{P_1}\right)\in \qquad \textbf{(1.6)}$$

$$\in = \frac{A_2}{A_t}$$

Equation 1.7 applies for ideal rocket propulsion where γ being constant through the expansion process. The equation shows that thrust is proportional to the throat area A_t and to the nozzle inlet pressure P_1 and is a function of pressure in the nozzle P_1/P_2, and of the ratio of specific heat *k* of the propellant gas [1].Thrust coefficient can be defined as thrust divided by the chamber pressure P_1 and the throat area A_t.

$$C_f = \frac{F}{P_1A_t} \qquad \textbf{(1.7)}$$

The thrust coefficient is dimensionless and is one of the main parameters for rocket engine analysis. It depends on *k*, the geometric ratio of nozzle expansion ∈, the pressure ratio through the nozzle P_1 / P_2, but not directly on the combustion temperature. In the case of a fixed ratio P_1 / P_3, the thrust coefficient C_f f has a peak at P_2 = P_3 known as the optimal thrust coefficient, which is also an important parameter for the design of rocket engine nozzles [1].

$$F = C_f A_t P_1 \quad \textbf{(1.8)}$$

Equation 1.8 can be experimentally solved for the thrust coefficient based on measured values of chamber pressure, throat diameter and thrust. The thrust coefficient is a function of the chamber pressure and directly proportional to the throat area. It represents the amplification of the thrust due to the expansion of the gas in the area of the supersonic nozzle. The thrust coefficient is a flexible parameter for studying the effects of chamber pressure and changes in altitude in a given nozzle configuration.

1.1.3 Characteristic velocity (c^*)

The characteristic speed is a function of the properties of the propellant, regardless of the characteristics of the nozzle. It is used to compare the propulsive performance of different propellants [1].

$$c^* = P_1 A_t / \dot{m} \quad \textbf{(1.10)}$$

The characteristic speed also depends weakly on the combustion and expansion of the propellants in the thrust chamber. The ratio between its measured value and that predicted by the theory of the ideal rocket is used to evaluate the degradation of the performance of the thrust chamber with respect to its maximum ideal value [1].

1.2 Major components of the combustion chamber

1.2.1 Combustion chamber

The thrust chamber is the main component of the rocket engine where the propellant is burned and transformed into gaseous products at high pressure and temperature. The combustion temperature of the propellants is in general higher than the melting point of the materials used for the realization of the combustion chamber. Therefore, it is important to use an effective cooling method to maintain the chamber wall temperature within the allowable limits for the materials used. The volume and shape of the thrust chambers are designed according to the operational requirements. Currently cylindrical chambers are often used, with flat injection plates and convergent-divergent nozzle [7].

1.2.2 Injectors

The injectors are located in the upper part of the combustion chamber and are used to feed liquid propellants with the appropriate mixing ratio and to atomize them finely in small drops, so that they can evaporate more easily and rapidly react in the gaseous state. The geometry of the injectors depends on the operating requirements and the shape of the combustion chamber [7].

1.2.3 Propellant feed system

The propellants can be fed to the thrust chamber by pressure, due to the pressurization of the tanks, or by means of turbopumps. The function of the feeding system consists in supplying the propellants to the thrust chamber with a pressure greater than that in the chamber, in order to adequately control the flow rate and atomization of the propellants. The selection of a pressurized propellant feeding system or a turbopump-fed system depends on the thrust control requirements and on the mass of propellants to be injected. The entire propellant supply system consists of pipes connected to valves, regulators, purge systems, filters and control devices. The pressurized feeding system provides excellent performance when the mass of the propellant to be injected is relatively small and high precision in thrust control is required. The turbopump-fed system offers the advantage of significantly reducing the weight of the tanks when the propellant mass is significant and the injection pressures are very high [3].

1.2.4 Valves

Valves are important components of any liquid propellant rocket engine as they control the flow of propellants and other fluids in the engine. The valves can be classified as normally open or closed, two-way, three-way, ball, gate, butterfly and spring valves. The size and shape of the valve are determined by the flow to be controlled [3].

1.2.5 Regulators

Regulators are one of the main components of liquid propellant rocket engines to achieve fluid pressure control. Normally the delivery pressure of a fluid line is controlled by an adjustable pressure valve. Regulators are often equipped with filters to remove any debris in the flow. The regulators used in the MESSENGER rocket engine system operate for most of the time with constant flow gas pressure [3].

1.2.6 Propellant tank

To store liquid propellants, tanks are used. In pressure-driven propulsion systems the tanks are pressurized with an inert gas or, more rarely, with hot gases generated by dedicated devices or drawn from the engine in order to avoid the additional weight of the pressurization system. The tanks can be shaped according to requirements, but the spherical or cylindrical-spherical shape is widely used because it is lighter [3].

1.2.7 Nozzle

The nozzle plays an important role in a rocket engine, effecting the expansion and acceleration of the burnt propellant to hypersonic speeds. The thrust chamber and the nozzle are traditionally of circular cross-section and have a converging part, a throat and a diverging part.[3].

1.3 Material selection of combustion chamber and nozzle extension

The selection of materials for the construction of the thrust chamber and the extension of the nozzle plays a fundamental role in the design of liquid propellant rocket engines. This section describes the main considerations for the choice of the material for the combustion chamber and the extension of the nozzle.

The choice of material for the inner wall of the thrust chamber and the throat region of the nozzle (the most critical areas from the thermal point of view) is influenced by the composition of the hot gas, the maximum admissible value of the wall temperature, the rate of heat transfer and the engine lifetime. Only a limited number of materials are

typically selected for the realization of combustion chambers. Aspects such as high performance, high thermal conductivity, emissivity, cooling method and wall thickness of the thrust chamber material will reduce the thermal stresses. Copper and its alloys are good heat conductors and do not oxidize in a mixture of non-corrosive fuel rich gases. These alloys include materials such as zirconium, silver or silicon that confer resistance at high temperatures. The configuration of the thrust chamber depends on the choice of their cooling method. It includes curved or doubly curved components and associated junctions. The use of milled cooling channels usually guarantees the most effective removal of the heat transfer. The materials used to make a thrust chamber must be examined under all possible operating conditions such as mechanical and thermal loads, thermal transients, transient conditions, pressure variations. The examination of the material must take into account about their physical properties such as tensile and compressive strength, yield strength, fracture toughness, modulus of elasticity, thermal conductivity, coefficient of thermal expansion, specific heat, reflectivity and density. These parameters change with temperature and sometimes also as a result of small changes in the composition of the material. The temperature at which the material loses 60-75% of its resistance at ambient temperature is usually considered as the maximum allowable temperature for that material [3]. The properties of materials such as erosion resistance, an acceptably low chemical reactivity with propellants or hot gases, a reproducible decomposition for ablative materials and the ease and cost of manufacturing are also important aspects to consider [1].

1.4 Cooling channel analysis

The main objective of the cooling process is to protect the walls of the chamber and of the nozzle from the damage induced by the applied loads. The material of the inner wall of the chamber loses its mechanical strength due to the increase in temperature due to contact with the combustion gases. Thus, effective cooling is crucial in liquid propellant rocket engines.

The fundamental cooling techniques currently in use are:

- Steady state regenerative heat transfer to a propellant flow used as refrigerant, or radiative heat transfer towards the environment. In both cases thermal equilibrium is reached.
- Non-stationary heat transfer by ablative cooling or heat conduction. In both cases the thermal equilibrium is not reached and the temperature profile in the wall exposed to the thermal flow continues to increase [3].

In regenerative cooling, a propellant flow is circulated in appropriate channels between the inner and outer surfaces of the heated wall, before being injected into the thrust chamber. The inner part of the wall is made of a high thermal conductivity material to effectively transfer heat to the refrigerant. The outer part is made of a high-strength material to withstand the pressure of propellant gases in the thrust chamber. This cooling method is the most used in high-pressure bipropellant engines as it absorbs large amounts of heat [3].

In radiation cooling the chamber and the nozzle are made of a single wall. Materials such as molybdenum, L-605 cobalt, carbon-carbon, rhenium capable of withstanding high temperatures are used. The temperature stabilizes when the heat absorbed by

the inner wall is equal to that removed by regenerative cooling or radiated by the outer wall towards the surrounding environment. Radiation cooling is used in gas generators, nozzle extensions and in the mono- and bi-propellant propellant engines with medium-low thrust and moderate chamber pressures (less than 17.23 bar), in order to limit the heat flux from the combustion gas [3]. In transient heat transfer, the temperature in the wall continues to increase during operation and the combustion process must be interrupted if the wall tends to exceed the maximum allowable temperature. This cooling method is mainly used in applications with moderate values of chamber pressure and heat transfer to the wall. Transient cooling often uses ablative thermal protections, typically made of reinforced organic resins, to absorb most of the heat transferred from the propellant gases to the wall. This method is widely used in solid propellant rockets. In some cases, fluid-film cooling is used in LPREs, where the refrigerant is injected at the interface between the heated wall and the combustion gases. Cooling methods also contribute to reducing the oxidation of the wall materials, as high temperatures increase their chemical reactivity with the oxidizing species of the combustion gases. Oxidation can also be reduced by applying an impermeable and chemically inert coating to the wall [3].

1.4.1 Cooling with steady state

The regeneratively cooled thrust chambers are provided with internal coolant channels for cooling all the parts in contact with the hot gases. The choice of coolant velocity in the channels depends on the thermal and mechanical loads of the wall, the changes in temperature and pressure of the coolant and the production techniques. Most pressure-fed thrusters operate with moderate pressures in the chamber and use radiative cooling instead of regenerative cooling because the heat flow to the walls of the thrust chamber is lower [3].

In regenerative cooling, the heat absorbed by the propellant increases the internal energy of the propellant before injection, marginally improving therefore also the specific impulse of the engine (from 0.1% to 1.5%). The structure of the nozzles is often made by brazing the coolant tubes on a thin wall in contact with the propellant gas, in order to reduce the thermal stresses and the wall temperature [3].

Radiation cooling is another constructively simple cooling method widely used in applications with not excessively high steady/unsteady thermal loads. In order for the heat to be radiated, it is important that the nozzle and the outer wall of the chamber protrude from the vehicle to avoid heating the surrounding structures of the vehicle[3].

Film cooling is another cooling method often used in thrust chambers and nozzles to protect the most highly loaded surfaces from excessive heating. The first liquid film cooled thrust chamber was developed by Robert H. Goddard in 1920. Film cooling is applicable in both stationary and transient conditions, often only in the nozzle throat region where the thermal loads are higher. In film cooling, a small portion of the propellant flow is injected through numerous orifices on the surface of the wall exposed to heat transfer, forming a layer that helps protect it from thermal contact with the combustion gases. The gases that are discharged from the turbines of the propellant feed pumps at temperatures between 400 and 800 ° C have often been used as film coolants in the nozzle output section of liquid propellant rocket engines [3].

1.5 Thesis structure

The next chapter of this thesis, Chapter 2, focuses on green propellants and the different types of propellants used in liquid propellant rocket engines and their benefits. A brief description of the traditional model for the analysis of rocket engines and another green propellant engine is provided. The new engine under development, its technical specifications are presented.

The next three chapters focus on a detailed thermo-structural analysis of the rocket thrust chamber and the nozzle extension with radiation cooling. Chapter 3 describes the two-dimensional (2D) axial-symmetric analysis of the thrust chamber, in which a stationary analysis with constant pressure is performed. A non-stationary axisymmetric 2D structural analysis is also performed and described.

Chapter 4 shows the results of the complete validation of the thrust chamber performed by means of a series of 2D analyzes at different axial stations. Radiative heat transfer along the chamber axis is studied. Validation is performed in two phases. First, a steady state analysis is performed with a variable pressure along the axis. Subsequently, this comparison is extended to the heat exchange model, illustrating which part of the thrust chamber undergoes the highest temperature. Loads and stresses due to the temperature field are studied.

The ANSYS APDL software is applied to simulate the rocket motor nozzle extension in Chapter 5. This is the final analysis of the thesis; the nozzle extension is analyzed with a 2D model of radiative cooling and the simulation is performed in two phases. The first phase includes analysis at different axial stations with pressure variation along the axis. In the second phase the effects of temperature variation along the axis and of thermal stress are taken into consideration.

Finally, Chapter 6 summarizes the results and conclusions of the thesis, also indicating the recommendations for possible improvements of the analysis presented in this work.

2 A new liquid rocket engine

2.1 Green propellants

Green propellants will need to be used more in the future because some of their advantages that cannot be obtained from other types of propellants. The use of green propellants entails the reduction of the environmental impact and of the overall cost of the mission. The term "green propellants" generally describes a category of propellants (liquid, solid, mono- or bi-propellant) that meets requirements such as the reduction of toxicity, low pollution, excellent storability, wide material compatibility and high propulsive performance [4]. Today, the propellants traditionally used in space missions have a number of adverse environmental effects such as soil, water and atmosphere contamination. In space applications the demand for green propellants is therefore increasing, in view of the replacement of more toxic propellants [5] [6]. The European Space Agency (ESA) and a number of other national space agencies are actively promoting the application of green propellants [5] [7].

2.2 Green propellants and their standards

To reduce the environmental pollution caused by a rocket engine, many scientists have conducted research on how to replace current propellants with green, more ecologic and less toxic propellants. Green propellants are preferable and safer than traditional propellants and also contribute to reducing recurrent costs and increasing operational safety. In particular, storable green propellants are being developed to replace hydrazine and NTO, which are dangerous, toxic and carcinogenic compounds. The main characteristics of green propellants are [8].

- Lower toxicity, which makes them less expensive, simpler and safer in the liquid state because the safety precautions during handling and storage are lower than the other types of propellant.
- Lower pollution, both in space and on the earth, in production plants, at the launch sites and in the atmosphere (greenhouse effect). In space, problems such as the failure of optical sensors are reduced by the introduction of green propellants.
- Reduction of production, transport and operating costs due to lower toxicity.
- Good propulsive performance that, taking into account the requirement of mass and density, is already comparable to that of traditional propellants.
- Based on these standards, a large number of green-propellants can be classified [8].

Sl.no	Elements	Advantage
1	Non-toxic and storable	Commercial, valves, pipes and tube. Propellants are easy in filling, transportation and packing
2	Favourable thermo-chemistry	Easier thermal management, amiable, high-density impulse
3	Oxidizer / monopropellant	The pump-fed system is lower cost, thrust variation in high range, smooth start and stop, individual ignition system
4	Gas-liquid injection	Easy injection, combustion efficiency is high, the stability margin is high
5	Developed technology	Economic development

Table 2.1 Advantage of green propellant [12].

2.3 Types of green propellants

There exist different propellants for usage in different space applications based on the specific requirements and cost, few selected green propellants which are expected to be widely used in the near future are illustrated below.

2.3.1 LOX (Liquid oxygen)

Liquid oxygen (LOX) is the most commonly used oxidizer in space propulsion and is considered a green propellant due to its moderate toxicity and excellent environmental compatibility. As an oxidizer, it is only inferior to fluorine, which however it is very toxic, expensive and difficult to manage because of its high reactivity. Liquid oxygen is inexpensive, and its handling is relatively safe, so it is widely used in space launchers. It is a light-blue, transparent and odorless liquid, with a boiling point of 90 K (-183 ° C) at room pressure. Therefore it must be transported and stored in liquid form in thermally insulated cryogenic tanks and used within a relatively short time after lunch to avoid evaporation [9].

2.3.2 LOX/Kerosene

Liquid oxygen and liquid kerosene are liquid propellants for rocket engines that have been widely used for a long time. Kerosene for space uses is a mixture of various hydrocarbons, known as RP-1 in the United States and as T (S) -1 in Russia. Kerosene has a relatively high density, which allows for a compact design of its feed turbopumps and small storage tanks. Kerosene develops a lower specific impulse than liquid hydrogen, but is often chosen for many space missions because of its low cost, good stability at ambient temperature and safety of use [9].

2.3.3 LOX/LCH4 (Liquid methane)

Liquid methane, also known as liquefied natural gas, has been introduced in 1960 as an alternative fuel to hydrogen. A lot of research is being done on the use of oxygen and liquid methane for high thrust and intermediate thrust rocket engines, as they offer several advantages over kerosene and hydrogen. A lot of today's liquid propellant combinations are expected to be replaced by LOX/LCH4. Methane is a cryogenic propellant, which needs to be stored at 111 K. Among all hydrocarbons it provides the highest specific impulse, lower pressure drops in the cooling channels, superior

cooling properties, lower soot formation and unburnt hydrocarbons deposition [10].

2.3.4 LOX/LH2 (Liquid hydrogen)

Liquid oxygen and liquid hydrogen have long been used as rocket propellants. Liquid hydrogen is a cryogenic propellant with a saturation temperature of 21 K at ambient pressure. It is produced by cooling it under pressure below its critical temperature (33 K), which makes its liquefaction more difficult than for other gases. Therefore, liquid hydrogen is relatively expensive, difficult to transport and store, with a very low density, and capable of deflagrating with the oxygen of the atmosphere if ignited. The LOX / LH2 combination is still widely used mainly in launchers even if it requires large thermally insulated tanks because it provides a relatively high specific impulse [9].

2.4 Types of green propellant engines

2.4.1 RD-58MF

The RD-58 is a liquid propellant rocket engine for the upper stages, developed in 1960 by OKD-1 (now RKK Energeia) and in production since 1967. The engine was designed to power the Block-D stage of the N-1 Rocket. The RD-58MF engine, also known as the 11D58MF, is an upgraded version of the RD-58 engine family that uses liquid oxygen and kerosene as propellants and offers higher performance[11]. Figure 2.1Image courtesy [12].

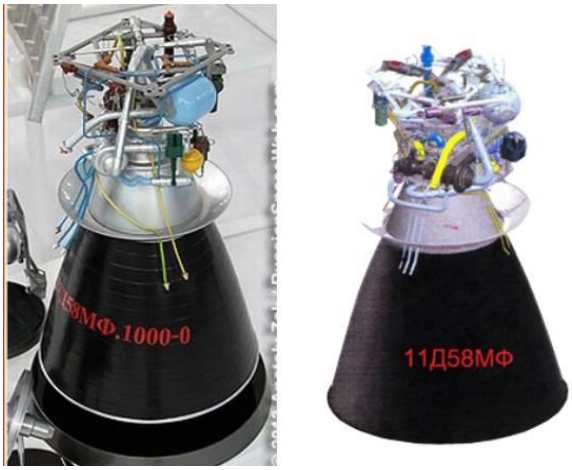

Figure 2.1 RD-58MF Engine by OKD-1 / RKK Energeia

2.4.2 HM7-B

The HM7-B engine belongs to the HM7 engine family produced by SEP and derived from the HM7 engine used in the Ariane2 and Ariane 3 rockets. The HM7-B has been realized for the upper stage of the Ariane 4 and 5 launchers and uses LOX and LH2 as propellants. It offers a higher specific impulse compared to the HM7 engine thanks to the use of a nozzle extension and to the increase in the combustion chamber pressure from 30 to 35 bar. It contributed to increasing the performance of the Ariane 4 and 5 launchers [13]. Figure 2.2 Image courtesy[14]

Figure 2.2 HM7-B liquid propellant rocket engine by ottoburnn

	RD-58MF	HM7-B
Thrust (KN)	83.40	70
Specific Impulse (s)	353	447
Burn time (s)	660	1.80
Height (m)	2.27	1.80
Chamber pressure (bar)	77.50	35
Propellants	LOX/Kerosene	LOX/LCH4

Table 2.2 Technical specifications of RD-58MF and HM7-B engines

2.5 Hypergolic propellants

Normally, the thrust chambers are fitted with an igniter to initiate the combustion process. However, there is a class of propellants, known as hypergolic propellants, which burn on contact at room temperature. These propellants are often toxic and relatively unstable, and therefore their handling requires special precautions. In addition, the hypergolic propellant injectors are designed in a different way with respect to the ones used for non-hypergolic propellants.

The reaction of hypergolic propellants develops in a few milliseconds giving rise to a deflagration with the rapid release of the combustion energy.

2.5.1 Hydrazine (N_2H_4)

Hydrazine is a hypergolic propellant that is widely used as monopropellant and as a bipropellant fuel. It is a poisonous, carcinogenic and colorless liquid with a freezing

point of 275.16 K, lower than the ambient temperature. In the space, hydrazine tanks, tubes, valves and injectors must often be electrically heated to prevent the propellant from freezing. Hydrazine is hypergolic with nitric acid and nitrogen tetroxide, with a short ignition delay. Pure anhydrous hydrazine is a storable propellant because it can be kept in a sealed tank for more than 15 years and safely heated up to 416 K. For several years, hydrazine has been used in the space industry for the in-orbit propulsion of space vehicles and satellites. During a rapid adiabatic compression or under a pressure shock at 367 K the hydrazine vapor can decompose [3]. In some situations, this decomposition can be explosive and cause problems in the cooling passages of the injectors and the thrust chamber. Inhalation of vapors, ingestion or direct contact of hydrazine with the skin is harmful to humans. Hydrazine is therefore considered a poison, with a maximum exposure limit of 0.013 mg/m^3 for eight hours (ACGIH, American Conference of Governmental Industrial Hygienists) [1].

Liquid hydrazine also reacts with different materials and its vapors form an explosive mixture in atmospheric air. Therefore their storage requires special precautions to avoid dangerous decomposition [1]. Hydrazine tanks, pipes and valves must be free of impurities and it is necessary to avoid the use with some materials, such as iron, copper and aluminum alloys which can promote its catalytical decomposition. Finally, hydrazine is a relatively poor refrigerant because its decomposition temperature is relatively low [3]. They are often used as a monopropellant, especially in small rocket engines for attitude control and trajectory control of space satellites [1].

Hydrazine can be decomposed by an electric heater or by contact with an iridium catalyst on a permeable alumina support. The catalytic decomposition of hydrazine occurs in two phases [21] [3], initially with exothermic production of ammonia and subsequent endothermic decomposition into nitrogen and hydrogen.

Nitromethane and ethylene oxide have also been tested as monopropellants, but they are no longer used today.

2.5.2 Unsymmetrical dimethylhydrazine (UDMH) $[(\boldsymbol{CH_3})\boldsymbol{NNH_2}]$

UDMH is derived from hydrazine and is thermally more stable, with a freezing point at 215.9 K, boiling at 335.5 K and a specific impulse lower than that of hydrazine. Due to its property of remaining liquid over a wider temperature range across the ambient temperature, UDMH is widely used as a propellant, for example in Chinese and Russian rocket engines, often mixed with hydrazine [15] [1].

2.5.3 Mono methylhydrazine $(\boldsymbol{CH_3NHNH_2})$

Monomethylhydrazine (MMH) provides a high thrust in combination with N_2O_4 as an oxidant and is often used for small rocket engines for attitude control and orbital maneuvers. Compared to hydrazine, MMH is more toxic, provides a smaller specific impulse, is liquid over a wider range of temperatures and its decomposition temperature (491 K) is higher. Its vapor forms a potentially reactive mixture with the atmosphere at ambient pressure and temperature[15][1].

2.5.4 S-400 Apogee engine

In the last three decades, bi-propellant rocket engines operating with NTO (nitrogen tetroxide) and MMH with a thrust level on the order of 400 N have been widely used both for propulsion of space probes as well as for apogee and orbital maneuvering engines of geostationary satellites [16]. The thrust chamber is often made of rhenium, internally lined with platinum to prevent oxidation. The use of this technology resulted in a mass saving of about 5 kg and a 1 second increase in the specific impulse. For

higher performance, the rocket engine must operate at the maximum temperature compatible with its service life requirement. The technology of the 400 N class engines is constantly updated with the introduction of materials that have a higher resistance to high temperatures. Iridium thrust chambers with internal rhenium (Ir/Re) coating have a maximum operating temperature above 2000°C. The thrust chambers made of platinum alloy do not reach the same temperature but can operate at 200 °C higher temperature than those realized in columbium alloy and reduced risk of oxidation [16][17]. The technical specifications of 400N are shown Table 2.3 [18] [19].

Figure 2.3 S-400 bi-propellant apogee motor.

Sl.no	S-400 N Technical characteristics	Values
1	Thrust	425 N
2	Specific impulse	321s
3	Flow rate	135g/s
4	Mixture ratio	1.65
5	Chamber pressure	10.35bar
6	Inlet pressure	12.5-18.5bar
7	Propellants	MMH and N_2O_4
8	Cooling concept	Film and radiative cooling
9	Propellant Valves	R-4D engine valves
10	Throat diameter inner	16.45mm

Table 2.3 Technical specification of S-400 engine.

2.6 Technical specification of a new engine

Success in space activities requires perfection. Many expert scientists, scholars and technicians have contributed to the success of extraordinary enterprises in this field. Behind every such success there is an impeccable performance of a highly complex system. Every detail and even the mistakes are important, in that they contribute to future refinements. If a part of the spacecraft does not work, the failure often leads to the loss of the entire mission. In-depth knowledge is needed to realize a perfect propulsion system. If it does not work flawlessly, none of the other systems has the possibility to operate in space [20].

To continue the exploration of the solar system and its planets it is necessary to be able to effectively design liquid propellant rocket engines for launch operations, orbiting, orbit circularization and maneuvers, spatial rendezvous and deorbit. The choice of propellants is a critical aspect of the design of liquid propellant rocket engines to meet the performance and payload requirements of the spacecraft. In particular, hypergolic and storable propellants are a very attractive solution for upper stage and orbital engines. Nitrogen tetroxide (NTO) and hydrazine have been selected as reference propellants for the present thermo-structural analysis because of their advantages in terms of hypergolicity, storability and propulsive performance [20].

The design of a rocket engine using high performance storable liquid propellants requires the improvement of the solutions used in previous engines. These challenges involve aspects such as fatigue resistance, thrust, assembly and disassembly, choice of materials and production processes. Special materials must be used to meet the operational requirements. The newly designed rocket engine object of this preliminary study must have the ability of operating at variable power levels. The R-4D engine produced by Marquardt (Aerojet Rocketdyne) has been chosen as a reference in this analysis for the preliminary design of a new engine and for the attainment of satisfactory requirements in terms of specific impulse and thrust. It is a rocket engine successfully used in the lunar module of the Apollo mission. The R-4D engine uses radiation and fluid-film cooling. The material chosen for the combustion chamber is molybdenum, which has a high mechanical resistance at high temperatures. The material selected for the nozzle extension is L-605 (Cobalt), which has good mechanical properties and is compatible with radiation cooling. In this study it has been preliminarily assumed to use these materials, even if this choice should not be considered as final [20].

The technical specifications of the new engine are listed in Table 2.4, The results obtained from the preliminary design are close to those of the R-4D engine. The engine's propulsive performance has been estimated using the CEA code, developed by NASA to study fuel-oxidant combustion. Data obtained from the CEA code assuming chemical equilibrium conditions at the end of combustion are presented below [20]. CEA is a software designed by NASA for modelling the chemical reaction of fuel and oxidizer. It has been used to estimate the rocket engine propulsive performance. Data obtained from the CEA code for rocket operation at chemical equilibrium listed below [21].

Sl.no	Technical Data	Value
1	Combustion pressure (nominal)	6.55 MPa
2	Mixture ratio O/F	2
3	External wall emissivity	0.64
4	Propellants	Hydrazine and Nitrogen tetra oxide.
5	Combustion temperature	2929.51 K
6	Characteristic velocity (c*)	1624.3 m/s
7	Average molar mass	22,733 g/mole
8	Average c_P	4508.1 J(kg/K)
9	Mass flow rate	0.153 kg/s
10	Thrust (nominal)	445 N
11	Specific impulse	280 s
12	Average gamma	1.1414

Table 2.4 Technical specification of the new engine.

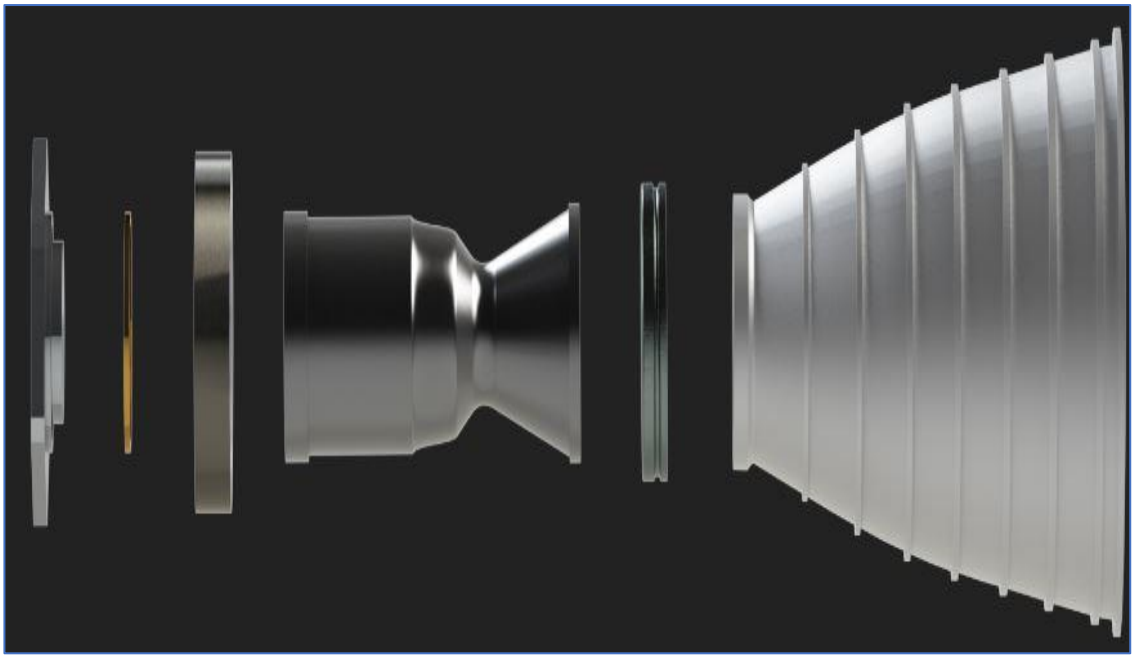

Figure 2.4 Concept of the new engine modelled by Solid Works

3 Cylinder analysis

3.1 Methodology

The finite element analysis (FEA) is a simulation method that, by discretizing the mathematical problem, allows one to obtain a numerical solution in order to study, among other things, how the forces, vibrations, thermal effects etc., influence the structural integrity of the object of the analysis. The first step consists in examining the real object to identify possible simplifications for more effectively converting it's geometry into a finite element model [22].

The first FEA of this work has been carried out with reference to a cylindrical thrust chamber with the dimensions indicated Figure 3.1. The advantages of performing FEA of the cylinder are.

- The possibility of comparing the solution with the behavior of the cylindrical part of the engine thrust chamber.
- The possibility of comparing and verifying the FEA results with those of analytical models.
- The possibility of studying any deformation or structural failure of the thrust chamber (the part connected to injection plate) by applying the same BCs and initial conditions to the cylindrical chamber model.

The main objective when performing a structural FEA is to verify that the structure will perform its design function under the action of the applied mechanical and thermal loads. It is essential to identify all possible failure modes and to design the structure accordingly. For any component of a rocket engine for space vehicles the most common causes of failure are as follows [23].

- Exceeding the maximum strength of the material, causing its rupture and collapse.
- The development of structural instabilities under the action of the applied loads, which can lead to collapse.
- The fatigue failure of the material under the cyclic loads due to the generation and propagation of cracks after a relatively large number of load/ unload cycles.
- The elasticity of the component, under steady or unsteady conditions, which if excessive can cause its malfunction or induce unacceptable vibrations.
- The structural damage caused by high temperatures. Since metals are good thermal conductors and their mechanical characteristics decrease with the temperature, structural failures can occur due to exceeding the ultimate stresses or due to the generation of unacceptable stresses as a consequences of differential thermal expansion (thermal stresses) [23].

Therefore, studying all these factors will help to guide the design of the spacecraft or its components and yield a high degree of reliability. Structural analysis is an essential step for reducing the cost and development time of rocket engine design and development. The execution of a FEA analysis allows one to evaluate the sensitivity of the project to the input data, optimize the engine geometry, increase its reliability and reduce its costs and weights, all beneficial aspects for any space mission. The present FEA has been carried out using the ANSYS APDL 2016 software [23].

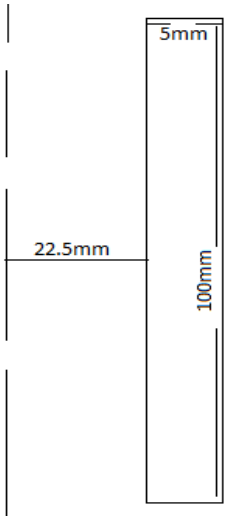

Figure 3.1 2D typical cylinder, with dimensions in mm.

3.2 Steady-state structural analysis of cylinder

The 2D cylinder representing the side wall of the thrust chamber has been designed in Ansys APDL. The element type selected for this model is the Solid 4 183 node. The axisymmetric option has been selected because the model shape, thermal and mechanical loads, and constraints are also axisymmetric. Axisymmetric modeling reduces the computing time with respect to three-dimensional (3D) modeling. The Element Plane 183 with 8 nodes has been chosen, which can be used for flat stresses and strains, as it is of superior 2D order with quadratic displacement accuracy and is suitable for irregular meshes, with the possibility of modeling viscous creep, stress stiffening, hyper elasticity effects and large deformations. The dimensions of the axisymmetric 2D cylinder model are: height 100 mm, thickness 5 mm and radius 22.5 mm. The material has been subjected to pressure and thermal loads to study its elasticity and linearity, verified by calculating the principal and equivalent 1D stresses.

The choice of materials plays a fundamental role in the design of the thrust chamber, as discussed in Section 1.1 and must be made before analyzing the mechanical and thermal properties of the thrust chamber. In particular, for this analysis, molybdenum has been chosen, a silver-white metal that can withstand high temperatures and pressures. Its mechanical proprieties at 25 ° C are listed in Table 3.1[24].

Sl.no	Technical properties	Values
1	Density [kg/m^3]	10.24
2	Young's modulus [GPa]	320
3	Poisson’s ratio [-]	0.32
4	Yield strength [MPa]	110
5	Coefficient of thermal expansion [1/K]	$5.20x10^{-6}$

Table 3.1 Mechanical properties of molybdenum.

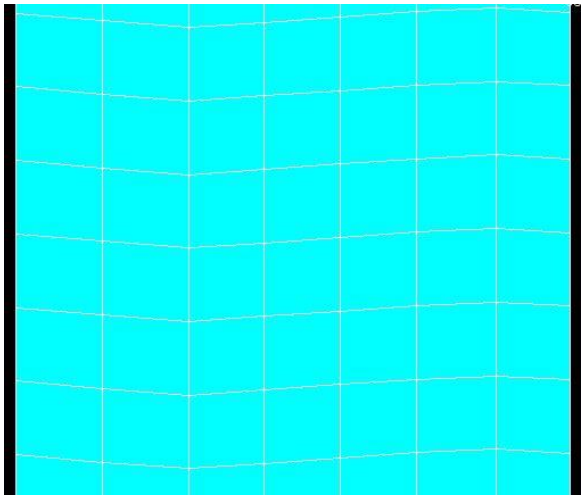

Figure 3.2 Meshed 2D cylinder.

The cylindrical model is based on the geometry of the cylindrical part of the thrust chamber. Then, the meshing has been performed by assigning the length of the edge of the FEA element as equal to 1.Figure 3.2 shows the cylinder mesh in which the chamber model has been divided into 2000 elements connected by 6240 nodes. The BCs for the analysis of the cylindrical model are 6.5 bar of constant pressure acting on the inner wall and the position of one end of the chamber being assigned (degree of freedom (DoF) UY = 0) while the other end is free. The results for the simulation are shown below plotted for steady state conditions in Figure 3.3 through Figure 3.5.

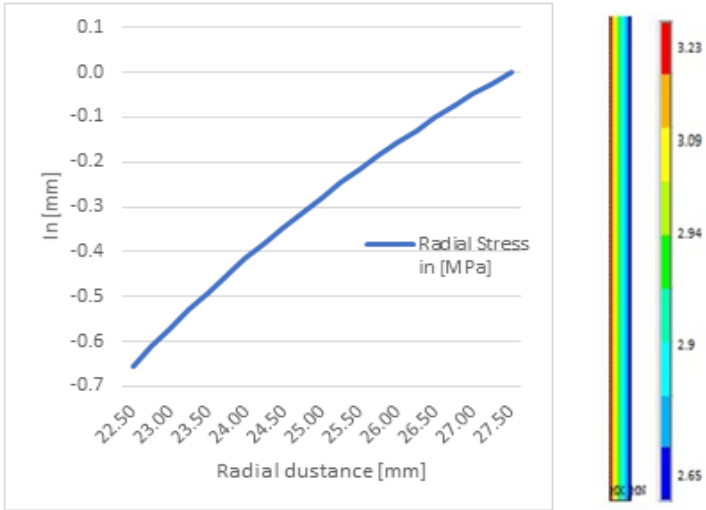

Figure 3.3 Radial stress of 2D cylinder.

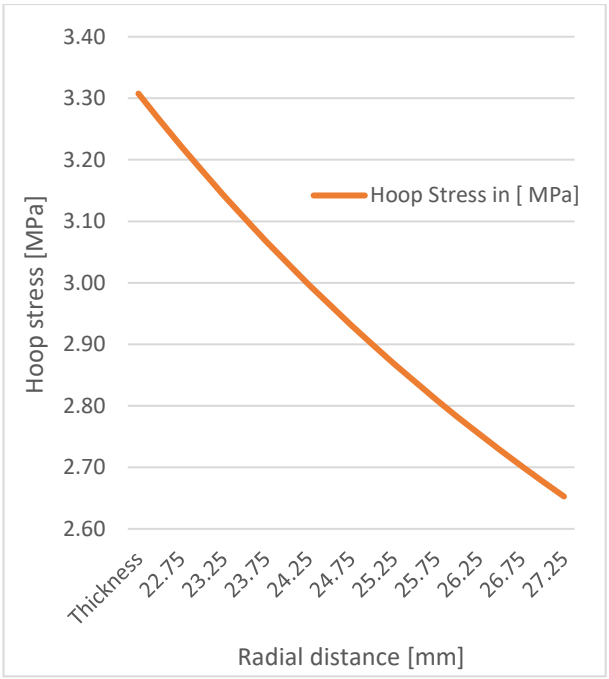

Figure 3.4 Hoop stress of 2D cylinder.

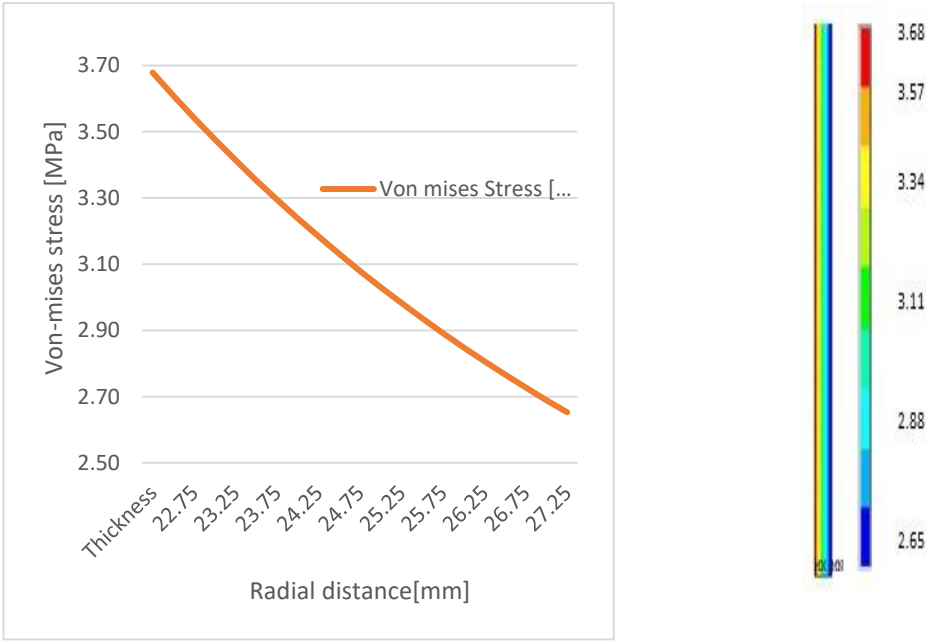

Figure 3.5 Von-Mises stress of 2D cylinder.

Results	Analytical	APDL	Error
Maximum radial stress	-0.42683 MPa	0.000055463 MPa	1%
Maximum hoop stress	2.8 MPa	3.31 MPa	2.5%

Table 3.2 Maximum radial and hoop stress for the 2D cylinder

The analytical result has been calculated by using the formula:

$$\sigma_r = -\frac{1-\rho^2}{\rho^2}\left(\frac{\beta^2}{1-\beta^2}\right)p_i \quad \textbf{(3.1)}$$

$$\sigma_r = \frac{1+\rho^2}{\rho^2}\left(\frac{\beta^2}{1-\beta^2}\right)p_i \quad \textbf{(3.2)}$$

for the radial stress and hoop stresses respectively.

The maximum stress Von Mises obtained from ANSYS APDL is 3.8 MPa. Comparing this result with the yield stress of molybdenum (110 MPa) we can conclude that there will be no failure nor plastic deformation. Therefore, the cylindrical part of the thrust chamber does not change its geometry at the assigned operating pressure and the risk of permanent deformation or rupture is low.

3.3 Unsteady -thermal structural analysis of cylinder

Stress is one of the major design factors of rocket engine combustion chambers. When an object is cooled or heated it changes its shape by contracting or expanding. An uneven temperature in an element causes stress and distortion. The resulting thermal stresses are determined by the temperature field in the material. The unsteady thermal analysis of the side wall of the thrust chamber has been carried out on the same 2D cylindrical model used for the calculation of the stresses produced by the internal pressure. The heat transfer to the inner wall of the chamber has been calculated for a value of the heat exchange coefficient equal to 416.89 W/m² K and a constant temperature of the gas in the chamber equal to 2929.27 K. The heat transfer by radiation to the inner wall of the chamber has been calculated assuming the emissivity of the inner wall to be equal to 0.038, constant gas pressure inside the chamber to be equal to 6.55 bar, the emissivity of the external wall of the chamber to be equal to 0.64, with unitary view factor towards the deep space (see Figure 3.6) and stress analysis has been performed by assigning the temperature field as an input [25] [26].

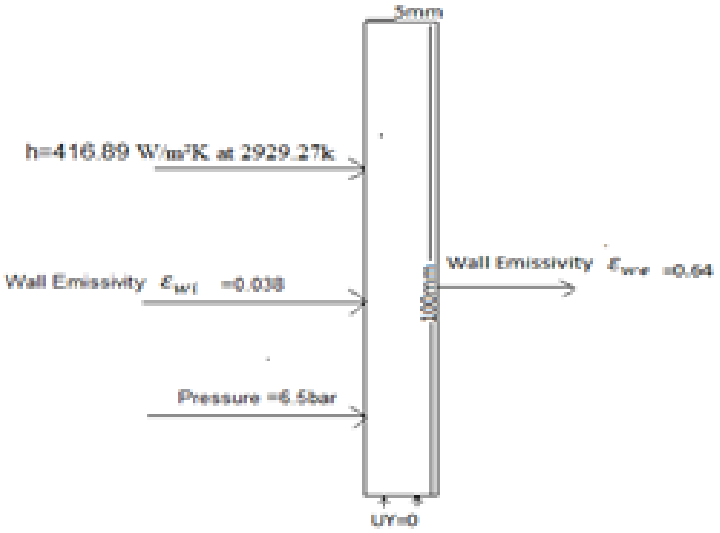

Figure 3.6 Cylinder with boundary conditions

The chamber cylinder model has been calculated as a 2D axisymmetric body using Ansys APDL. The type of element selected in this case has been the plane model 77, a four-node thermal element, of a higher order, with a temperature DoF in each node. The 8-node flat element 77 is suitable for thermal analyses because it is able to represent a temperature profile and can model curved boundaries. The results have been obtained for each node of the structure. The thermal properties of molybdenum are listed below in Table 3.3 (the reason for selecting molybdenum is to the possibility of comparing the results with those of the reference thrust chamber, also made in molybdenum).

Sl.no	Thermal Specification	Values
1	Thermal conductivity [W/(mK)]	142
2	Specific heat [J/(kg K)]	251
3	Thermal expansion coefficient [1/K]	5.20×10^{-6}
4	Melting temperature [K]	2883

Table 3.3 Thermal Properties of molybdenum.

The cylindrical model of the chamber has been defined by assigning the thermal properties of the materials and by realizing the mesh with the edge length of the element equal to 1 (Figure 3.2). The BCs were assigned to the cylindrical model on the basis of data obtained at chemical equilibrium from the CEA code, a software developed by NASA that calculates the composition and properties of gas mixtures produced by combustion in rocket engines for the evaluation of its propulsive performance [27].

For this analysis the initial temperature of the chamber and the internal gas temperature are set equal to 273.15 K and 2929.51 K respectively. With a heat exchange coefficient equal to 416.89 W / m² K. From the emissivity of the external wall is equal to 0.64, obtained from the R-4D engine. Heat transfer by convection and radiation is given as a BC, with emissivity from hot gases to the inner wall (assuming a simplified radiation model in a single cavity with participating thermal gas) of 0.038. Since this is a transient analysis, the calculation has been performed for a total duration of 150 s. The automatic choice of the time step has been deactivated and the number of sub-phases (which should be lower than the total duration of the simulation) is assigned equal to 0.025 s. The results of these thermal simulations are shown in Figure 3.7 through Figure 3.9 and show how the temperature in the chamber wall varies over time. Based on these results, the thermal stresses for the same cylindrical chamber model have been evaluated.

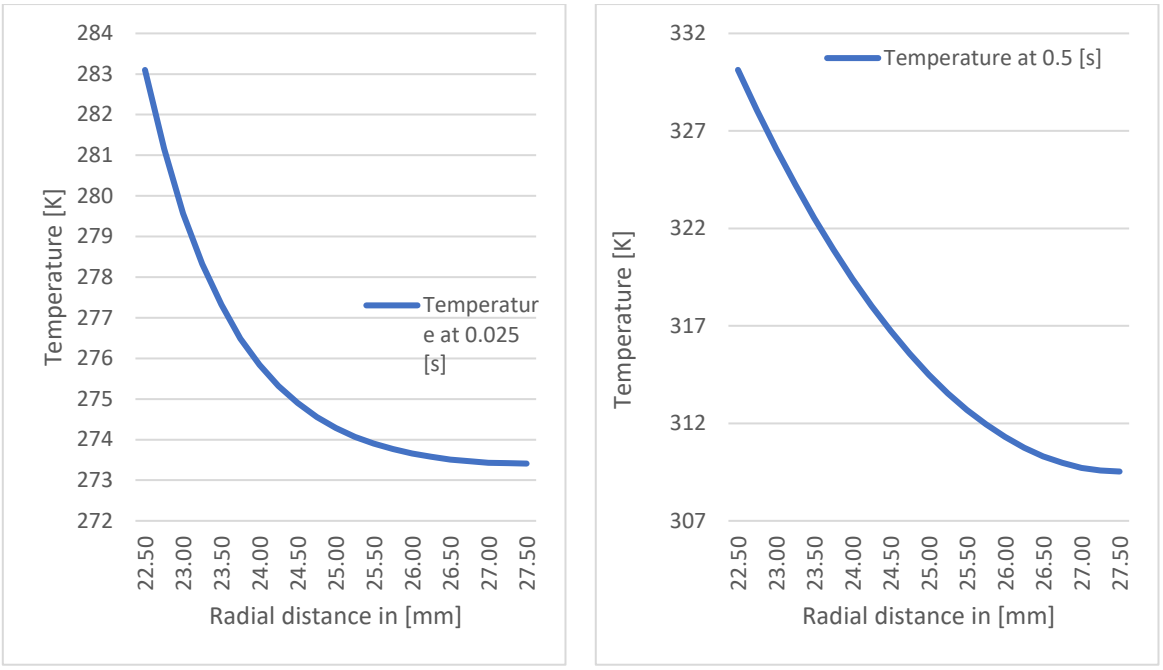

Figure 3.7 Temperature profiles of 2D cylinder at 0.025 s (left) and 0.500 s (right).

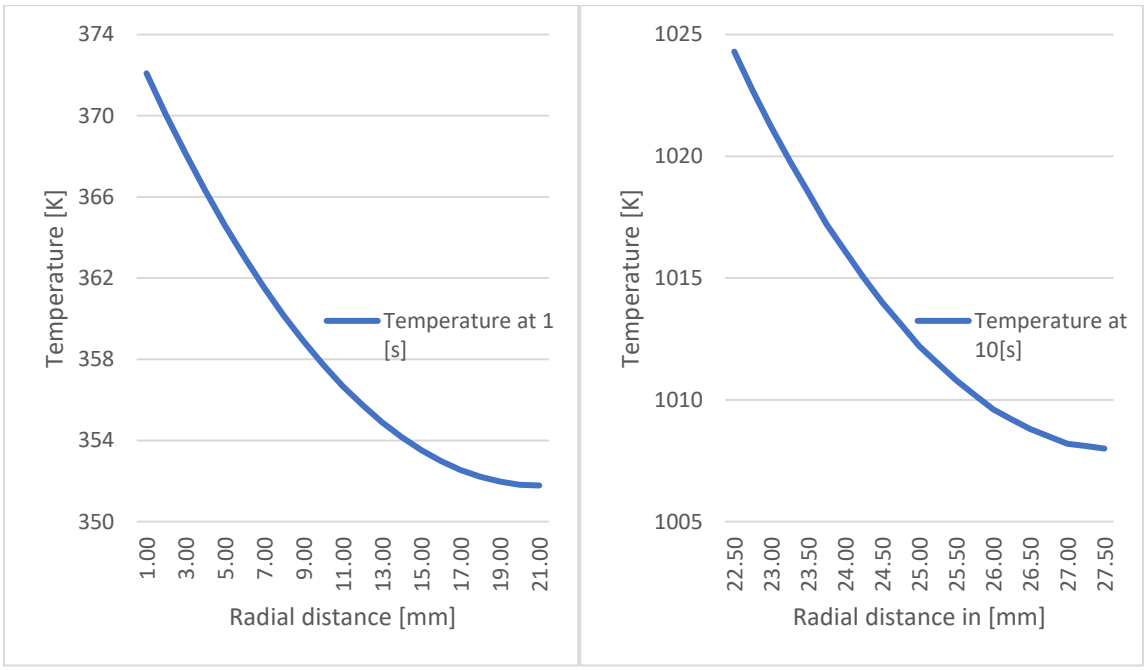

Figure 3.8 Temperature profile of 2D cylinder at 1 s (left) and 10 s (right).

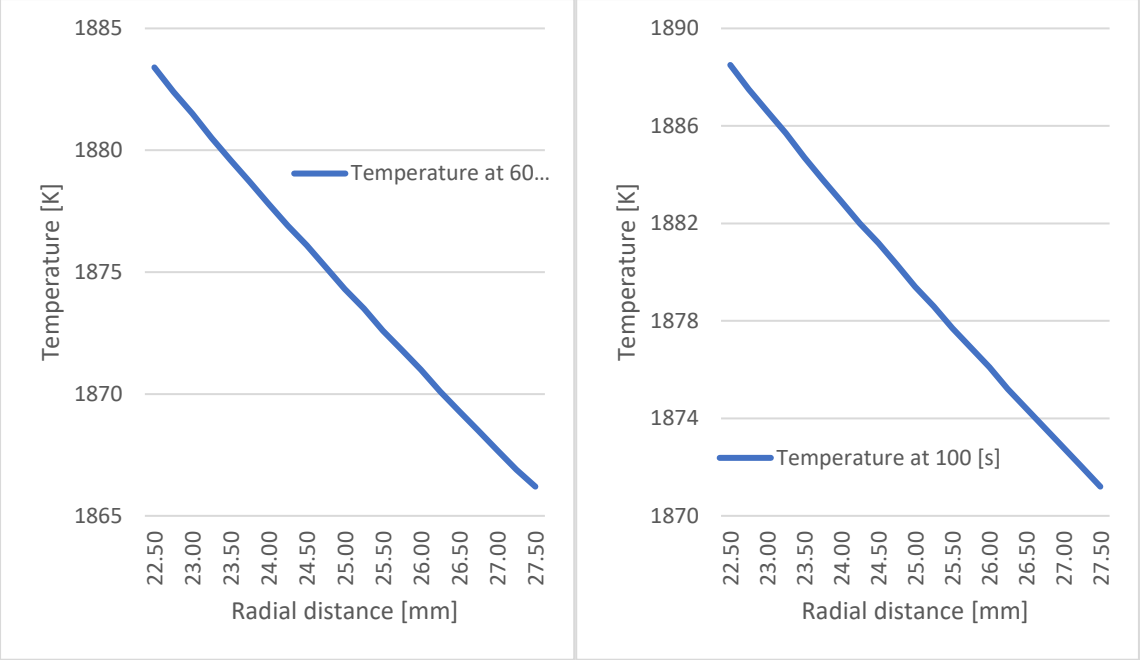

Figure 3.9 Temperature of a 2D cylinder at 60 s when steady state conditions have been attained.

The above diagrams show the temperature profile in the cylindrical part of the combustion chamber, where the temperature reaches the steady value of 1888 K after about 60 seconds from propellant ignition. With these thermal fields it is possible to develop the analysis of the thermal stresses that act on the model. The properties of the material for the structural analysis are provided as input to the model (see Table 3.1), and a constant pressure of 6.5 bar is assumed to act on the inner wall as a BC of the structural analysis. This analysis is steady. It is therefore important to change the option in APDL ANSYS from unsteady to steady. The temperature fields are applied at each time by selecting ".rth" file. As soon as one switches from thermal to structural analysis, the ANSYS software saves the ".rth" file and reads a new file for the structural analysis. The results obtained from this analysis are shown below in Figure 3.10 through Figure 3.12.

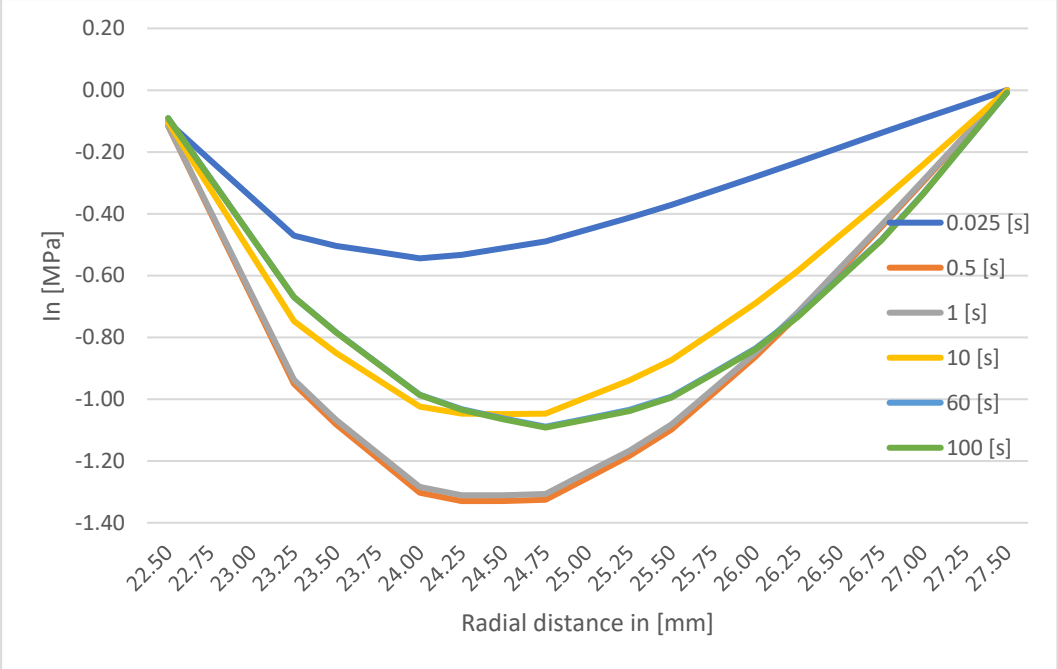

Figure 3.10 Radial stress of 2D cylinder due to the temperature field along the radial direction at different times after ignition.

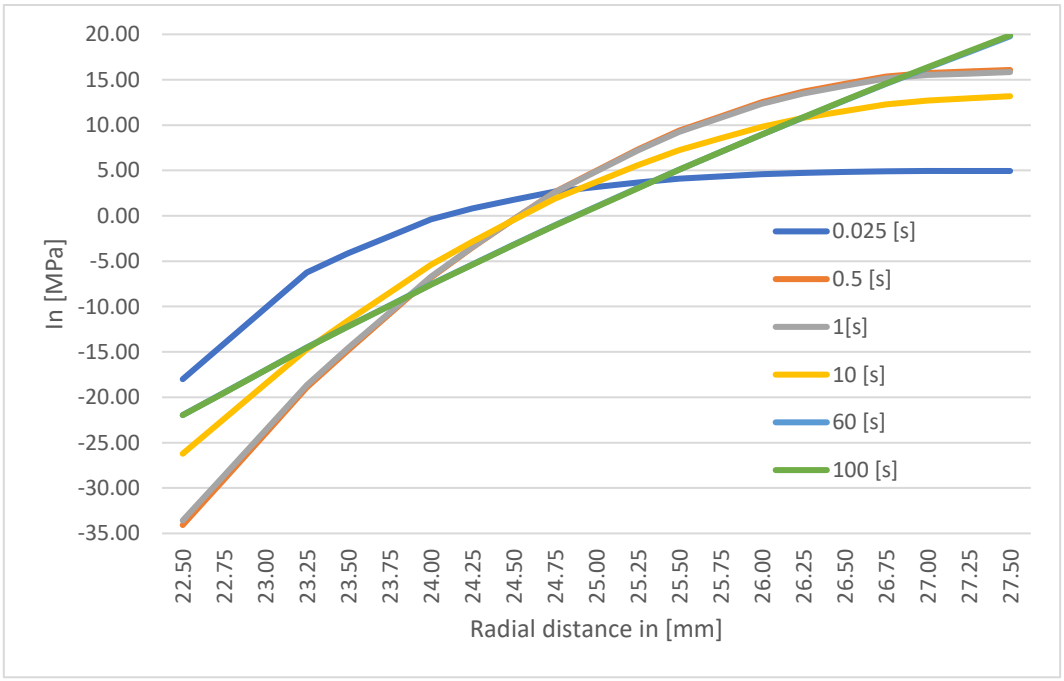

Figure 3.11 Azimuthal stress of 2D cylinder due to thermal field along the radial direction at different times after ignition

The results obtained are shown in the diagrams in particular, Figure 3.9 shows that for a gas temperature in the thrust chamber equal to 1888 K the azimuthal stress in the chamber wall reaches the stationary value of 20 MPa after 100 s.

The Von Mises stress is used to reduce a general state of stress in an equivalent uniaxial stress to be compared with the yield stress of the material for assessing the

possibility of structural failure. The graph shows that the maximum Von Mises stress, equal to 34 MPa, occurs at 500 ms from the chamber ignition. In view of the fact that the yield strength of molybdenum is 110 MPa, the results of the analysis indicate that the wall of the chamber will not fail.

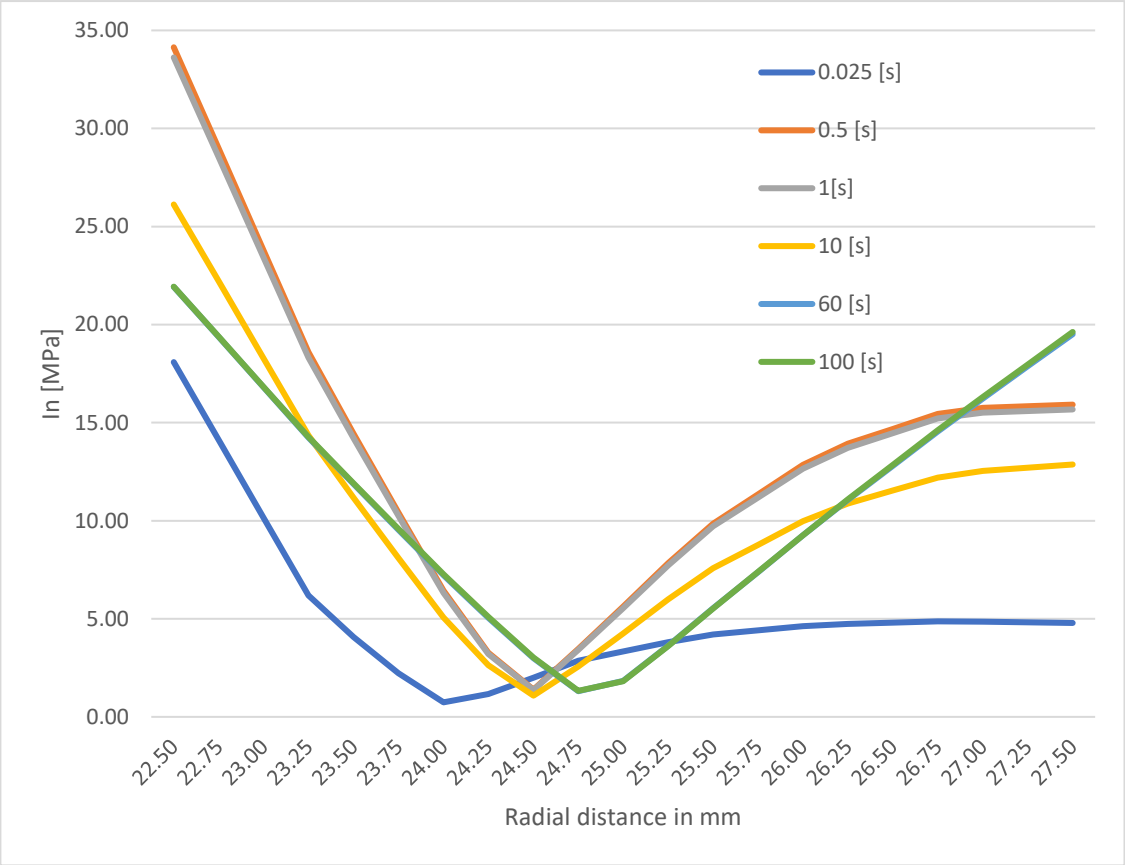

Figure 3.12 Von Mises stress of 2D cylinder due to thermal loads acting with respect to time

4 Combustion chamber analysis

The design of a liquid propellant rocket engine (LPRE) is developed below. The combustion chamber of the engine, which converts the chemical energy into kinetic energy of the jet to generate the thrust, is considered as a structural element. The chamber wall material and its cooling method must be carefully selected taking into account the operational requirements and structural resistance constraints [28].

The rocket engine design has been developed using the R-4D bi-propellant engine as a reference. The combustion chamber of this engine is single-walled with a throat radius of 11 mm. Molybdenum has been selected for the realization of the chamber as it is a material that combines high mechanical strength at high temperatures with high thermal conductivity. These properties are particularly important as they allow one to increase the pressure in the chamber and reduce the thermal stresses during its operation. Molybdenum also has a high emissivity, compatible with the use of radiation cooling to control the temperature of the chamber wall. The method used in this study for the structural analysis of the thrust chamber is planned and executed as summarized in Table 4.1[23].

4.1 Analysis of the steady state combustion chamber

The first step of the analysis consists in defining the structural requirements and evaluating the applied loads. Parameters such as forces, loads, cycle times and displacements must be considered and verified during the analysis. In the end, the dimensions and design of the chamber are determined by the conditions of maximum deformation, also taking into account that the combustion chamber is subject to constantly changing loads due to variations of the vehicle acceleration, the chamber operating pressure and temperature, and sometimes of the engine vibrations. All these factors affect the rocket engine performance. In the transient analysis, the dynamic load acting on the combustion chamber and the load history can be calculated based on position, stiffness and heat flux. It is important to ensure that the combustion chamber is not subjected to excessive mechanical loads in order to avoid malfunctions and the failure of the mission [29].

The steady-state analysis of the stresses in the combustion chamber has also been performed using ANSYS APDL 16.0. The objective consists in determining its behavior in response to the load conditions. The chamber design has been carried out with the Solid Works code. The key points have been indicated in mm and it has been useful to develop a model in ANSYS using these key points. The steady-state structural analysis has first been performed using the Solid node183 element, which has been selected because it is axisymmetric and because the meshing can be performed in a flexible way. Furthermore, this element is suitable for 2D structural analysis of any component. The material selected for this model is molybdenum and its mechanical properties are listed in the Table 3.1.

1. Needs and load calculation: • Loads→ static load and transient load • Stiffness, displacement
2. Material evaluation • Material parameters and technical specification needed
3. Structural Modeling: • Structural modelling of the combustion chamber in ANSYS APDL 16.0 4. Determination of combustion chamber response: • Static analysis→ Pressure varying along Z-axis in the combustion chamber and radial distance • Transient Analysis → Determination of Thermal load while Temperature varying along Z-axis, and determination of stress caused by thermal loads which are static analysis
5. Combustion chamber failure mode check: • Checking the margin of safety for yield strength • Cooling method

Table 4.1 Methodology of stress analysis

Figure 4.1 The 2D thrust chamber of the rocket engine designed using ANSYS APDL 16.0 software and it is mesh. The structure is divided into 4895 elements, formed by connecting 15970 nodes.

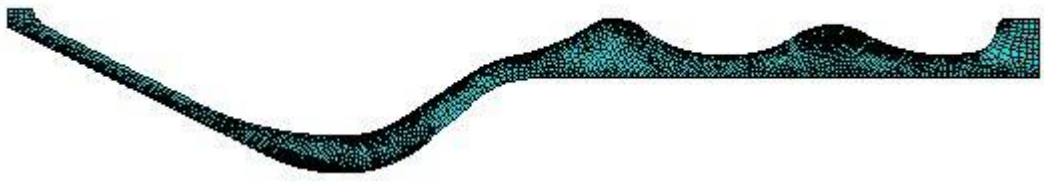

Figure 4.1 Finite meshed 2D thrust chamber.

The loads can be applied to each element and to each node. Any selected node of the combustion chamber yields its result corresponding to the applied loads. After meshing the chamber model it is necessary to impose the BCs. The combustion chamber is fixed at one end (that is, the bottom line or the part that connects to the injection plate is fixed UY = 0) and a non-uniform pressure acts along the Z axis of the inner wall. In particular, the combustion chamber is divided into seven stations (see Figure 4.2) along the Z axis, with a different pressure acting at each station.

The axial stations are defined for the converging/diverging portion of the chamber, since the temperature and pressure in the cylindrical part are constant and equal to the stagnation values, obtained from the CEA code developed by NASA (see Table 4.2) using nitrogen tetroxide (NTO) as oxidant and hydrazine as fuel with an oxidizer / fuel ratio O / F = 2 (see Table 4.2).

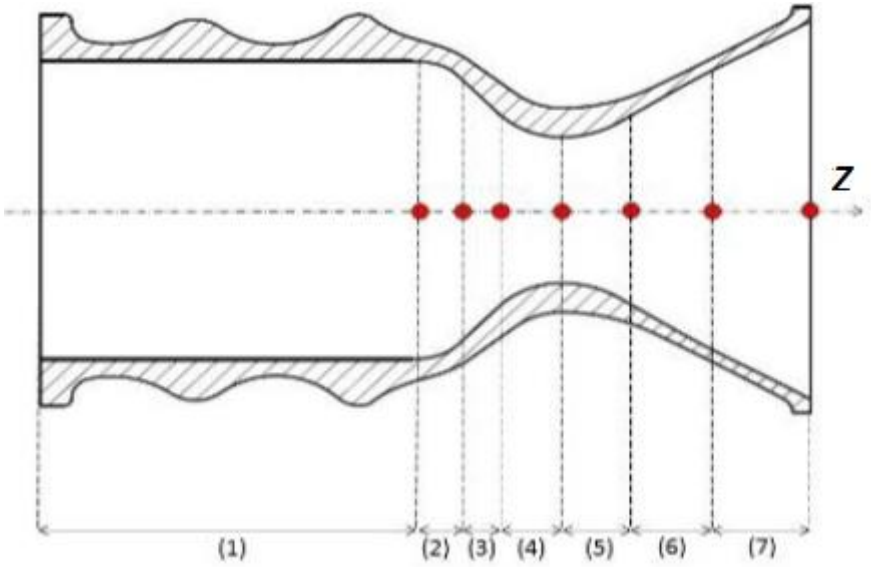

Figure 4.2 Stations of the thrust chamber selected for applying specific values of the pressure and temperature.

Sl.no	CEA online tool data	Values
1	Average molar mass [g/mole]	22.733
2	Average gamma	1.1414
3	Average specific heat [J/kg K]	4508.1
4	Combustion temperature [K]	2929.51
5	Mass flow rate [kg/s]	0.153
6	Combustion Pressure [bar]	6.5

Table 4.2 Data obtained from the CEA code.

Using this data, it is possible to calculate the non-uniform pressure and temperature acting at the different stations Table 4.3 shows the location along the z-axis. $A_t \,/\, A$ is the ratio of the throat area (A_t) with respect to the area of the selected station (A), the number Mach number *M* and the pressure p_g in the selected station. For the calculation of the Mach number for isentropic flow, Equation 4.1 is used, when A_t/A and gamma (obtained from the CEA online tool) are known. After calculating the Mach number, it is possible to obtain the non-uniform pressure acting at each axial station using Equation 4.2.

St.no	X [mm]	Mach Number	p_g [MPa]	$\frac{A_t}{A}[-]$
1	52.74	0.158363	0.6457	0.2621
2	57.81	0.176473	0.643474	0.2911
3	64.12	0.322326	0.617426	0.5115
4	73.09	1.000	0.377363	1.00
5	81.59	1.725702	0.14008	0.6811
6	96.66	2.5265	0.0323944	0.2525
7	109.12	2.8666	0.0162358	0.1498

Table 4.3 Boundary conditions for the thrust chamber steady-state analysis.

$$\frac{At}{A} = M\left(\frac{2+(\Upsilon-1)M^2}{\Upsilon+1}\right)^{-\frac{\Upsilon+1}{2(\Upsilon-1)}} \quad \textbf{(4.1)}$$

$$p_g = \frac{p}{p_c} = \left(1+\frac{(\Upsilon-1)}{2}M^2\right)^{\frac{-\Upsilon}{\Upsilon-1}} \quad \textbf{(4.2)}$$

Figure 4.3 illustrates how the pressure varies along the z. At the first station, as soon as the cylindrical part ends, the pressure starts to decrease up to the nozzle exhaust. The Mach number is smaller in the cylindrical part of the combustion chamber. In the convergent/divergent part a drastic increase of the Mach number occurs.

The uneven pressure obtained has been applied to the inner wall of the combustion chamber. In the APDL ANSYS code it is necessary to assign in tabular form the pressure as a function of the axial coordinate. Since these are steady analyses, the pressure does not change over time.

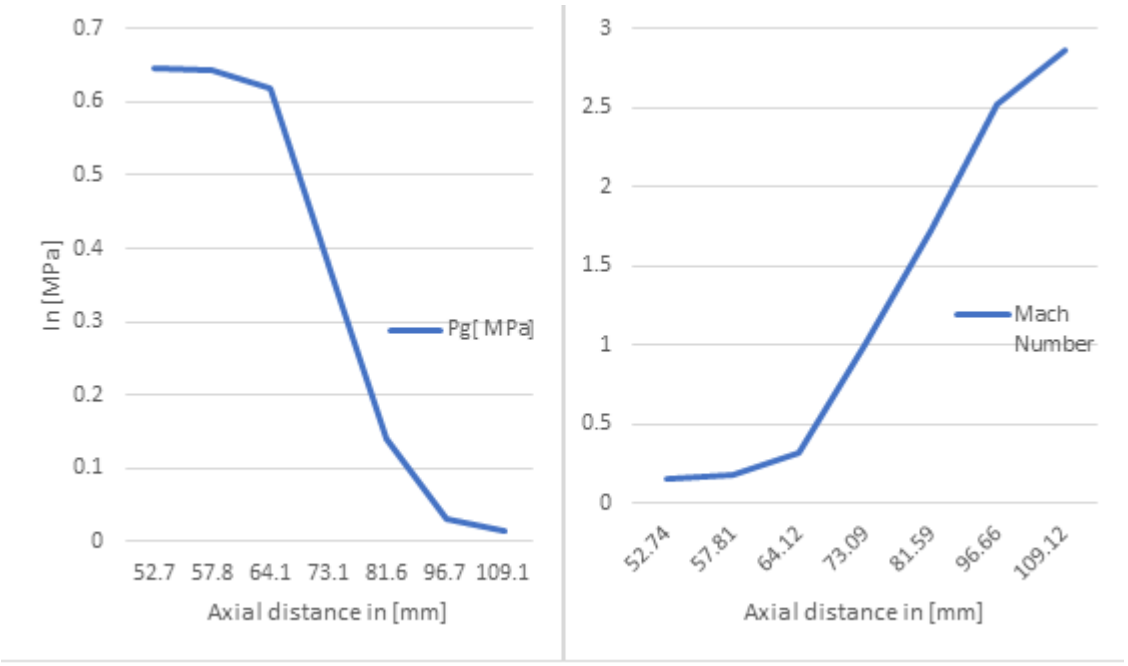

Figure 4.3 Pressure profile and Mach number profile in the thrust chamber

Figure 4.4 to Figure 4.9 show the results of the simulation for the assigned BCs of non-uniform pressure acting on the inner wall of the combustion chamber along the Z axis. The results show that the azimuthal and radial stresses experienced by the combustion chamber are small, and that the Von Mises stress is 4.96 MPa, lower than the yield limit of molybdenum. All seven stations are subject to pressure, but this does not cause any structural damage. Thus, the material can withstand the pressure of 6.5 bar in the thrust chamber. The maximum values of the azimuthal and Von Mises stresses occur in the cylindrical part of the chamber.

Two points have been selected in the combustion chamber to study the stresses along the radial direction: point 1 has been selected at the center of the cylindrical region of

the combustion chamber and point 2 in the throat region of the nozzle. The non-uniform pressure acting on the inner wall not only creates a radial stress in the chamber wall, but also creates an azimuthal stress. The azimuthal stress is equal to 4.7 MPa and is higher than the radial stress. This is anyway a low stress, which does not involve an appreciable deformation of the outer diameter of the chamber. The Von Mises stress created by the internal pressure in the chamber is 4.76 MPa, which is within the yield limit of the wall material. Hence, the walls of the thrust chamber can withstand the assigned value of the operating pressure equal to 6.5 bar.

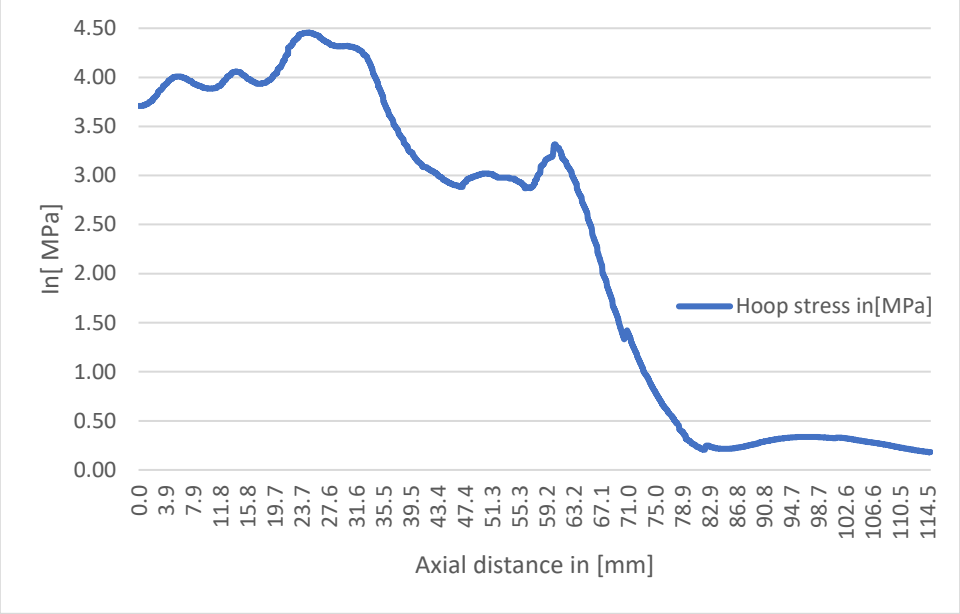

Figure 4.4 Azimuthal stress in the 2D thrust chamber along the axial direction

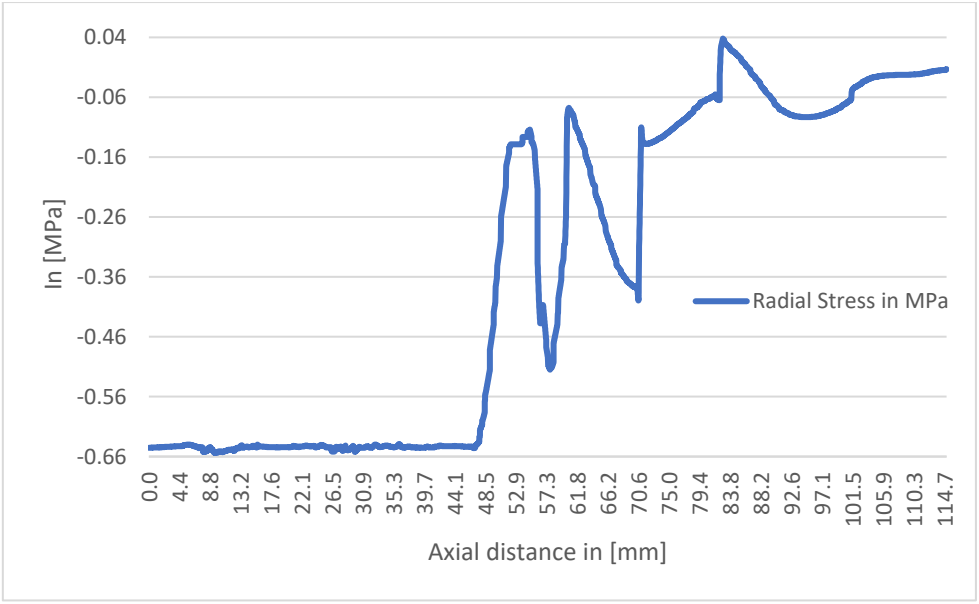

Figure 4.5 Radial stress in the 2D thrust chamber along the axial direction.

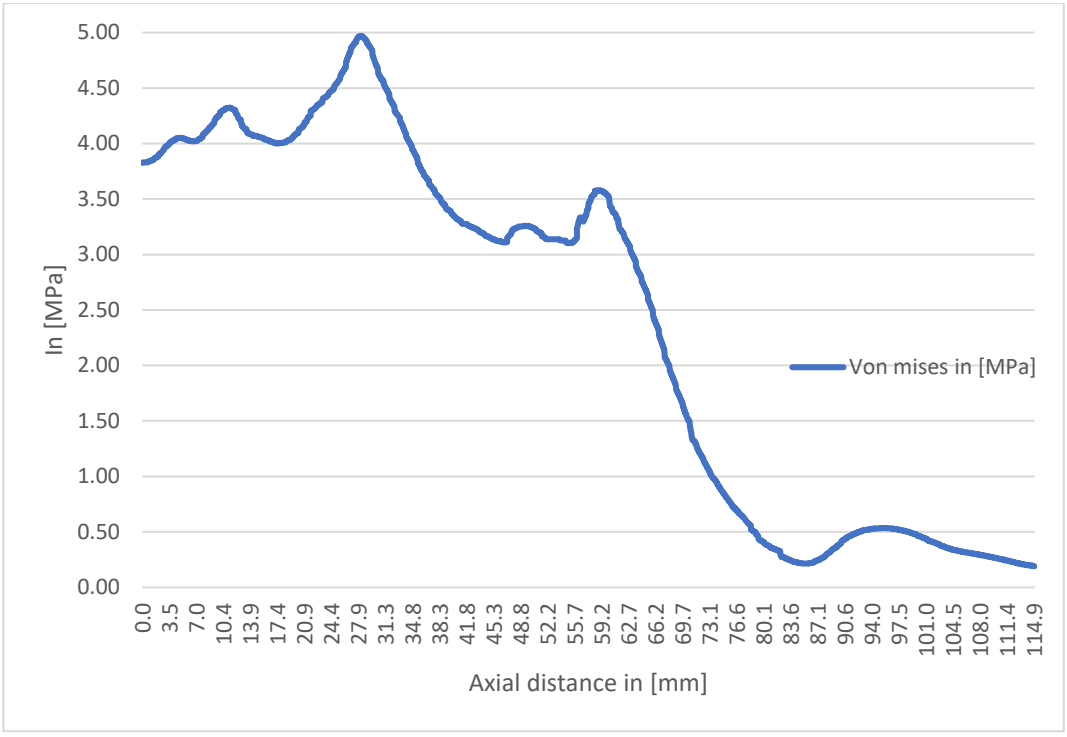

Figure 4.6 Von-Mises stress in the 2D thrust chamber along the axial direction.

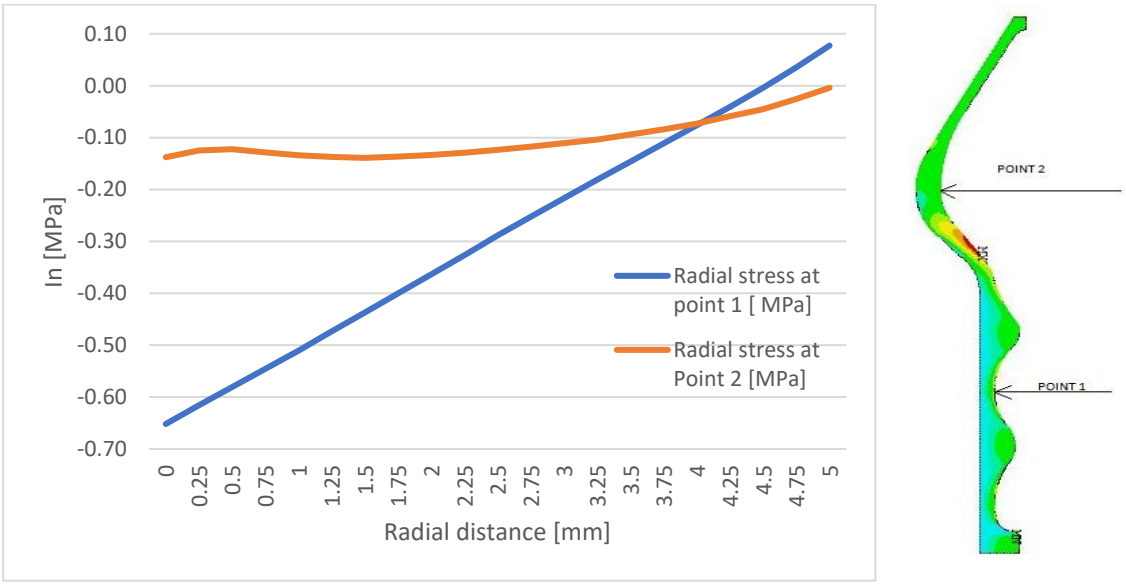

Figure 4.7 Radial stress in the 2D thrust chamber along radial direction.

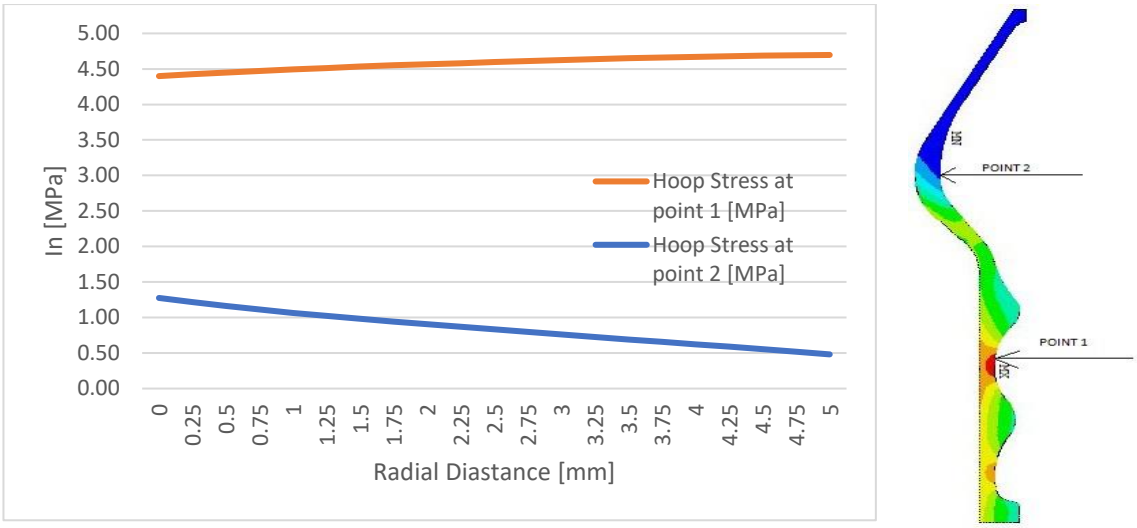

Figure 4.8 Azimuthal stress at two different axial stations in the 2D thrust chamber along the radial direction.

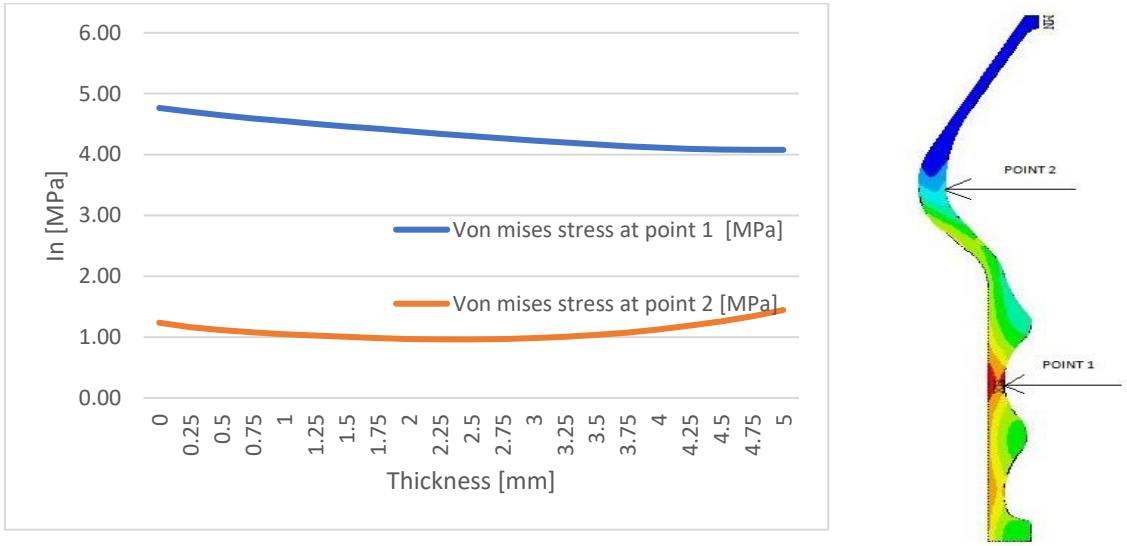

Figure 4.9 Von-Mises stress in the 2D thrust chamber along the radial direction**.**

4.2 Unsteady thermal analysis of thrust chamber

Any solid body subjected to a heat load exchanges heat with temperatures that vary over time until the body's heating or cooling reaches a steady state. The transient heat transfer during this process is said to be unsteady The study of unsteady heat transfer helps to define the thermal-structural response of the combustion chamber in a transient regime [30].

The objective of the analysis is to derive the temperature distribution in a combustion chamber during operation, and to determine the intensity of the heat flow and the radial and axial profile of the temperature in the chamber wall. Temperature distribution in unsteady heat transfer conditions *T (x, t)* is considered to be a function of position (*x)* and time (*t)*.

As long as it remains below the melting point it is relatively easy to analyze the temperature, as there are no phase transformations or chemical changes. However, it is impossible to realize a thrust chamber for a bi-propellant rocket engine without

cooling since the combustion temperature is higher than the melting point of most usable materials, and in any case so high as to reduce excessively the structural resistance even of the materials refractory to heat. In our case, during the combustion of the propellant, there is a temperature gradient in the chamber wall due to the heat flow transferred by its thermal contact with the hot gases[31]. Because the heat flux varies along the axial direction, each section of the wall undergoes a different temperature rise. In the unsteady one-dimensional heat conduction approximation, the heat transfer in the axial direction of the chamber is neglected and the thermal field is governed by equation [32],

$$\frac{\partial T}{\partial t} = \alpha \frac{\partial^2 T}{\partial x^2} \qquad \left(\alpha = \frac{k}{\rho c_p}\right) \tag{4.3}$$

where *x* is distance across the chamber wall, *k* is constant thermal conductivity, c_p is specific heat and ρ the density of the wall material.

During the analysis it is necessary to make sure that the thermal field generated by the heat transferred from the hot gases to the inner wall of the combustion chamber does not determine stresses exceeding the allowable stresses of the material. Based on this consideration, the nozzle throat and the initial part of the nozzle extension are the most critical areas, as they are subject to the highest thermal loads.

4.2.1 Methodology

The axisymmetric 2D combustion chamber has been designed using ANSYS APDL 16.0 to study the unsteady thermal effect that could generate structural failures and analyze the rocket engine performance at elevated temperatures. In the event that some of the characteristics of the chamber, such as geometry, loads or materials, were not axisymmetric, it would be necessary to perform a 3D analysis.

4.2.2 Computational plan

The performance and life of a liquid propellant rocket combustion chamber are constrained by the thermal stress of the material due to load cycles (ignition/shut-off). Therefore, an accurate thermo-mechanical analysis of the engine chamber wall must be performed to avoid the occurrence of critical failures during operation. Figure 4 shows the table reporting the results of the thermo-structural performance simulations and the heat transfer intensity in the combustion chamber, providing the convective thermal loads and structural loads for the analysis[29].

The 2D thrust chamber is designed using ANSYS APDL software. The element usually selected to perform thermal analysis is the Plane 77 element, a higher order version of the 4-node 2D thermal elements. The Plane 77 element is characterized by one DoF and by the temperature of the respective node and is applicable for the study of the heat flow that describes the origin of the matrices of the thermal elements, of the load vector and of the heat flow.

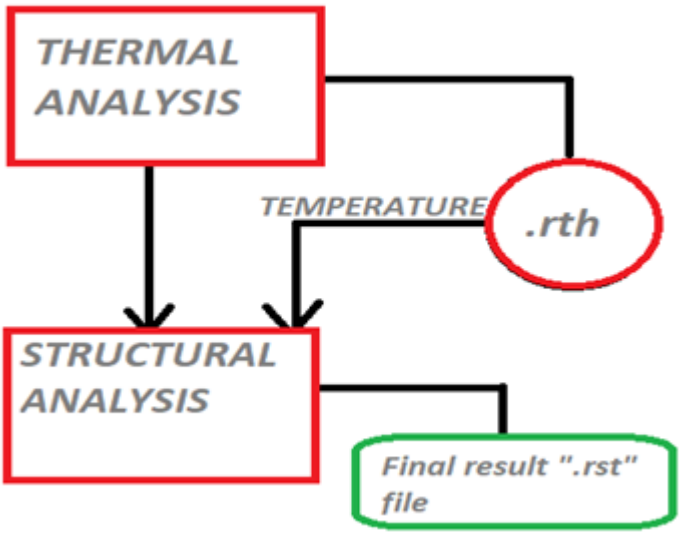

Figure 4.10 Flow chart of the unsteady thermo-structural analysis.

4.2.3 Material parameter

Molybdenum has been chosen to realize the Marquardt R-4D engine thrust chamber. The same material has also been chosen for the engine analyzed in this study, in order to better validate the results of its design. To verify the influence of the characteristics of the selected material, several analyses have been performed using Pt-Ir (90% platinum and 10% iridium) and Pt-Rh. The main criteria for the choice of molybdenum were:

- The combustion chamber can be operated with a radiation cooling and film cooling because molybdenum has high emittance and therefore radiates heat effectively.
- Combustion chamber can be manufactured more simply in a single material rather than by combining layers of different materials.
- Molybdenum can withstand temperatures of up to 1922 K and tensions up to 20.62 MPa for 10 minutes without creep failures.

Once the material has been selected, the thermal properties of molybdenum (see Table 3.3) have been assigned as inputs to the numerical model.

4.2.4 Modelling

The specifications and original dimensions of the R-4D engine are very difficult to obtain and many of the related documents are reserved. The diameter of the R-4D engine throat is approximately 22 mm. Based on this dimension, a model of the thrust chamber has been realized in Solid Works (see Figure 2.4). The key points of this model have been provided as input to the ANSYS APDL 16.0 code, realizing the shape of the combustion chamber for the thermo-structural verification.

4.2.5 Meshing

In the preliminary phase of this analysis, the thrust chamber has been meshed with an edge length of the elements equal to 0.50 mm. The thrust chamber has been divided into 1,025,000 elements and over 2,500,000 knots, to obtain a sufficiently accurate result. The non-stationary thermal simulation for a duration of 300 s required more than 24 hours of calculation. For an excessive number of elements, the time required for the simulation can become too long. To reduce the computational time the thrust

chamber has been divided into 4386 elements connected with 14253 nodes. With this choice, each simulation has been completed in about 3 hours (Figure 4.11).

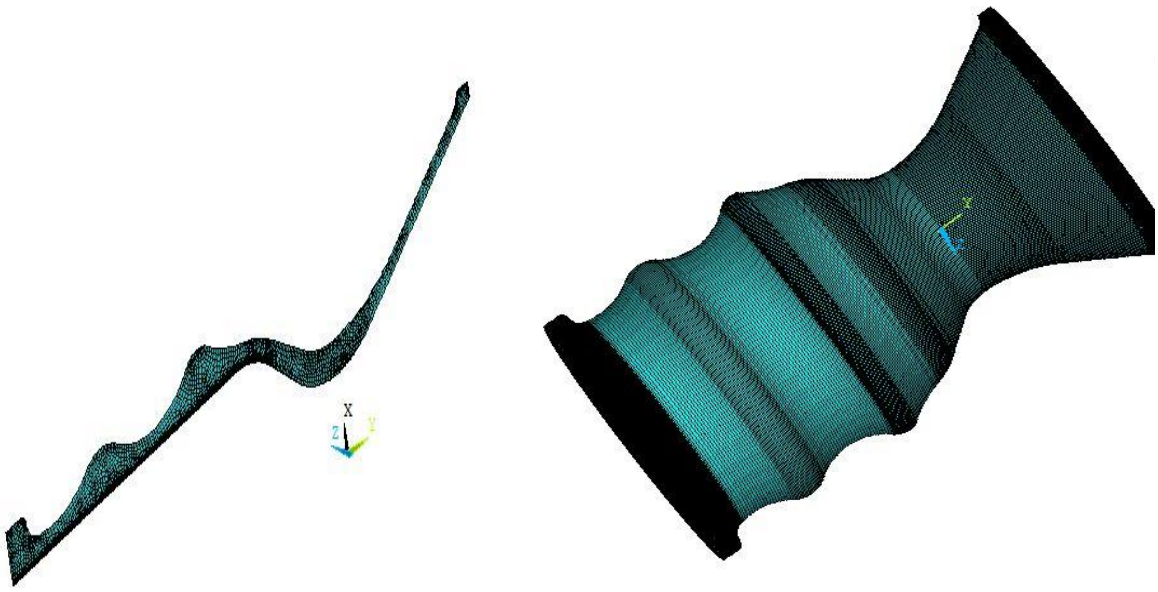

Figure 4.11 Meshed 2D thrust chamber and full expansion view.

4.2.6 Convective heat transfer of wall

The selected liquid propellants, Hydrazine (N_2H_4) and Dinitrogen tetroxide (N_2O_4), are converted into gaseous products during the combustion. The parameters of the gaseous flow have been calculated using NASA's CEA online code. Given the propellant and the pressure, CEA determines composition of the combustion products, the combustion temperature, the specific heats and their ratio gamma, the density, the pressure, the viscosity, characteristic velocity (c*), Prandtl number etc., of the propellant gas.

The chamber is in contact with the boundary layer of the internal gas, which determines the flow of heat towards the inner wall ($\dot{q}_{conv}$). The convective heat transfer coefficient (h_g) has been estimated using the Bartz method to define the thermal BC to the inner wall of thrust chamber [33].

$$q_{conv} = h_g(T_w - T_{bulk}). \tag{4.4}$$

The convective heat flux q_{conv} has been assigned at several axial stations, since the transfer coefficient varies along the z-axis and q_{conv} is not constant along the inner wall. Some areas of the inner wall of the chamber are in contact with a high-speed gas flow, where the wall temperature is intermediate between the static temperature of the gas and the adiabatic wall temperature [31].

$$T_{aw} = T_c \left(\frac{1 + Pr^{0.33} \left(\frac{\Upsilon - 1}{2} \right) M^2}{1 + \frac{\Upsilon - 1}{2} M^2} \right) \tag{4.5}$$

$$P_r = \frac{V}{a} \tag{4.6}$$

Prandtl number (P_r) is a non-dimensional parameter, defined as the ratio between kinematic viscosity(*V*) and thermal diffusivity (α) , using equation 4.6 the values of the number of Prandtl, of the combustion temperature and of the ratio of the specific heats provided by the CEA code, one obtains T_{aw}at the generic station where the flow has a Mach number equal to M [31]

Convective heat transfer is a different phenomenon with respect to conduction heat transfer because convection is increased by the movement of the fluid along the heated wall. The temperature T_{aw} is also known as bulk temperature (T_{Bulk}), and does not coincide with the wall temperature when the wall is cooled. [32].

The convective heat transfer coefficient (h_g) is determined by semi-empirical relationships: the most famous relation is Bratz equation, derived from the Dittus-Boelter relation for the Nusselt number in straight tubes. According to Bartz semi-empirical equation, the specific heat and the number of Prandtl remain constant with the temperature, the temperature and the pressure of the gas are calculated at a reference temperature to take into account the heat transfer [31].

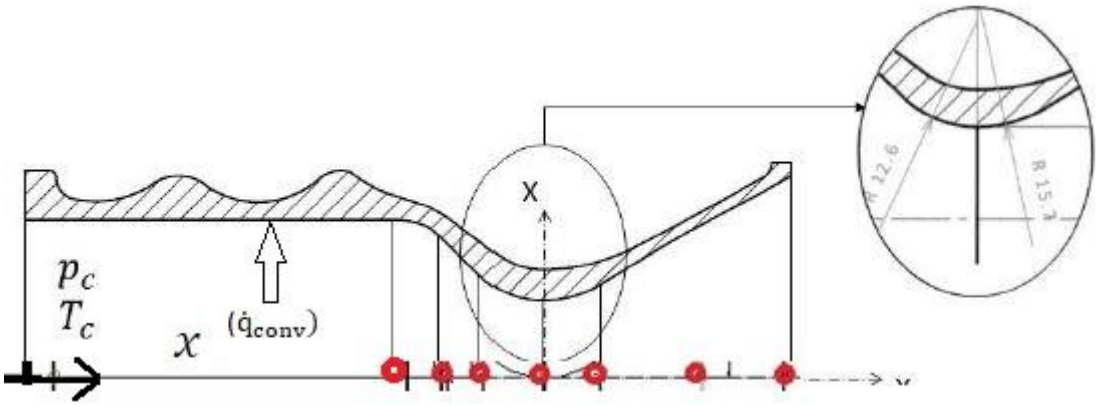

Figure 4.12 Radius of curvature

In Bartz equation the properties of the gas are determined at the film temperature, intermediate between the wall temperature and the temperature of the hot gas. The dimensions of the thrust chamber such as the radius of curvature *R* and the diameter of the grooveD_t (shown in Figure 4.12) average molar mass *M*, the viscosity of the gas mixture in stagnation conditions *μ* and the specific heat c_p are taken in consideration to evaluate the convective heat transfer coefficient h_g, as proposed by Bart'z [31].

$$R = \frac{12.6 + 15.7}{2} \text{ in mm} \qquad \textbf{(4.7)}$$

$$\mu=(1.78 \text{ X } 10^{-7})(M^{0.5})\left(T_c{}^{0.6}\right) \frac{Kg}{ms} \qquad \textbf{(4.8)}$$

$$c^* = \frac{P_c A_t}{\dot{m}}$$

$$h_g = \left[\frac{0.026}{D_t{}^{0.2}}\left(\frac{\mu^{0.2} Cp}{P^{0.6}}\right)\left(\frac{Pc}{c^*}\right)^{0.8}\left(\frac{D_t}{R}\right)^{0.1}\right]\left(\frac{A_t}{A}\right)^{0.9} \qquad \textbf{(4.9)}$$

The static temperature and pressure T_c and P_c of the gas flow are determined as functions of the local Mach number from the stagnation values with the formulas [34],

$$T_g = \frac{T}{T_c} = \left(1 + \frac{(\Upsilon - 1)}{2} M^2\right)^{-1} \quad \textbf{(4.10)}$$

$$p_g = \frac{p}{p_c} = \left(1 + \frac{(\Upsilon-1)}{2} M^2\right)^{\frac{-\Upsilon}{\Upsilon-1}} \quad \textbf{(4.11)}$$

The values so obtained are used for the evaluation of the thermal BCs for the inner wall of the thrust chamber and are listed in Table 4.4.

Station no.	X [mm]	A_t/A [-]	Mach number	T_g [K]	p_g [MPa]	T_{aw} [K]	H [W/m²K]
1	52.74	0.262106	0.158363	2924.32	0.6457	2929.27	416.89
2	57.81	0.291135018	0.176473	2923.07	0.643474	2929.21	458
3	64.12	0.511537575	0.322326	2908.15	0.617426	2928.52	760.99
4	73.09	1.000000383	1.000	2736.07	0.377363	2920.53	1391.21
5	81.59	0.681181972	1.725702	2419.99	0.14008	2905.87	984.75
6	96.66	0.252516668	2.5265	2018.55	0.0323944	2887.24	403.13
7	109.12	0.149870315	2.8666	1852.97	0.0162358	2879.55	252.07

Table 4.4 Boundary conditions for 2D thrust chamber.

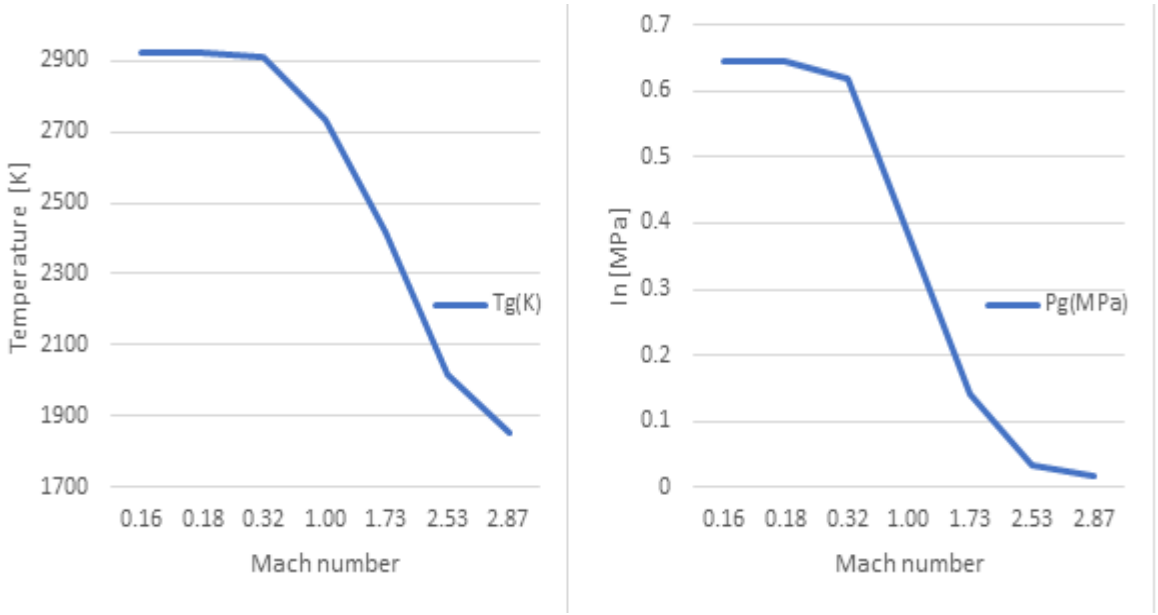

Figure 4.13 Temperature and pressure profile in the 2D thrust chamber as functions of the local Mach number.

4.2.7 Radiation heat transfer

Radiation contributes to the transfer of heat to the walls of the combustion chamber, playing a vital role in our analysis. Assuming optically diffusing internal walls of the combustion chamber to be diffuse with uniform emissivity and optically opaque the

gas in the chamber, the radiative heat transfer to the wall is expressed by Equation 4.12 [33].

$$\dot{q}_{rad} = A\varepsilon\sigma\left({T_w}^4 - T^4\right) \quad \textbf{(4.12)}$$

where *A* is the area of the wall surface, σ is a Stefan-Boltzmann constant $(5.67\ \mathrm{X}\ 10^{-8}\mathrm{W.m^2/k^{-4}})$, ε is the emissivity of the inner wall, surface T_w is wall temperature and *T* is emitting temperature [33].

In LPRE, the gas temperature ranges from 1900 to 3500 K. In these operating conditions the radiation can assume an important role by transferring, depending on the composition of the propellant, from 3 to 40% of the heat that reaches the inner wall [35].

Gases with symmetric molecules such as oxygen, nitrogen and hydrogen have relatively weak spectral bands. These molecules do not absorb or emit a lot of radiant heat. Heteropolar gases such as water vapor, carbon monoxide, carbon dioxide, hydrocarbons, hydrochloric acid, ammonia and alcohols, are characterized by intense emission bands in the infrared spectrum and thus effectively emit radiant heat.

The internal emissivity of the wall is determined by properties as:

- ε_{wi} = Emissivity of inner wall = 0.45
- ε_{we} = Emissivity of external wall surface=0.64
- $\varepsilon_{we} = \varepsilon_{w-g}$ = Emissivity of gas molecules

Figure 4.14 makes it possible to determine the lateral surface of the chamber volume between the injection plate and the nozzle groove.

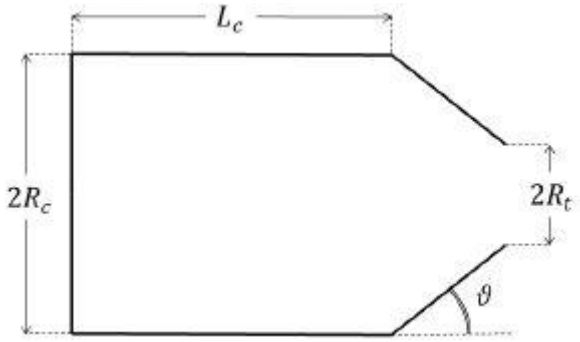

Figure 4.14 Typical thrust chamber.

$$V_{cc} = \pi {R_c}^2 L_C + \frac{\pi}{3}\frac{\left({R_c}^3 - {R_t}^2\right)}{tan\vartheta} \quad \textbf{(4.13)}$$

$$A_{cc} = 2\pi R_c L_c + \frac{\pi\left({R_c}^2 - {R_t}^2\right)}{sin\vartheta} \quad \textbf{(4.14)}$$

where R_c is the radius of the combustion chamber, L_c is the length of cylindrical portion of the combustion chamber, R_t is the throat radius, ϑ is the angle of convergence.

From this surface and the chamber volume it is possible to compute equivalent beam length.

$$L_{w-g} = 3.66\frac{V_{cc}}{A_{cc}} = 3.492cm$$

The emissivity of the gas mixture depends on the composition, pressure and temperature of the combustion products, as well as the equivalent beam length of radiation from the gas to the chamber wall:

$$\varepsilon_{w-g} \approx \varepsilon_{H_2O} \approx f(T_g, P_{H_2O}, L_{w-g}) \quad \textbf{(4.15)}$$

For the chosen liquid propellant N_2H_4 and N_2O_4 with O/F ratio equal to 2, the composition of the component species (i) and mole fractions of the hot gas have been calculated using online tool CEA.

Species (x_i)	Mole fraction	Species (x_i)	Mole fraction
H_2O	0.44079	H_2	0.01476
N_2	0.39725	O	0.00678
O_2	0.08141	H	0.00444
OH	0.03915	HO_2	0.00004
NO	0.01535	NO_2	0.00001

Table 4.5 Precipitation species with mole fraction Data.

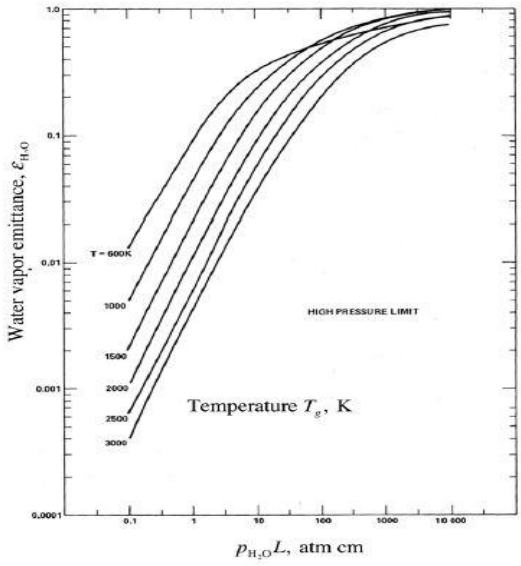

Figure 4.15 Emissivity of water vapor as a function of its partial pressure, the equivalent beam length and the temperature.

With this information the equivalent emittance of inner wall can be calculated using the formula [33]:

$$\varepsilon_{wi}{}^{eq} = \frac{1}{\left(\frac{1}{\varepsilon_{wi}} + \frac{1}{\varepsilon_{w-g}} - 1\right)} \quad \textbf{(4.16)}$$

By substituting the emissivity of inner wall and the hot gas in the equation above equation aids to obtain the total emittance of each axial station of the camber.

St.no	X [mm]	$P_{H_2o}L$	ε_{w-g}	T_g[K]	$p_g[MPa]$	$\boldsymbol{\varepsilon_{wi}}^{\boldsymbol{eq}}$
1	52.74	9.83	0.035	2924.32	0.6457	0.034
2	57.81	9.74	0.034	2923.07	0.6434	0.033
3	64.12	9.25	0.01	2908.15	0.6174	0.030
4	73.09	5.73	0.026	2736.07	0.3773	0.025
5	81.59	2.15	0.012	2419.99	0.1400	0.012
6	96.66	0.55	0.005	2018.55	0.0323	0.005
7	109.12	0.24	0.003	1852.97	0.0162	0.003

Table 4.6 Radiation heat transfer boundary conditions.

From the results obtained at the different stations (see Table 4.6) one can observe that the equivalent emittance of the inner wall varies along the axial direction and that it depends on the temperature of the gas flow. In addition, the emittance of the gas and the equivalent emittance of the inner wall are almost similar (they vary by 10% or less). The values of convection and radiation heat transfer in Table 4.4 and Table 4.6 have been assigned as BCs for the 2D thermal model of the thrust chamber. The initial temperature has been taken equal to 273.15 K.

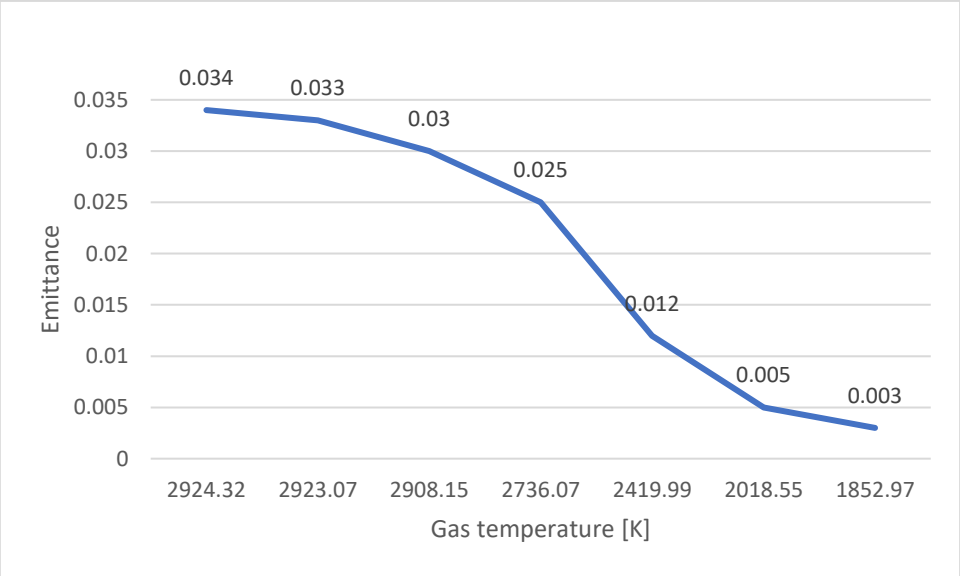

Figure 4.16 Emittance vs gas temperature as a function of the axial position.

The values of the heat exchange coefficient (h_g) of the mass temperature and of the film coefficient (T_{aw}) have been assigned for each axial station of the chamber as input for the calculation of the convective heat transfer on the inner wall. The emissivity of the external wall of the chamber has been obtained from the experimental ratio of the R-4D engine, which gave a value equal to 0.64 [36].

The outer temperature is set to zero before analysis is performed. Equivalent inner wall emittance value has been given in the radiation option corresponding to the given flow temperature, and it should match along with all the stations.

Since these are non-stationary thermal analyses, heat transfer by convection and by

radiation are time functions. The simulation has been performed for a total duration of 300 s. The integration time step has been chosen equal to 0.025 s. Steady-state thermal equilibrium has been reached after 60 s from ignition.

4.2.8 Results

The temperature distribution along the axial direction as a function of time is shown Figure 4.17 and Figure 4.18 and it achieves steady state condition at 60 s.

Figure 4.17, shows how temperature changes due to convective and radiative heat transfer. It can be seen that it reaches steady-state equilibrium after 60 s from ignition and remains constant at 2058 K. The simulation indicates that after 60 s all nodes (axial stations) have reached steady state conditions. The maximum temperature reaches 2058 K at the throat region or immediately before, where the convective transfer is more intense due to the combined action of the velocity and density of the propellant flow.

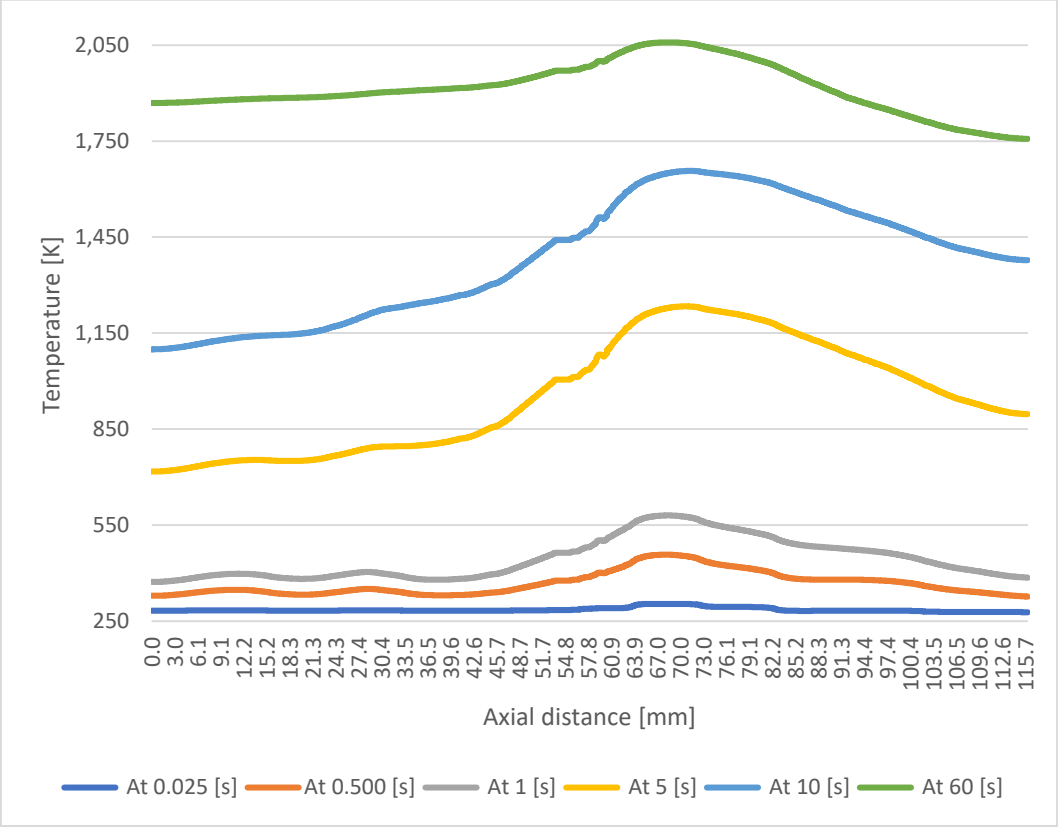

Figure 4.17 Temperature profile of 2D thrust chamber as a function of the axial position.

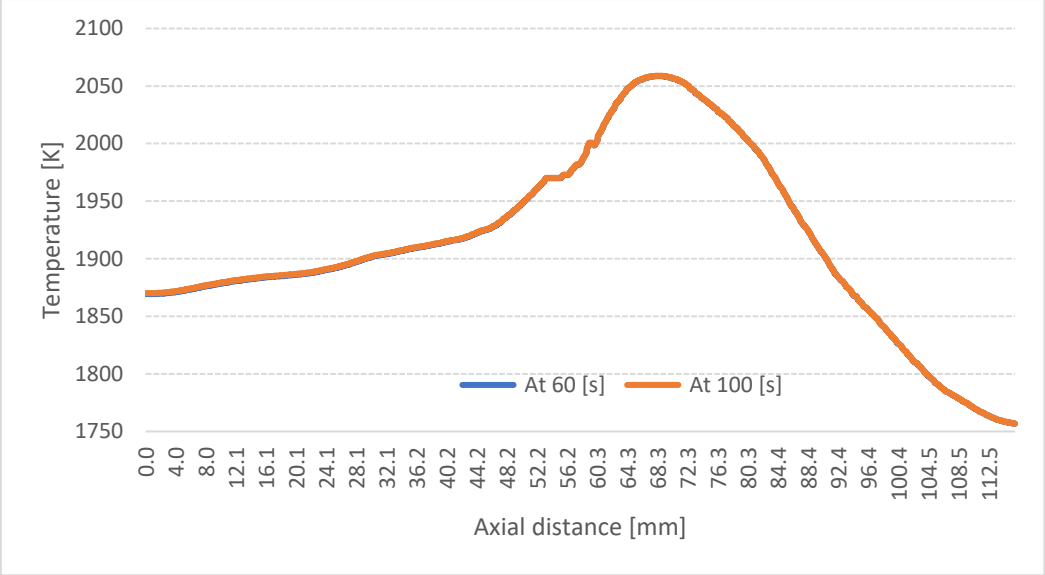

Figure 4.18 Steady-state temperature profile of the 2D thrust chamber as a function of the axial direction.

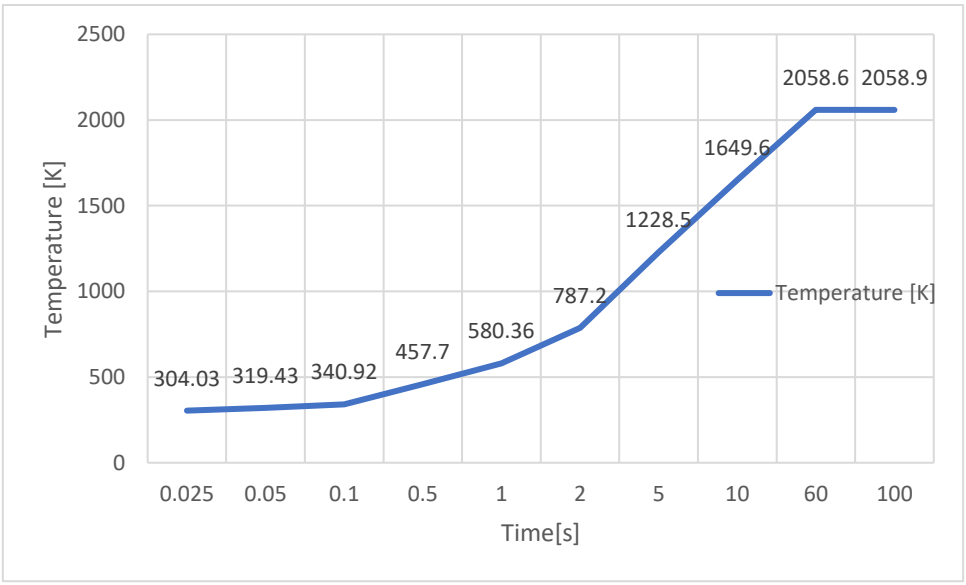

Figure 4.19 Temperature as a function of time after engine ignition in the 2D thrust chamber.

Two axial stations (Point 1 and 2) have been chosen, at the locations shown in Figure 4.7 to calculate the temperature profile in the radial direction, which is plotted in Figure 4.20 and Figure 4.21. The temperature in Point 1 and Point 2 as functions of time are plotted in Figure 4.22. The temperature decreases by more than 10 K from the inner wall to the external wall. At 5 and 10 s after ignition, the temperature drop in the chamber wall varies from 20 to 30 K and generates by conduction the heat that is irradiated in the outer space by the external surface of the chamber.

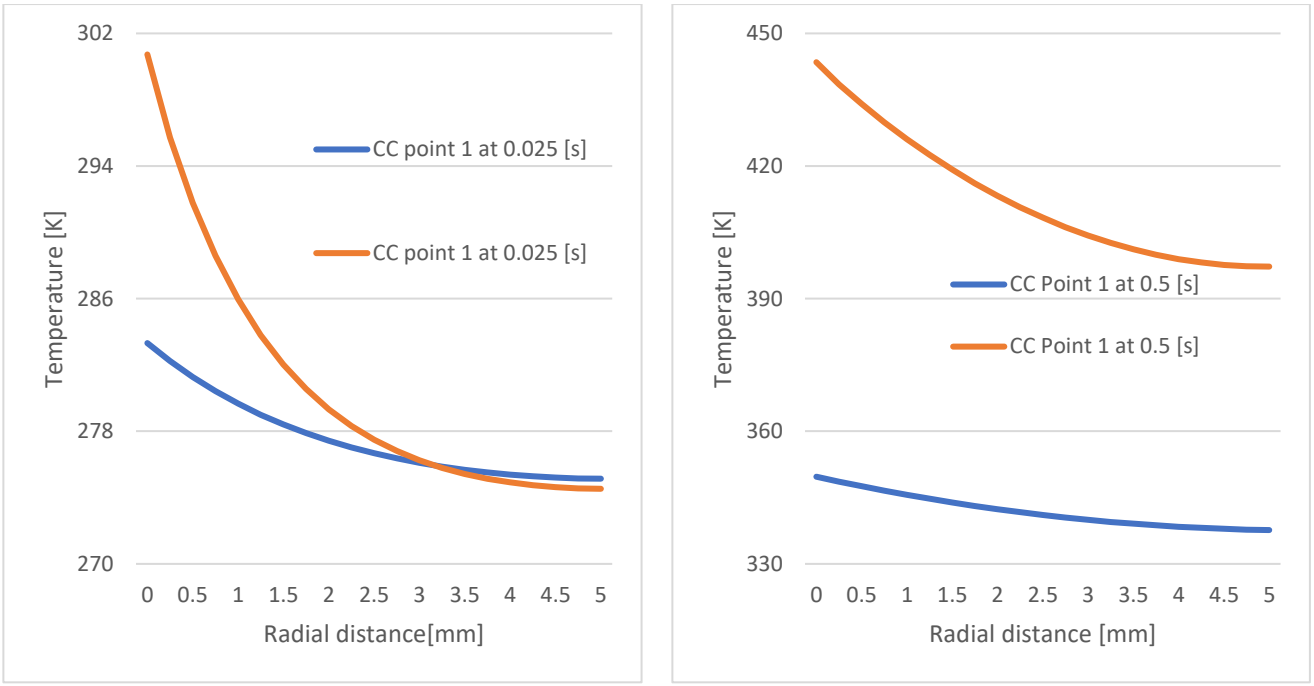

Figure 4.20 Temperature profile in the radial direction at 0.025 s (left) and 0.50 s (right) from engine ignition.

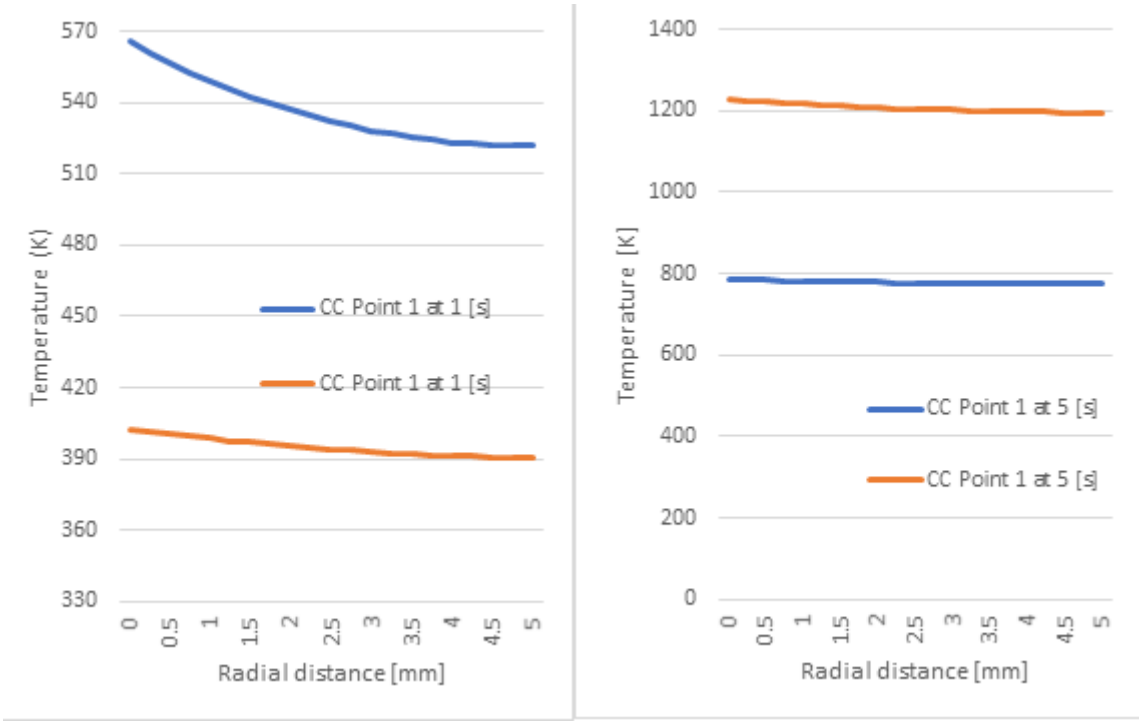

Figure 4.21 Temperature profile in the radial direction at 1s (left) and 5 s (right) after ignition.

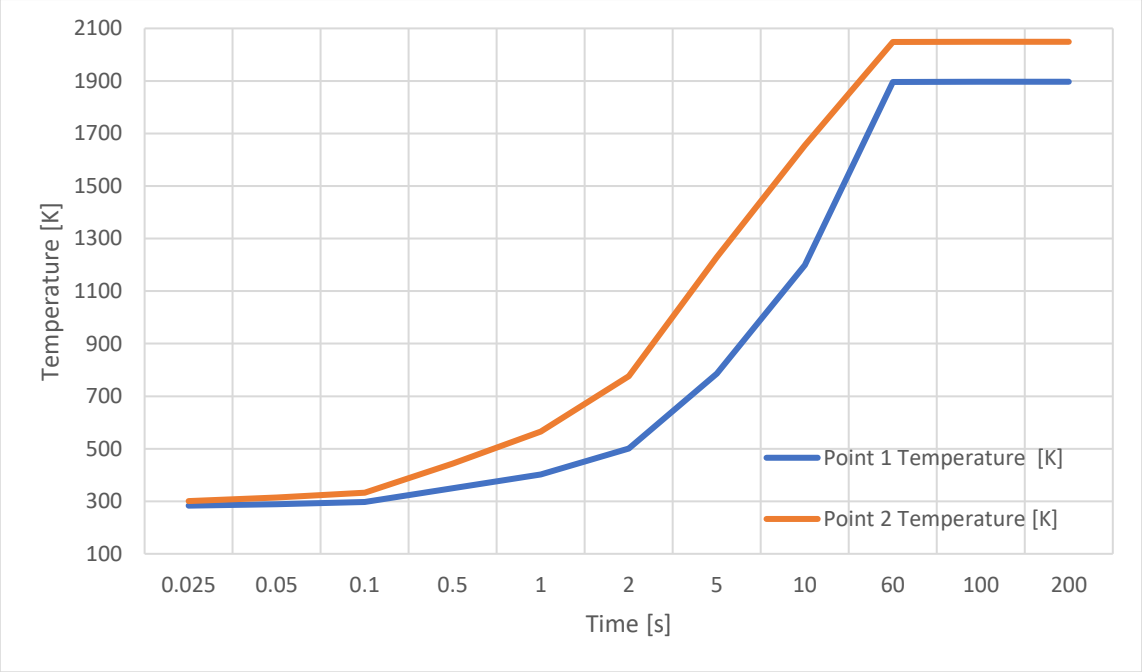

Figure 4.22 Temperature distribution of 2D thrust chamber as a function of time after engine ignition.

4.3 Unsteady thermo-structural analysis of thrust chamber

The thermal stresses in the chamber wall can cause damages, deformations or fractures and are determined by the temperature gradients. Therefore, they depend on the results of the thermal analysis, which help to improve the design of the rocket engine.

The only change in the structural simulation has been the replacement of the Plane 77 element (which is used specifically for thermal analysis) with the Solid Node element 183. The BCs for the combustion chamber have been assigned by fixing the lower, DoF UY = 0. The thermal field at the requested time has been saved in the ".rth" file and then imported to perform the thermo-structural simulation. The non-uniform gas pressure acts on the inner wall of the chamber as indicated by the data shown in Table 4.3. The various axial stations of the chamber are therefore subject to thermal and pressure loading. The LS file has been selected to record the results of the analysis. Finally, the data have been transferred to Microsoft Excel and plotted along the axial and radial directions of the combustion chamber.

4.3.1 Results along the axial direction

The stresses calculated as a consequence of the thermal loads on 2D thrust chamber are shown in Figure 4.23 to Figure 4.28.The hot gas increases the temperature of the inner wall of the combustion chamber. To ensure the proper operation of the engine the heat flux must be transferred to the external surface by conduction and radiation without creating any structural damage.

The thermal BCs cause the internal wall temperature to reach the maximum value of 2058 K near the nozzle throat. The maximum stress in the axial direction near the divergent nozzle section is 38 MPa. This stress occurs at the throat after 5 s from engine ignition. With a static temperature of the gas equal to 1228.5 K. Figure 4-23 indicates that the maximum axial tension occurs in the throat area or in the converging section immediately before the nozzle throat.

The radial stress generated by the static gas temperature of 1228 K is equal to 3.67 MPa (see Figure 4.25), relatively small with respect to stress in the azimuthal direction.

The Von Mises stress in the chamber wall is shown in Figure 4.28, the in order to evaluate the resistance of the chamber by comparison with the yield stress of molybdenum. The static temperature of the gas of 1228 K determines a Von Mises stress equal to 156.8 MPa near the throat of the convergent at 5 s from engine ignition. In this position the structure runs the risk of yielding since the Von Mises stress is higher than the yield stress of molybdenum (110 MPa). The best way to overcome this problem is to reduce the temperature of the gas in contact with the chamber wall by using an additional cooling method such as fluid-film cooling.

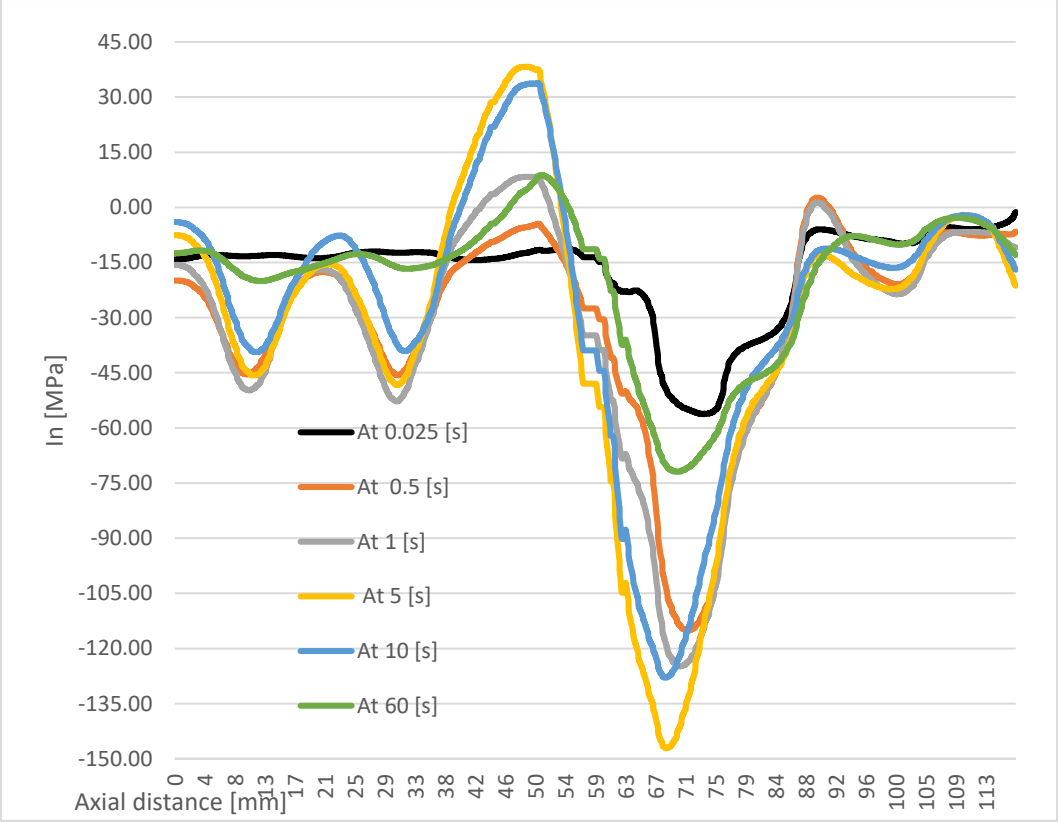

Figure 4.23 Azimuthal stress of 2D thrust chamber acting in the axial direction

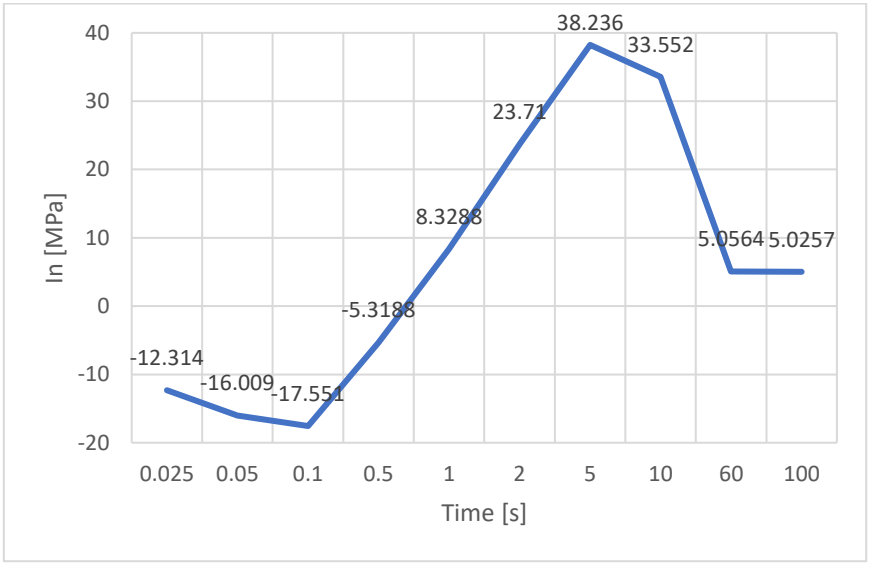

Figure 4.24 Azimuthal stress as a function of the axial position.

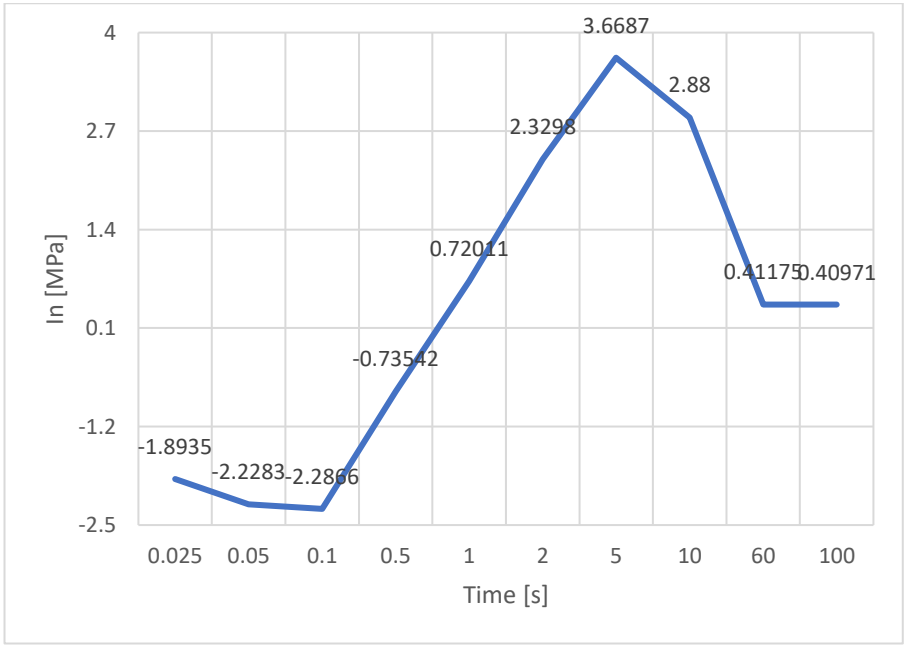

Figure 4.25 Radial stress as a function of time after engine ignition in the axial position.

Figure 4.26 Radial stress of the 2D thrust chamber in the axial direction

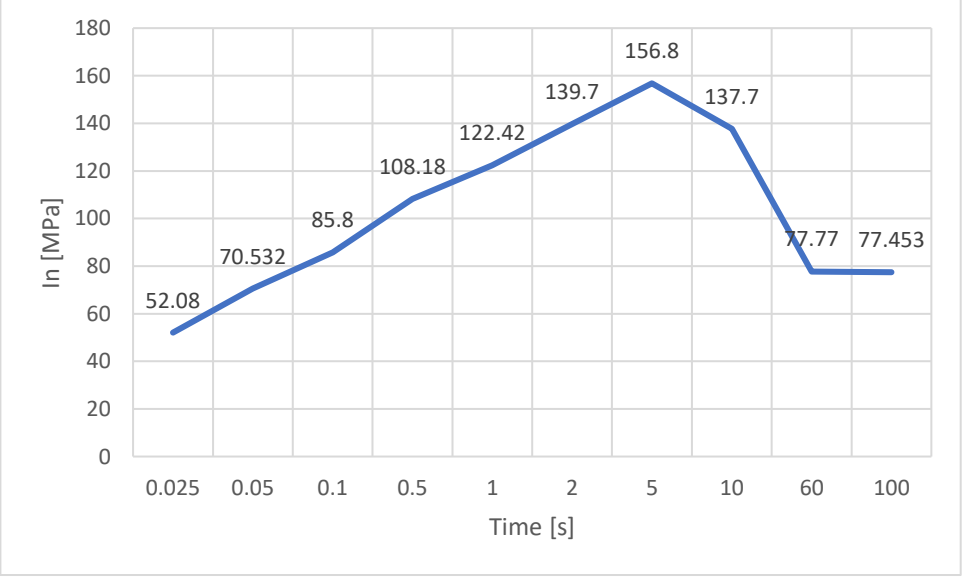

Figure 4.27 Von-mises stress as a function of time after engine ignition.

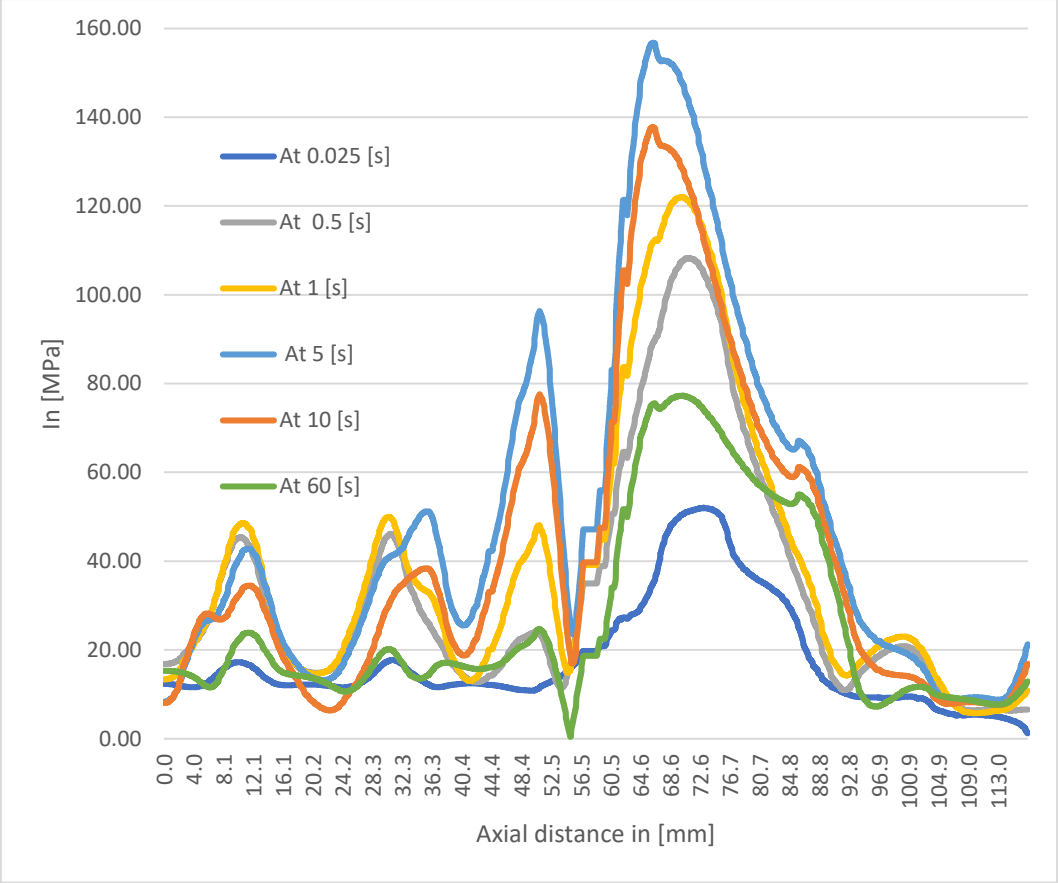

Figure 4.28 Von Mises stress as a function of the axial position along the thrust chamber.

4.3.2 Results along the radial direction

The stress profile in the radial direction of 2D thrust chamber is shown in Figure 4.29 to Figure 4.40.

- The reduced area of the throat determines a higher heat flux.
- The maximum temperature is observed at nozzle throat, where cooling must be improved to ensure the structural integrity of the structure.
- A higher heat flux is obtained at the throat due to the combined effect of the velocity and density of the gas flow.
- The gas in the boundary layer is colder than the gas outside the boundary layer and therefore is denser.

The results for the radial stress are reported. Point 1 and point 2 show the minimum radial stress in the combustion chamber. The stress values of point 1 and point 2 differ in the radial direction. The radial stress observed at point 2 is 3.76 MPa after 5 s from engine ignition, with a static gas temperature of 1228.5 K. The azimuthal stress in the chamber wall thickness is 48 MPa near the nozzle throat with a static gas temperature of 1228 K after 5 s from engine ignition.

The stress of Von Mises is indicative of the yield risk of the structure. The maximum stress of Von Mises observed at point 2 is equal to 105 MPa, which is slightly lower than the yield stress of molybdenum (110 MPa). It can be concluded that the stresses caused by the thermal and mechanical BCs should not cause structural damage to the combustion chamber since all the values are within the yield limit.

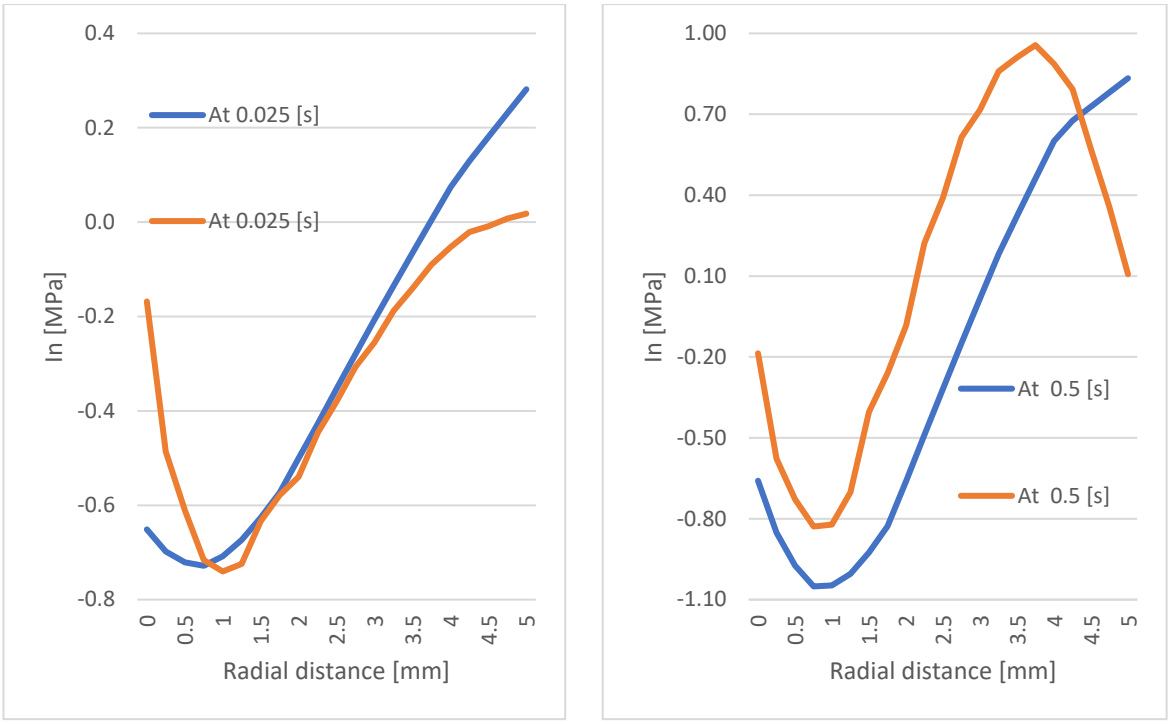

Figure 4.29 Radial stress at 0.025 s (left) and 0.5 s (right) in radial direction at selected points in the axial direction.

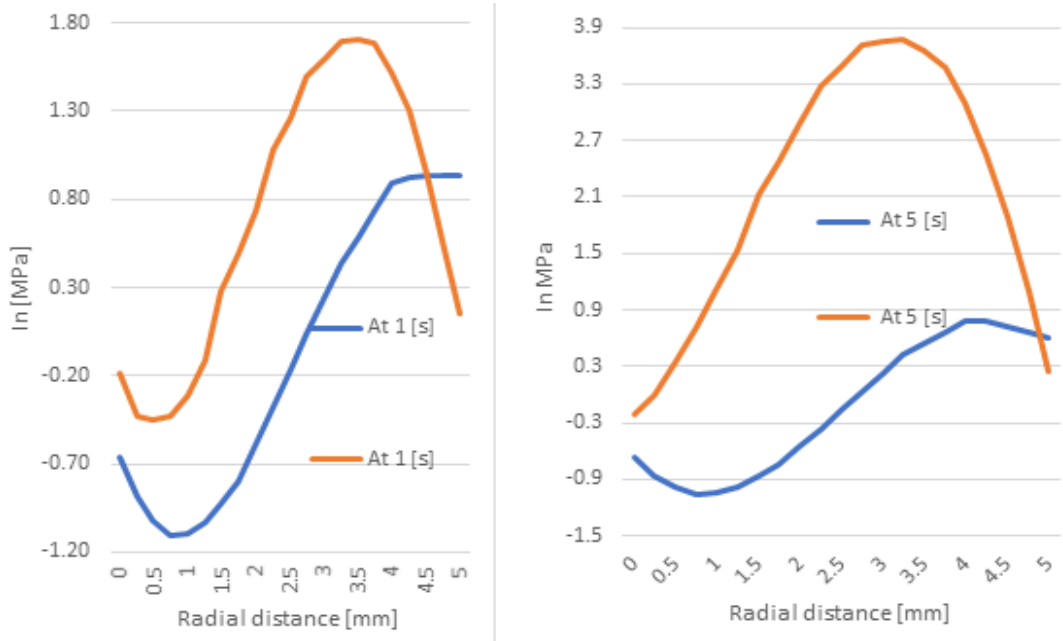

Figure 4.30 Radial stress as a function of the axial position at 1 s (left) and 5 s (right) after engine ignition.

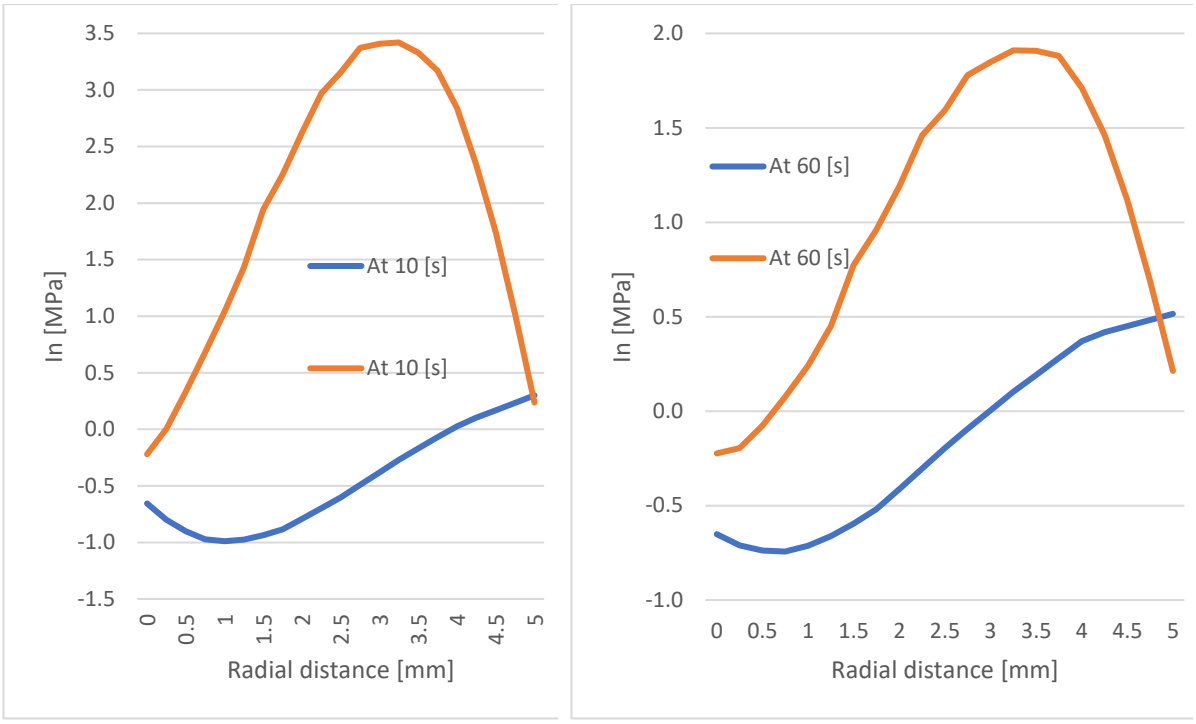

Figure 4.31 Radial stress as a function of the axial position at 10 s (left) and 60 s (right) along in after engine ignition.

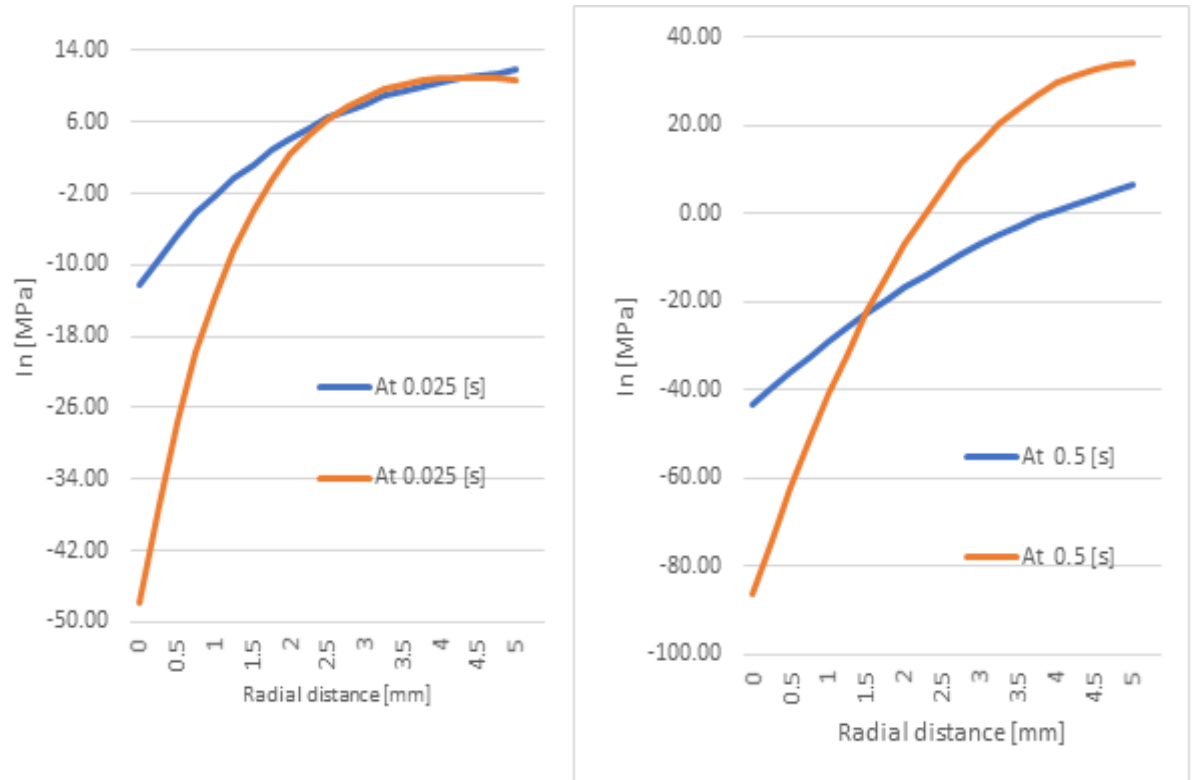

Figure 4.32 Azimuthal stress as a function of the axial position at 0.025 s (left) and 0.5 s (right) from engine ignition.

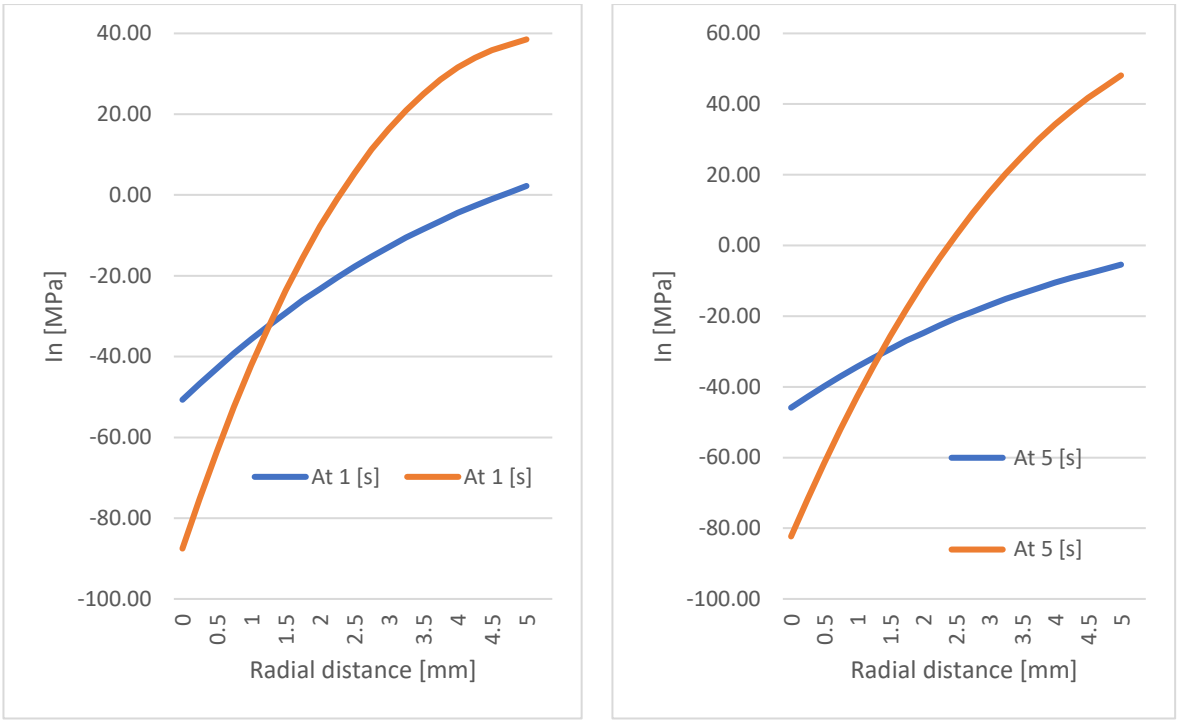

Figure 4.33 Azimuthal stress as a function of the radial position at 1 s (left) and 5 s (right) after engine ignition.

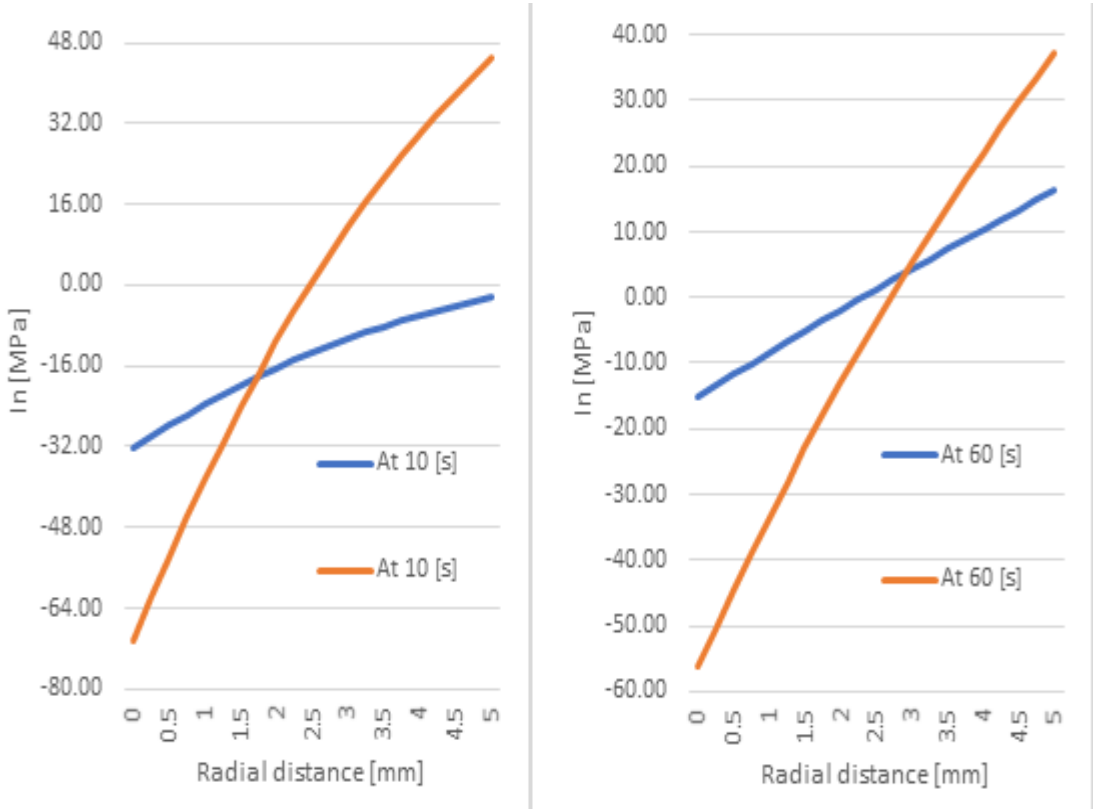

Figure 4.34 Azimuthal stress as a function of the radial position at 10 s and 60 s in from engine ignition.

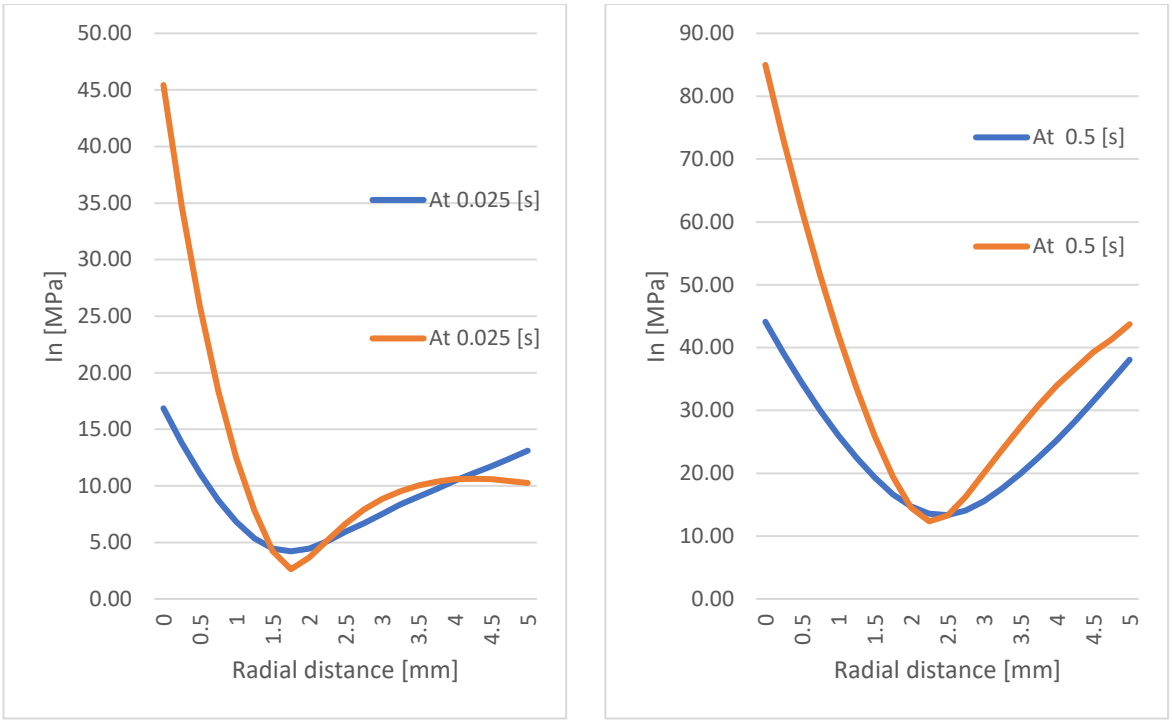

Figure 4.35 Von Mises stress as a function of the radial position 0.025 s (left) and 0.5 s (right) in after engine ignition.

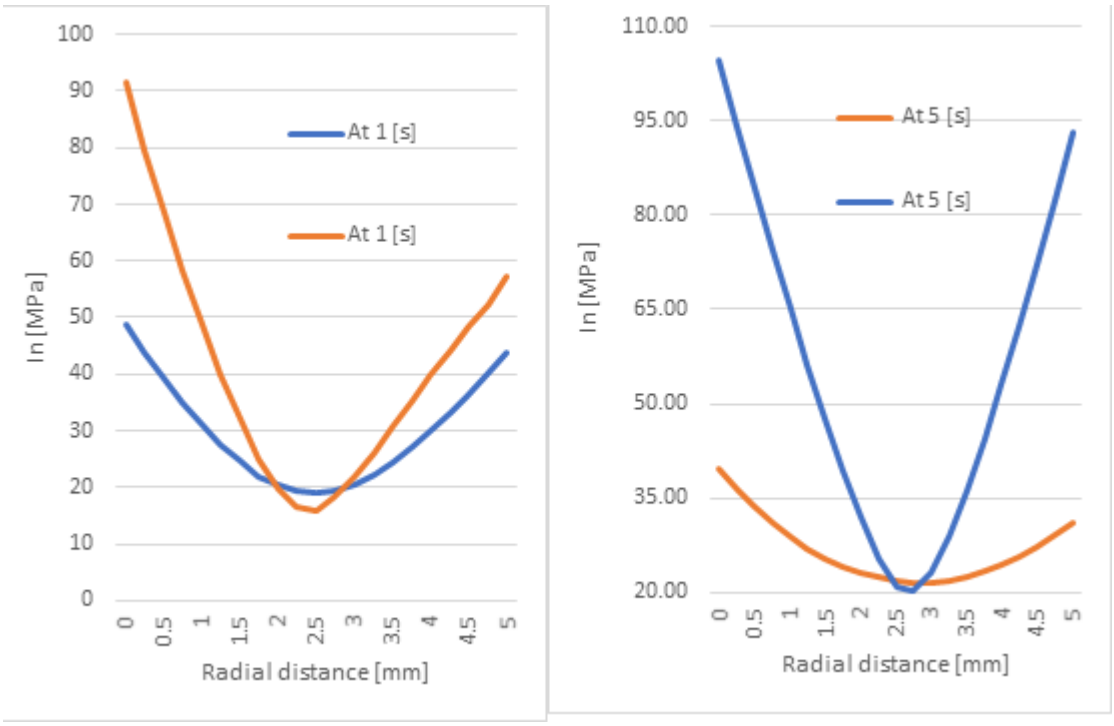

Figure 4.36 Von Mises stress as a function of the radial position at 1 s (left) and 5 s (right) after engine ignition.

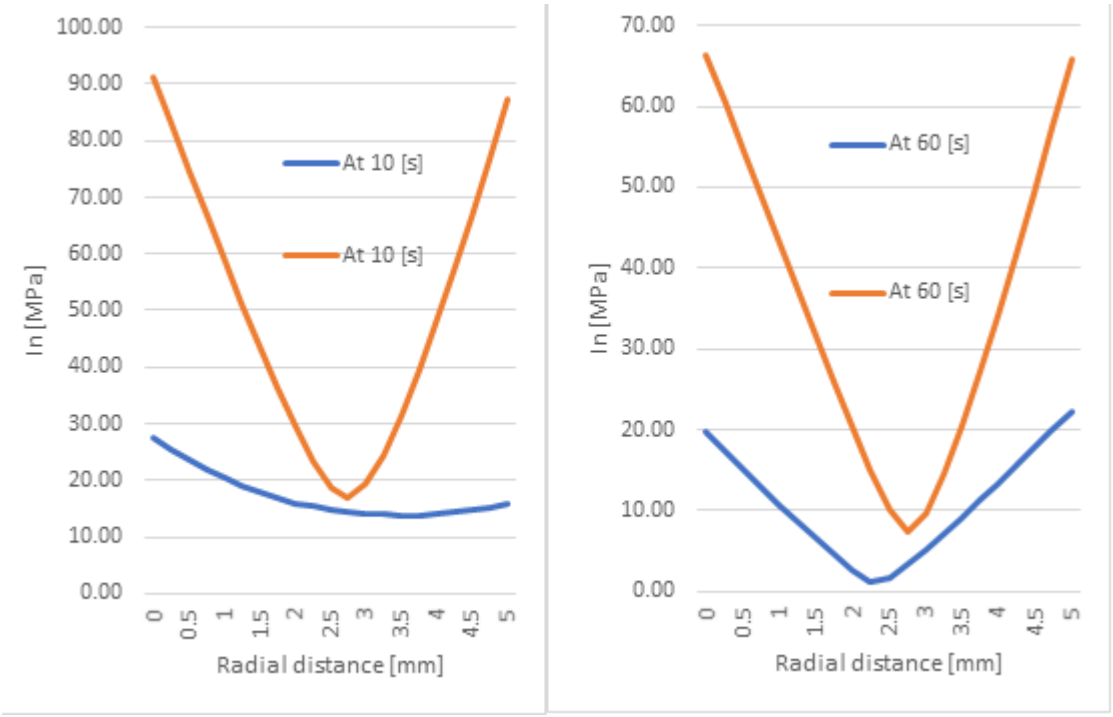

Figure 4.37 Von Mises stress as a function of the radial position at 10 s (left) and 60 s (right) after engine ignition.

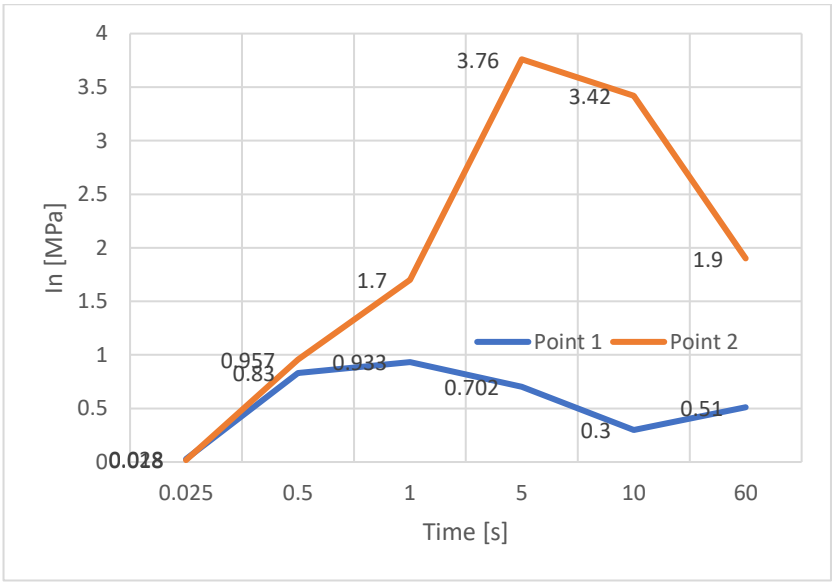

Figure 4.38 Radial stresses as functions of time after engine ignition.

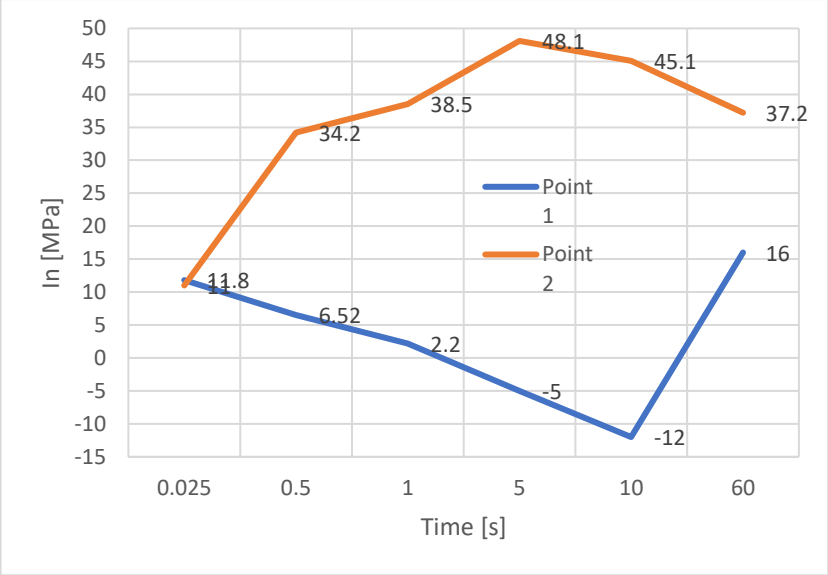

Figure 4.39 Azimuthal stresses as functions of time after engine ignition.

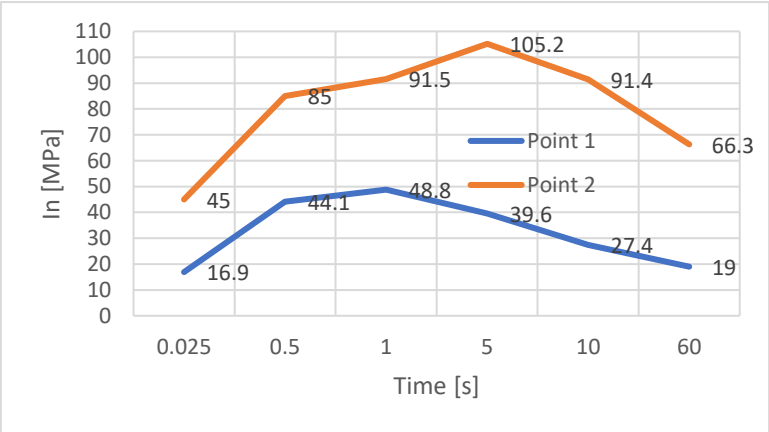

Figure 4.40 Von-Mises stress in a radial direction as function of time after engine ignition.

5 Nozzle extension analysis

5.1 Nozzle background

Many scientists and researchers are working to improve the performance of liquid propellant rocket engines [37].

In LPREs, the fuel and oxidizer are injected, atomized and ignited in the thrust chamber. After combustion, the liquid propellants are transformed into high pressure and high temperature combustion products. The engine nozzle starts from the converging section of the combustion chamber, just after the end of the cylindrical part. In this part of the nozzle the gas is expanded and sub sonically accelerated until the flow reaches the nozzle throat [38] where the Mach number is 1 (critical conditions). In the divergent part of the nozzle the propellant increases its speed under supersonic conditions up to the exhaust cross-section. The main function of the nozzle is to convert most of the energy of the high pressure and high temperature combustion products into kinetic energy and then create the maximum possible thrust [37][38].

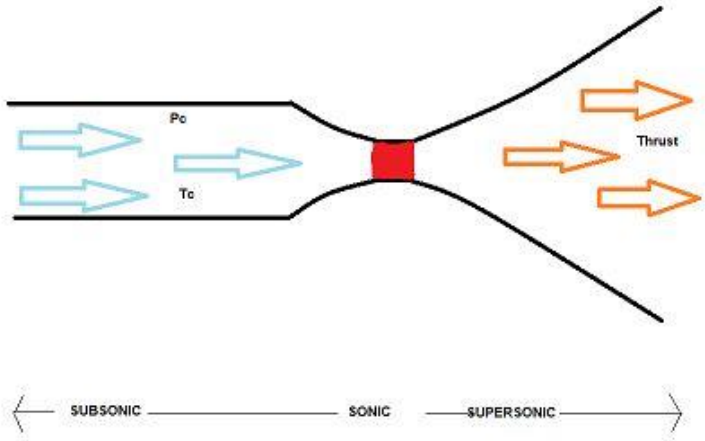

Figure 5.1 Typical rocket engine.

Nozzle operation is affected by many parameters such as viscous losses on the inner wall, flow separation and atmospheric pressure. The latter is a decreasing function of the altitude. Under atmospheric operation, a nozzle develops its maximum thrust when the exhaust gas is expanded to the same pressure of the ambient [39][38].

Rocket nozzles are traditionally designed with a continuous profile between the throat and the exhaust and, when working inside the atmosphere, expand the exhaust gas up to an intermediate pressure between the one at ground level and the one corresponding to the maximum altitude reached by the engine before shut-off. In this case, the nozzle is over-expanded at sea level or at low altitudes, because the exhaust gas pressure is smaller than the environmental pressure, and under-expanded at higher altitudes because the discharge pressure is higher than the ambient pressure [38].

In an excessively over-expanded nozzle the flow separates irregularly from the inner wall of the nozzle and can result in dangerous lateral loads due to the misalignment of the thrust from the axis of the engine. These loads are determined by the formation of

a recirculation zone, which often has an unsteady unstable behavior and variously interacts with the supersonic flow outside the recirculation zone generating shock waves [38].

The phenomena associated with flow separation lead to unsteady changes in the pressure distribution on the terminal part of the inner wall of the nozzle, causing lateral fatigue forces that can cause structural failure. Flow separation in the nozzle is therefore an important aspect to consider when designing engines that operate inside the atmosphere. If, on the other hand, the nozzle is operated in a vacuum, the expansion takes place in a regular manner without separation. The gas leaves the nozzle outlet with a residual pressure with respect to the environment, which cannot be converted into thrust [38]. In order to optimize the efficiency of the expansion, nozzle extensions consisting of two different profiles have been studied, the former starting at the nozzle throat and the latter ending at the nozzle exhaust. The two profiles are connected at a corner point. In operation at higher atmospheric pressure the flow follows the first profile and separates in a stable and axially symmetric manner at the point of connection with the second profile, where the flow is completely separated. At higher altitudes, when the external pressure decreases, the flow reattaches on the second profile, which expands it further up to the discharge conditions. The flow configuration in the nozzle is always stable and axially symmetrical, as required to avoid thrust misalignments and unsteady lateral forces, except during the short transition from one flow configuration to another [38].

The shape and dimensions of the nozzle extension are suitably designed to optimize the thrust performance over the desired range of altitudes.

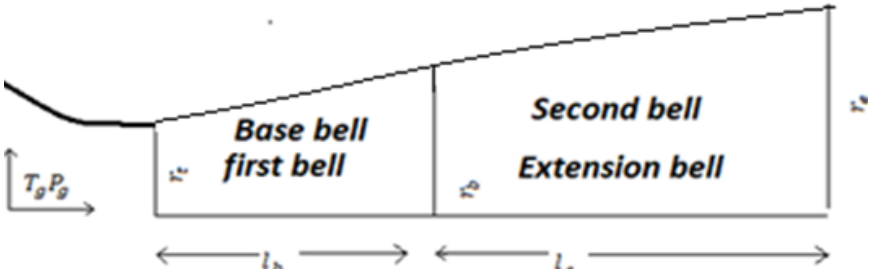

Figure 5.2 Design of nozzle extension.

For the purpose of this study, different geometries have been taken into consideration before adopting the single-bell nozzle of the R-4D engine, which worked successfully and with high efficiency in a number of space missions. The nozzle extension, made with a thin wall in cobalt alloy L-605 R-4D, has been designed to reduce weight and withstand the internal gas pressure, the thermal loads and the vibrations occurring during operation. The external ribs are sized to guarantee the stiffness of the component. The most critical point of the nozzle is its joint with the extension [37]. which is mounted to the combustion chamber using clamping nuts made of waspaloy. Therefore the loads acting on the nozzle extension are directly transferred to the clamping nuts, which can withstand significant thermal and vibration loads acting during the operation of the engine [37].

The extension of the nozzle is provided with 8 circumferential ribs 2.7 mm wide. These ribs have variable thicknesses to provide a rigid and light-weight structure [37].

5.2 A steady state analysis of nozzle extension

5.2.1 Methodology

The Finite Element Analysis (FEA) of the nozzle extension under steady state conditions has been conducted for the model designed in 2D with the aim of understanding how the components react when subjected to the imposed thermal and mechanical loads. The radial, azimuthal and Von-Mises stresses have been calculated for the purpose of verifying the feasibility and structural efficiency of the nozzle extension.

The model has been developed in Solid Works in accordance with all applicable requirements. The model dimensions have been assigned by defining the key points in the ANSYS APDL 16.0 software. The 2D model is then discretized in finite elements and the structural analysis has been carried out at steady state conditions. It was an extremely demanding simulation as the model includes many ribs and small parts. The FEA has been developed in order to understand the physical behavior of the nozzle extension, to know its performance, behavior and safety margins, and to verify where maximum stress is acting.

The element selected to develop the FEA is the axisymmetric Solid 8node 183. During the selection of the material for the nozzle extension, several potentially suitable materials have been taken into consideration, such as Rene41, Al 6061 T6, platinum alloys, etc. The material chosen is the L-605 cobalt alloy because it has been used successfully in many R-4D engines. It is an excellent material capability of withstanding the high thermal, pressure and vibrating loads that act on the internal wall of the nozzle extension. The mechanical properties (density, Poisson's modulus, Young's modulus and coefficient of thermal expansion) of the cobalt alloy L-605 at 25 °C have been provided as input data of the structural simulation (see Table 5.1).

Sl.no	Mechanical Properties	Values
1	Density [kg/m^3]	9.27
2	Poisons ratio [-]	0.29
3	Young’s modulus [GPa]	220
4	Thermal Co-efficient [1/K]	$1.30x10^{-5}$

Table 5.1 Mechanical properties of L-605 Cobalt alloy.

5.2.2 Modelling and meshing

The structural simulation of the nozzle extension using the ANSYS APDL 16.0 software is a demanding enterprise. The main problems are related to the geometric definition of the model.

The known key points of Solid Works have been provided as input to the ANSYS software, the model has been created along the X axis of the nozzle and the calculation grid has been created. To accurately model the bell shape of the nozzle it has been necessary to use cylindrical coordinates. Then the model in cylindrical coordinates has been transformed into Cartesian coordinates to improve the accuracy of the simulation. The nozzle profile has been represented by a succession of splines. The computational grid has been made with an edge length of the element equal to 1 and a fine mesh for the component. In this way the model has been divided into 7795 elements defined by 26930 nodes. The mesh is barely visible in Figure 5.3 because the component is made up of large number of elements and nodes.

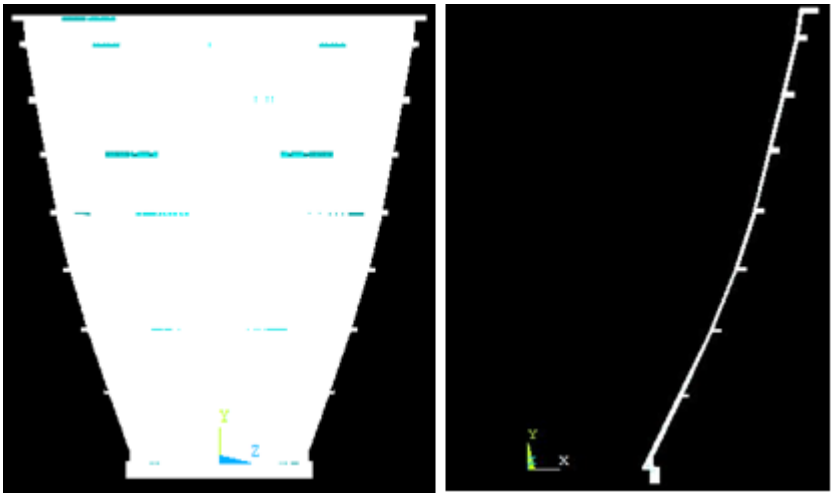

Figure 5.3 Expanded nozzle extension (right) Meshed 2D (left)

5.2.3 Boundary conditions

The flow of gas generated in the combustion chamber undergoes significant changes during the expansion in the nozzle. Therefore, six axial stations have been selected in the subsonic flow region inside the nozzle extension. The stations are equally spaced 23.3 mm apart in the axial direction for a total length of 139 mm. Figure 5.4 shows the stations used to model the nozzle extension, marked with red dots along the axial direction.

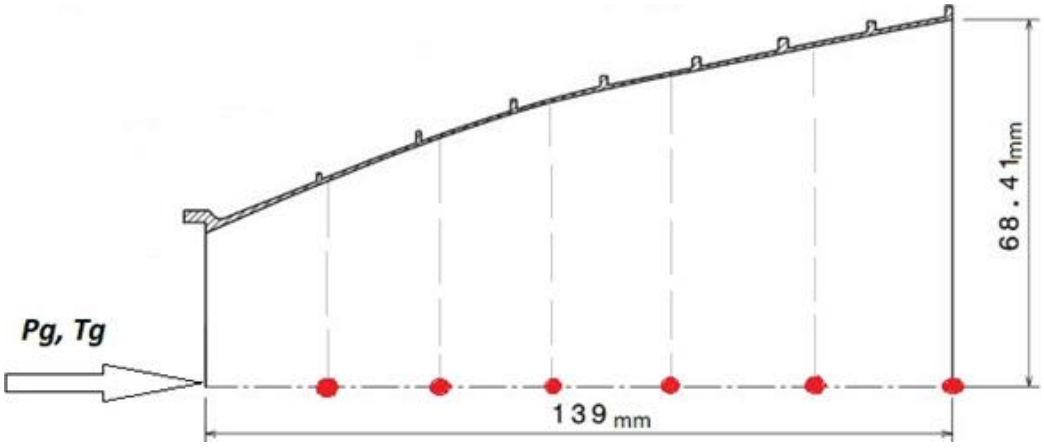

Figure 5.4 Different stations along an axial direction selected on 2D nozzle extension

The varying gas pressure and temperature acting on nozzle extension have been calculated using the isentropic gas equation (4.2). The Mach number at all stations has been computed from the area ratio using equation (4.1). The values of the Mach number and pressure so obtained are plotted in Figure 5.5 and Table 5.2.

Station number	X(mm)	$\frac{A_t}{A}$	P_g [MPa]	Mach number
1	23.27	0.08182	0.00748	3.235
2	46.33	0.05400	0.00444	3.479
3	69.43	0.04067	0.00313	3.643
4	92.53	0.03404	0.00251	3.745
5	115.63	0.02932	0.00209	3.83
6	139	0.02590	0.00179	3.90

Table 5.2 BC for steady state nozzle extension analysis

The non-uniform pressure acting on the inner wall has been assigned as BC by fixing the downstream line which is DoF (UY=0). The simulation has been carried out by selecting the current LS file.

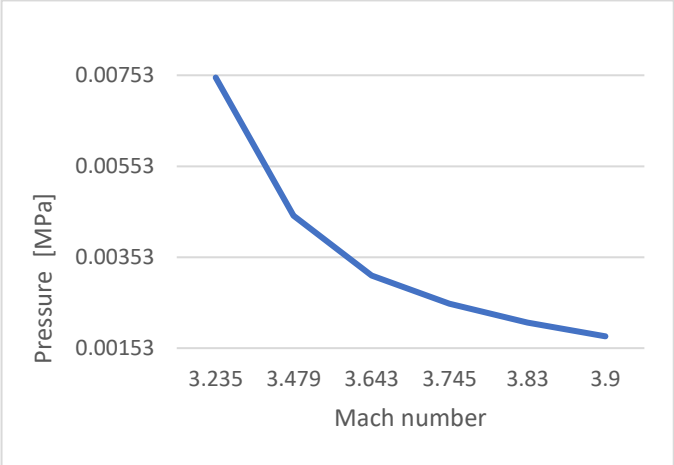

Figure 5.5 Pressure of the gas flow in the nozzle extension as a function of the axial position.

5.2.4 Result

The results for the radial, azimuthal stress and Von Mises stresses are reported as functions of the axial and radial position in Figure 5.6,Figure 5.7, Figure 5.8, Figure 5.9 and Figure 5.10. The gas flowing from the outlet of the nozzle in its extension creates a disturbance that can cause the failure or fracture of the structure and compromise the performance of the component. The extension of the nozzle is connected to the combustion chamber by means of clamping nuts, to which the stresses are then transferred. The hoop stress created in the axial direction is plotted in Figure 5.6 , and has a maximum value 0.30 MPa. This value is not particularly high because the gas has already expanded in the nozzle and therefore does not cause structural damage to the extension of the nozzle.

Figure 5.7 shows that the maximum radial stress acts at the initial point of the extension with a value equal to 0.03 MPa, practically negligible for the structural resistance of the nozzle extension.

The Von Mises stress in the nozzle extension is shown in Figure 5.8. Its maximum value of 0.4 MPa is below the yield limit of the cobalt alloy L-605.

The results obtained show that all the stresses generated in the nozzle extension do not create structural damage and therefore do not adversely affect the performance of the component.

The results obtained shows that all the above three stresses at all axial positions in the nozzle extension do not create any damage, nor they significantly affect the structural performance of the nozzle.

The stresses have also been calculated in the radial direction (see Figure 5.9 and Figure 5.10). Three nodes have been selected at the beginning of the nozzle extension and path created along the radial direction. The maximum values obtained for the stress of Von Mises are also low and within the yield stress of the material.

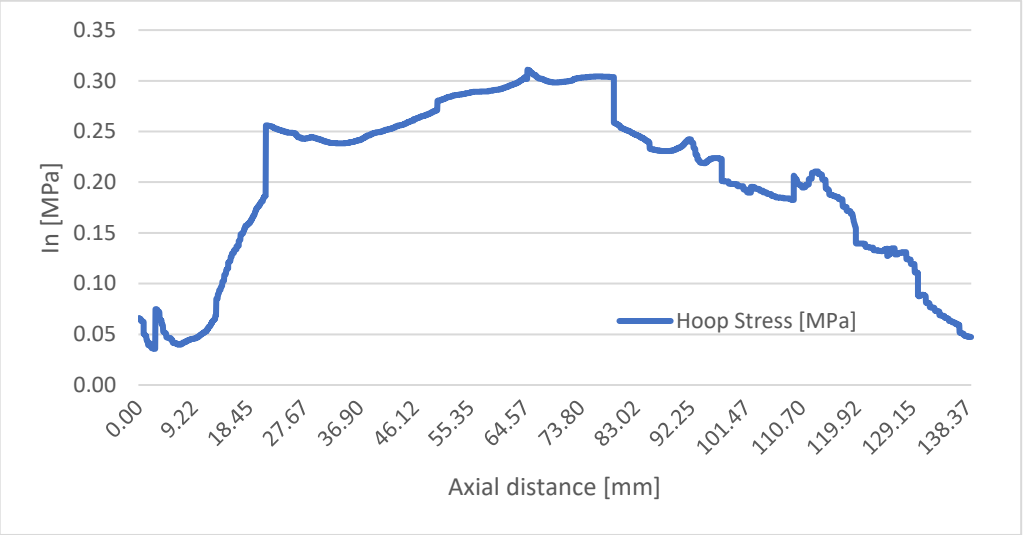

Figure 5.6 Azimuthal stress as a function of the axial position in the 2D nozzle extension.

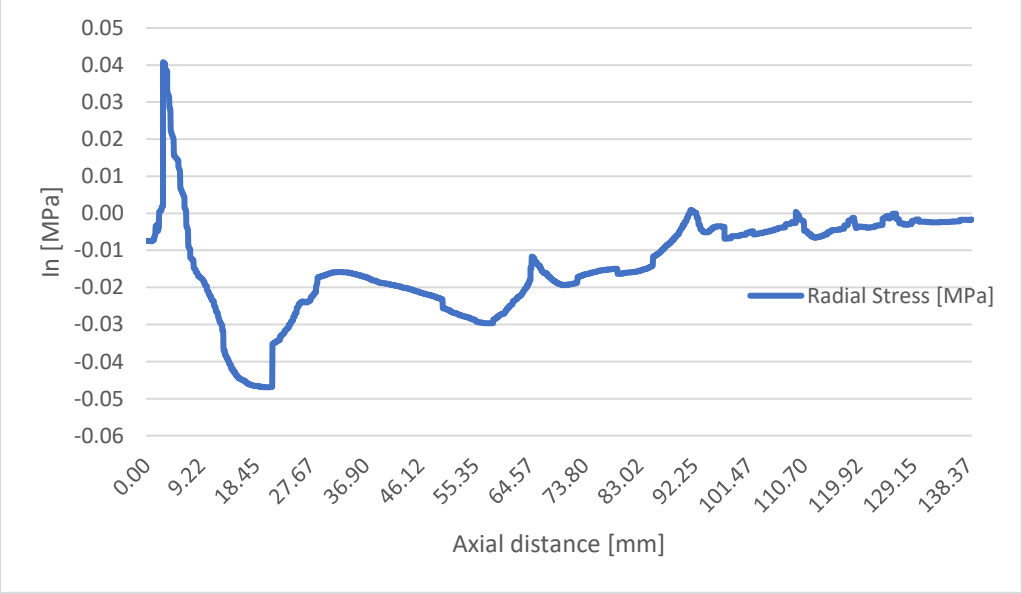

Figure 5.7 Radial Stress as a function of the axial position in the 2D nozzle extension.

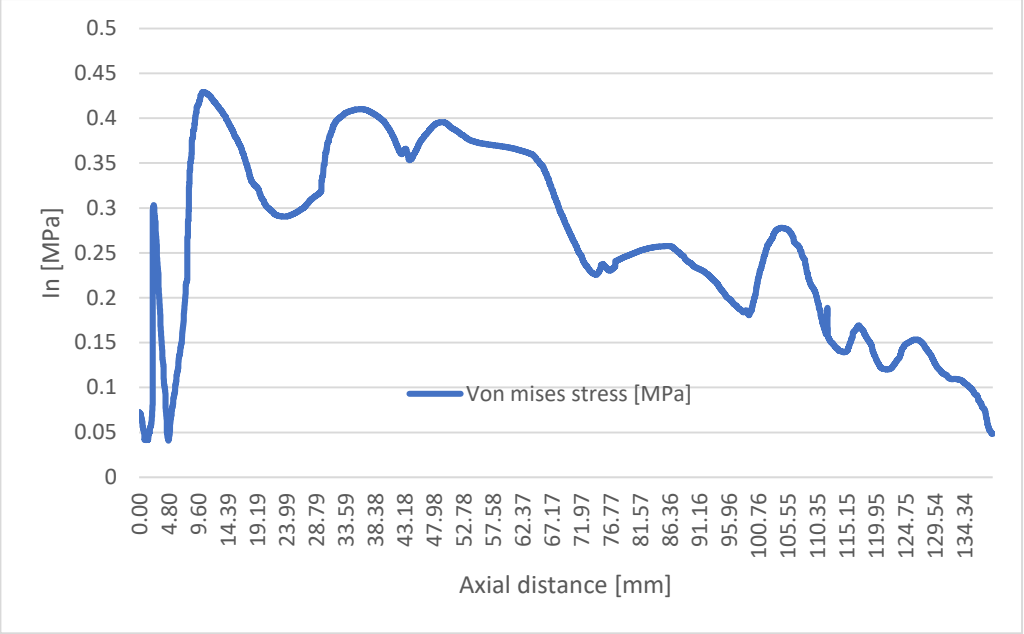

Figure 5.8 Von-Mises stress as a function of the axial direction of 2D nozzle extension

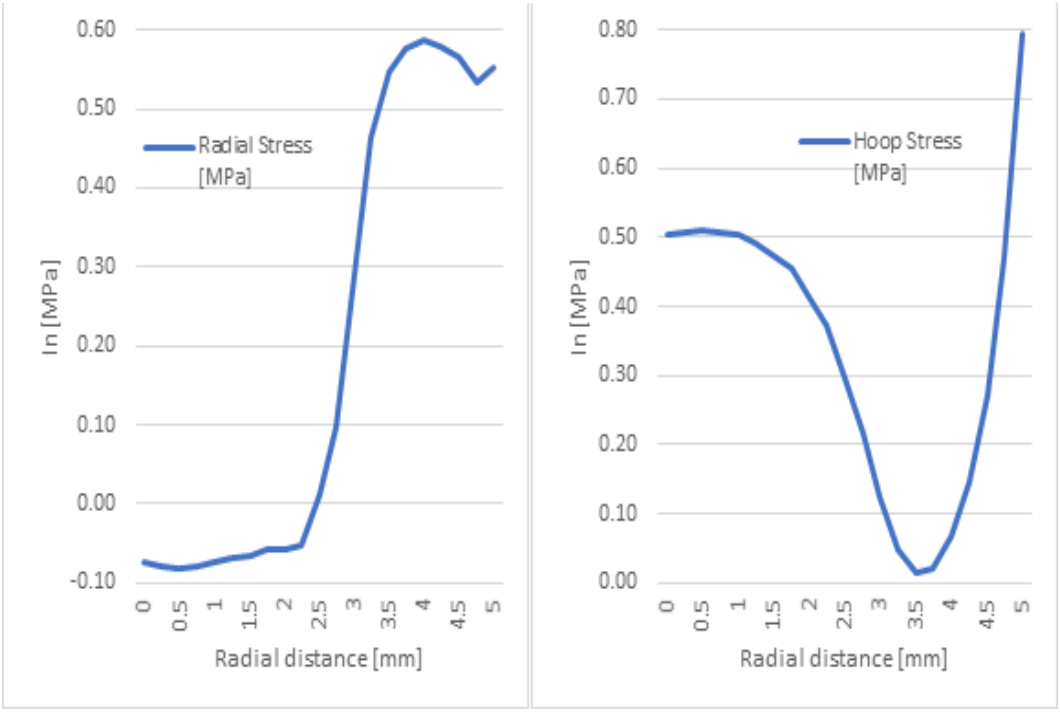

Figure 5.9 Radial stress (left) and azimuthal stress (right) in nozzle extension as a function radial position.

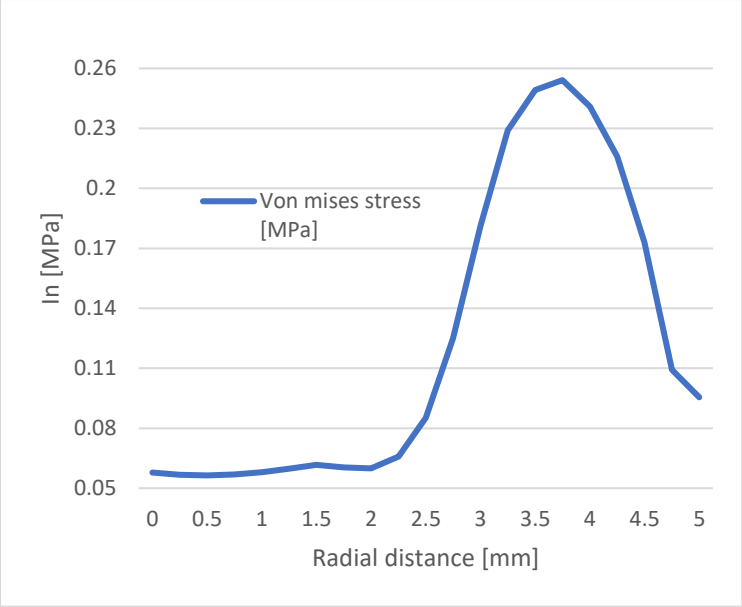

Figure 5.10 Von Mises stress in 2D nozzle extension as a function of the radial position.

5.3 Unsteady thermal analysis of nozzle extension

The preliminary transient analysis of the temperature field in the extension of the nozzle, where it is necessary to resolve the temperature distribution $T(x,t)$ where x is a distance or position and T is temperature and t is time, has been carried out.

Knowing the temperature field in the nozzle extension, it is then possible to verify its thermo-structural resistance. Furthermore, the analysis of the heat transfer provides a very useful guide in design tests and for the interpretation of possible failures. The temperature of the propellant gas is greater than the maximum operating temperature of the thrust chamber wall material (about 2000 K). So, the heat transfer to the chamber wall is a vital aspect in the design of a LPRE because it can cause structural failures.

The study of the heat transfer indicates that the maximum temperature of the wall in contact with the propellant is mainly caused by convection and radiation. In particular, radiation heat transfer only contributes a small part of the overall heat transfer, which depends on the type of liquid propellant used.

5.3.1 Methodology

The 2D rocket motor nozzle extension has been designed using ANSYS APDL 16.0 to analyze the temperature field that affect its structural performance. The procedure for the thermo-structural analysis of the rocket nozzle extension is very similar to the thermo-structural analysis of the combustion chamber illustrated previously (see in chapter 4.2)

The material chosen for the design of the rocket motor nozzle extension is the L-605 cobalt alloy, whose properties such as specific heat, thermal conductivity and density are assigned as input data to the model (see Table 5.3). The component has been finely meshed by dividing it into 13362 nodes connected in 3799 finite elements with an edge length equal to 0.75. The problem has been defined by assigning the thermal

BCs [40].

The temperature range obtained from the thermal analysis has then been used to develop the thermo-structural analysis. The structural properties of the material, such as the Young's modulus, the thermal expansion coefficient and the Poisson module, must be provided as input data for the structural simulation and their values at 25 ° C are listed in Table 5.3[40].

Sl.no	Mechanical and Thermal Properties	Values
1	Density [kg/m^3]	3.27
2	Young's modulus [GPa]	220
3	Poisons ratio [-]	0.29
4	Yield Strength [MPa]	466
5	Ultimate Strength [MPa]	994
6	Thermal expansion co-efficient [1/K]	1.30E-05
7	Thermal conductivity [W/(mK)]	9.4
8	Specific heat [J/(kg k)]	385

Table 5.3 Mechanical and thermal properties of L-605 cobalt alloy at 25˚C

The heat transfer coefficient and the bulk temperature of the gas flow have been assigned at various positions along the axial direction of the nozzle extension. The thermal problem has been solved and provided the temperature distribution as a function of time and position. For the structural analysis, displacement constraints and the pressure load have been applied at the inner wall along the axial direction of the nozzle extension. The results of the unsteady thermal problem have been saved in the ".rth" file and their content has been assigned as input to the structural simulation at the times 0.025 s, 0.050 s, 0.1 s, 0.5 s, 1 s, 2 s, 5 s, 10 s, 50 s, 80 s, 100 s after engine ignition. The results of the thermo-structural simulations are shown in Figure 5.12, Figure 5.13 and Figure 5.16.

The heat flow is transferred by convection and radiation from the hot gases to the internal wall of the structure, by conduction to the external wall and finally by radiation to the external space. The initial temperature condition is T = 273K and the BC for the thermal analysis has been assigned by calculating the heat exchange coefficient using the Bartz equation (Equation 4.9) for all six stations of the nozzle extension. Parameters such as Mach number, gas pressure, its static and bulk temperatures at each station along the axial direction have been calculated using equation (4.5). The BCs assigned for the thermal analysis at the various stations along the axial direction of the nozzle extension are shown in Table 5.4.

Station no	X [mm]	$\frac{A_t}{A}$	Mach number	T_g [K]	T_{aw}[K]	H[W/m²K]
1	23.27	0.081826019	3.2355	1683.51	2871.69	146.200
2	46.33	0.054000419	3.47967	1578.36	2866.81	100.578
3	69.43	0.040678137	3.643	1511.91	2863.69	77.9418
4	92.53	0.034046711	3.7456	1470.72	2861.82	66.406
5	115.63	0.029329212	3.83089	1437.74	2860.29	58.0652
6	139	0.025902881	3.90171	1410.93	2859.04	51.9229

Table 5.4 Boundary condition for thermal analysis of 2D nozzle extension

The CEA code provides the properties of the combustion gas, such as the specific heats and their ratio, the combustion temperature, the average molar mass, etc., depending on the liquid propellants used and their mixing ratio.

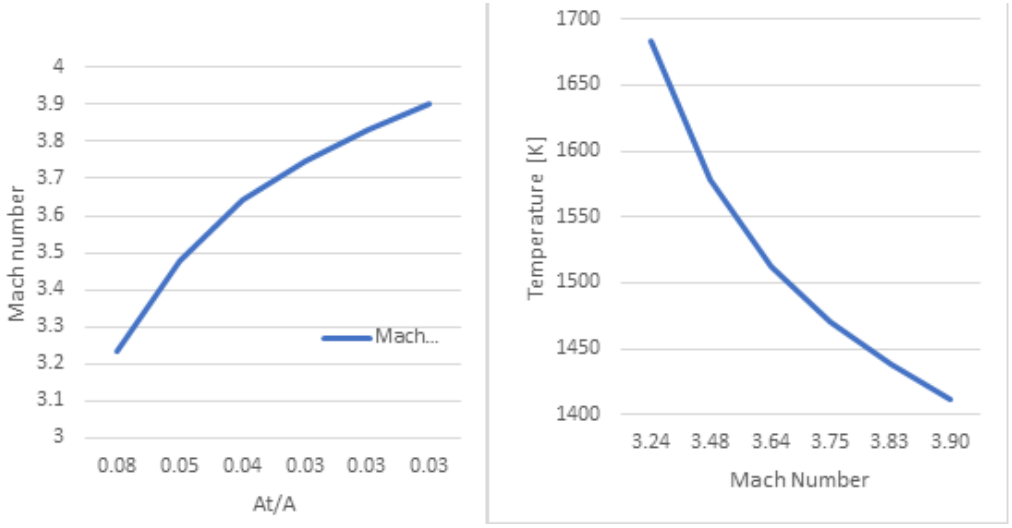

Figure 5.11 Mach number of the flow in the nozzle as a function of the inverse ratio (left). Temperature of the flow in the nozzle as a function of the local Mach number (right)

Figure 5.11 shows the calculated parameters for the gas expansion along the nozzle extension. On the left the Mach number is shown as a function of the geometric expansion ratio while the right part of the figure illustrates the variation of the static temperature as a function of the Mach number. When the temperature is reduced, the gas velocity increases. In particular, the diagram shows that the static gas temperature is reduced to 1400 K at the nozzle exhaust, while the Mach number increases monotonically in the axial direction.

Heat transfer by radiation depends on the emissivity of the material. The emissivity of the external wall of the chamber material has been assigned equal to ε_{we} 0.64 as for the R-4D engine. The internal emissivity has been calculated using the formulas indicated previously. Then, calculating V_{cc} and A_{cc} by Equation (4.13) and (4.14) and substituting in L_{w-g}, we obtain the equivalent beam length for radiation in the nozzle extension.

$$L_{w-g} = 3.66\frac{V_{cc}}{A_{cc}} = 8cm$$

Therefore, from equation (4.16) the internal emissivity ${\varepsilon_{wi}}^{eq}$ corresponding to the gas temperature equal to 1683.51 K resulted to be about 0.008. Since the emissivity of the radiation is low, also the intensity of radiation in the extension of the nozzle is low, between 1% and 2% of heat transfer by convection.

The analysis under unsteady conditions has been carried out for the final time of the thermal simulation (t = 250 s). The duration of the time step has been set equal to 0.025 s. Then, by providing the required input for the transient analysis, the thermal state of the nozzle extension has been obtained at each of its elements and nodes.

5.3.2 Results

The temperature profile in the axial direction of nozzle extension is shown in Figure 5.12 to Figure 5.16. The temperature reaches steady state after about 80 s from engine ignition. The result relative to the thermal BC for the heat flow to the wall by convection and radiation is shown in Figure 5 12. Initially (t = 0.025 s) the highest temperature is 298 K near the initial point of the nozzle extension. After 80 s from engine ignition the temperature reaches its maximum steady-state value of 1800 K near the beginning of the extension and remains constant thereafter.

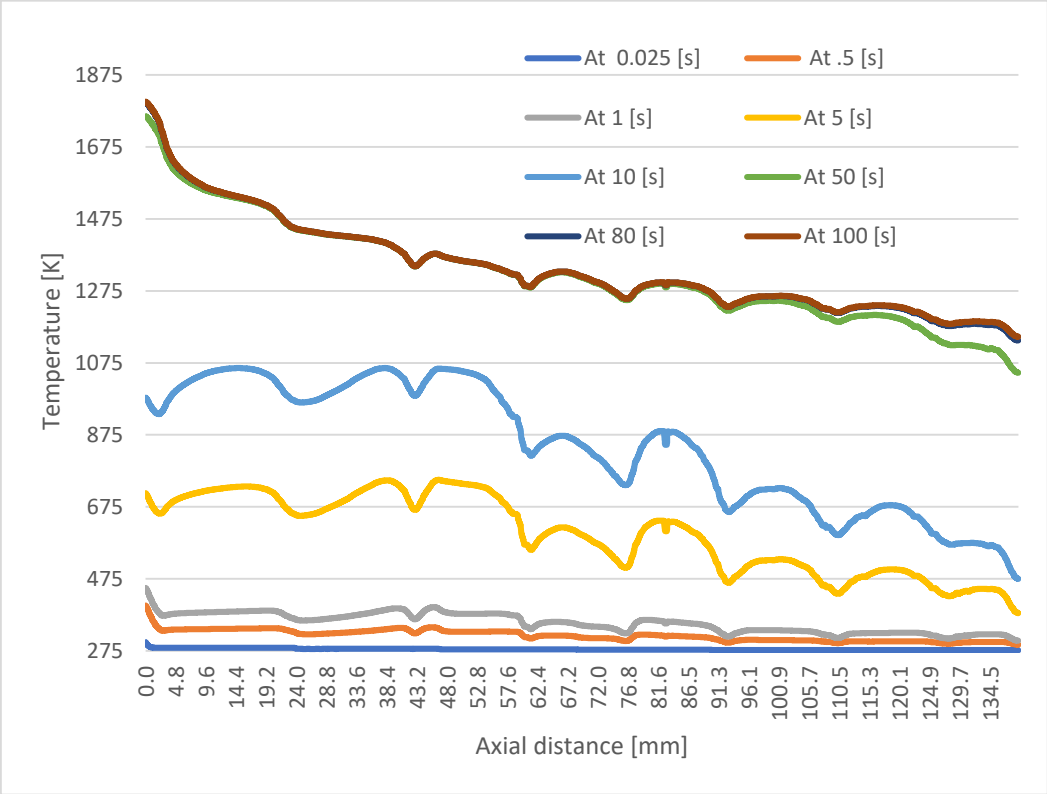

Figure 5.12 Temperature profile of the 2D nozzle extension in the axial direction

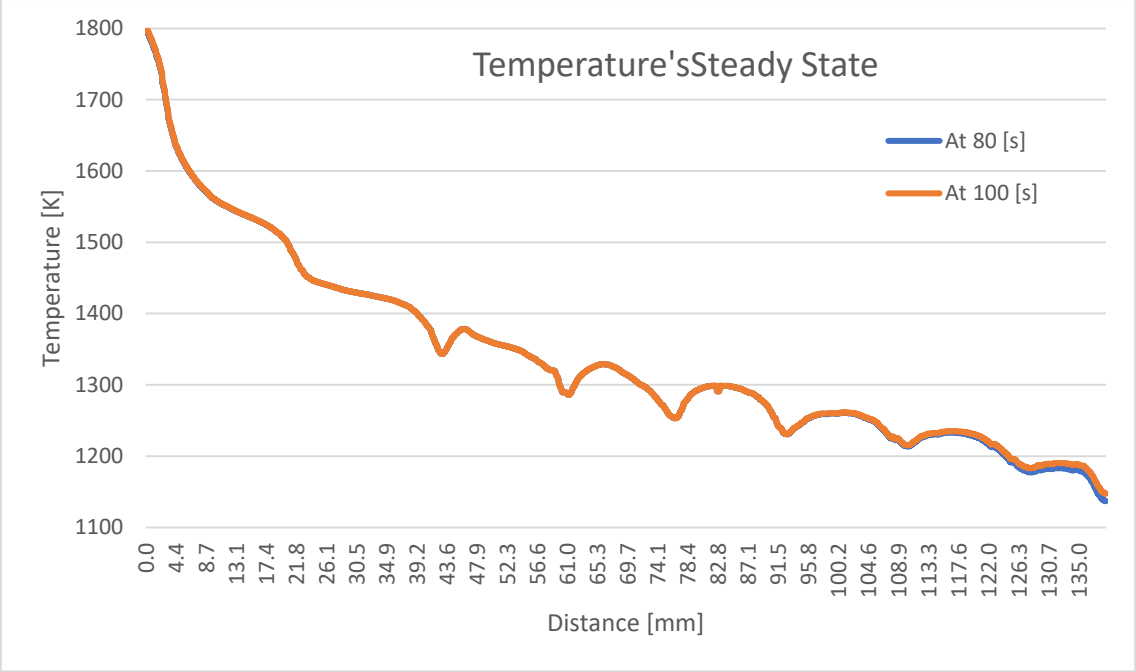

Figure 5.13 Temperature profile of the 2D nozzle extension in the axial direction at steady state.

Figure 5.13 shows the results obtained by means of the software ANSYS APDL 16.0 for the temperature of the nozzle extension as a function of the axial position. At time t = 80 s the maximum temperature is 1800 K, equal to the value obtained after 100 or 200 s from engine ignition. The corresponding thermo-structural loads are therefore the same at the time t = 80, 100 and 200 s (thermal equilibrium conditions).

The temperature profile in the nozzle extension is also plotted for three nodes in the radial direction (see Figure 5.15). Figure 5.14 shows how the temperature increases as a function of time and axial position. The minimum temperature is 298.58 K at 0.025 s, and gradually increases in time as a function of the axial and radial position X and Y. At the time t = 80 s the temperature is 1800 K, and it remains constant thereafter.

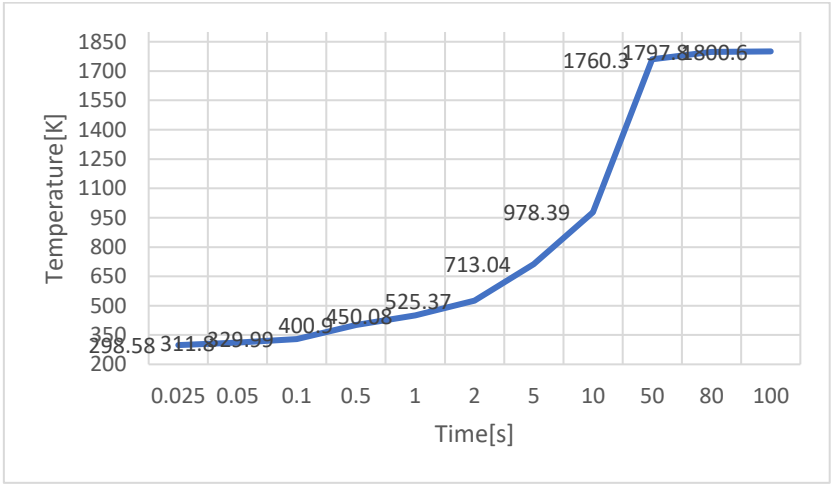

Figure 5.14 Temperature as a function of time from engine ignition.

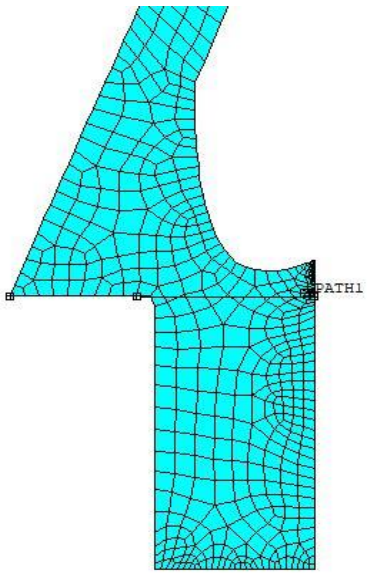

Figure 5.15 Meshed 2D nozzle extension downstream point (Path 1).

The temperature profile in the radial direction at three points of the nozzle extension is also illustrated. The radial temperature profile at point 1 is shown in Figure 5.16, It can be seen that the temperature is maximum at the inner wall, where the thermal stress is also maximum. The temperature profile decreases appreciably from the internal to the external wall. At time t = 1 s after engine ignition the maximum temperature occurs at the inner wall (450 K) and the minimum temperature at the external wall (302 K), with a total drop of about 150 K.

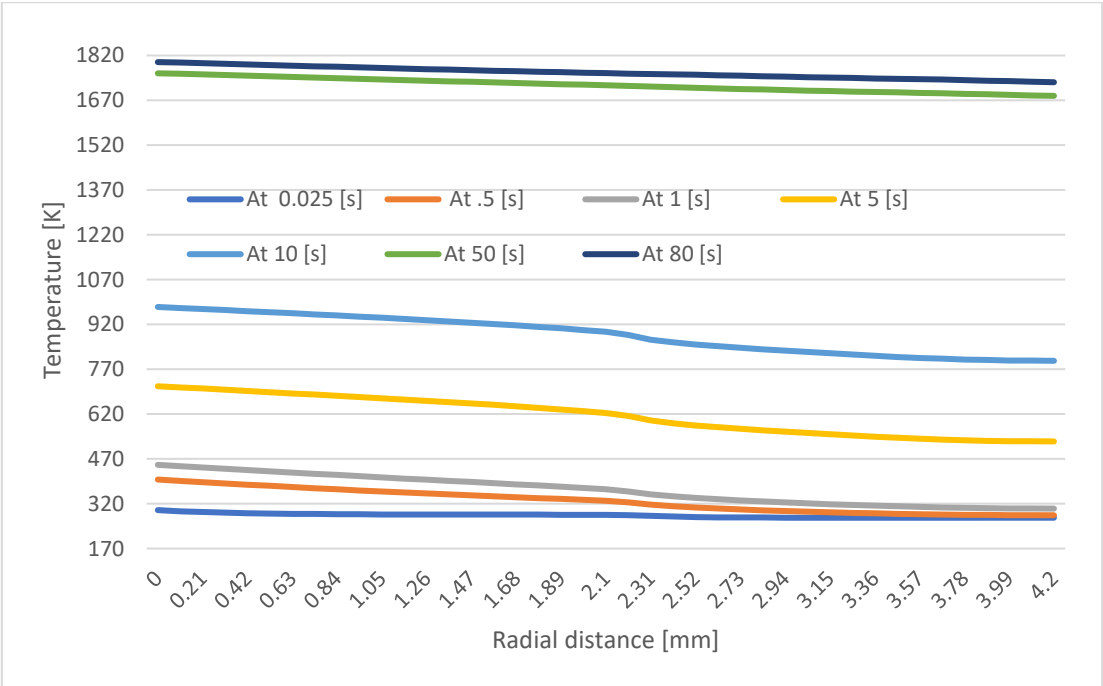

Figure 5.16 Temperature profile of 2D nozzle extension in the radial direction

5.4 Thermo-structural analysis of nozzle extension

The 2D axisymmetric finite element (FEA) model of the nozzle extension has been used for thermo-structural analysis. In this model the material is considered isotropic and non-linear. The analysis combines the thermal analysis for the evaluation of the temperature field and the thermal-structural analysis for the valuation of the resulting thermal stresses. The Plane element 183 has been chosen because it supports an axisymmetric model of the structure.

One of the BCs for the thermo-structural analysis is the pressure on the inner wall of the nozzle extension, which is non-uniform in the axial direction. The gas pressure has been calculated using the isentropic gas flow formula. The thermal conditions in the nozzle extension have been applied by selecting a file saved with the name "rth", which provides the temperature field corresponding to the given time *t* after engine ignition.

5.4.1 Results

The results of the thermo-structural analysis of the nozzle extension for the radial, azimuthal and Von-Mises stresses have been calculated as functions of the axial and radial positions, as illustrate in Figure 5.17 up to Figure 5.21. The high-temperature gas flowing in the axial direction heats the inner wall of the nozzle extension determining both thermal and pressure loads. According to the results of the previous steady-state analysis of the nozzle extension, also the unsteady simulations demonstrate that the stresses generated by the non-uniform pressure distribution along the nozzle extension are negligible.

The highest thermal stresses occur in the initial part of the nozzle extension. The maximum radial stress in the nozzle extension is 35.7 MPa at the time t = 10 s from the ignition of the engine and occurs at the inner wall where the temperature is 978 K. Figure 5.17 shows that the maximum radial stress occurs in the central region of the nozzle extension.

The corresponding azimuthal stress for the temperature T = 978 K at time t = 10 s after engine ignition is equal to 162 MPa. The comparison with the yield stress of the material allows one to verify the structural resistance of the nozzle extension. From the results of the simulation, the maximum Von Mises stress acting on the nozzle extension is 407 MPa, lower than the yield stress of the cobalt alloy L-605, which is equal to 466 MPa. Therefore, the extension of the nozzle can withstand the thermo-structural stresses acting on it.

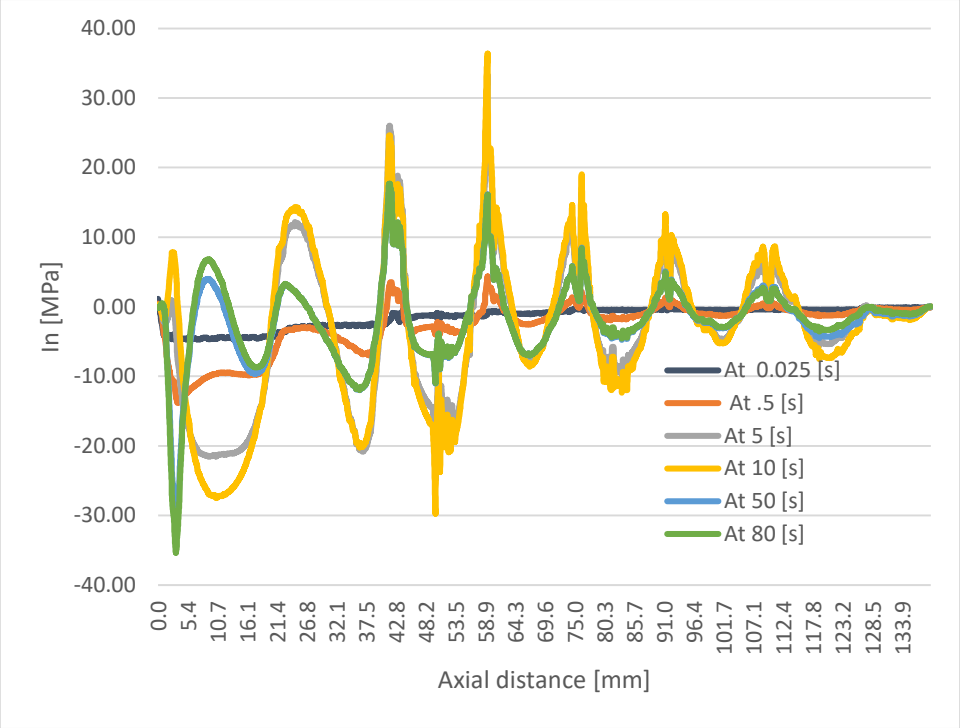

Figure 5.17 Radial stress along the axial direction in the nozzle extension

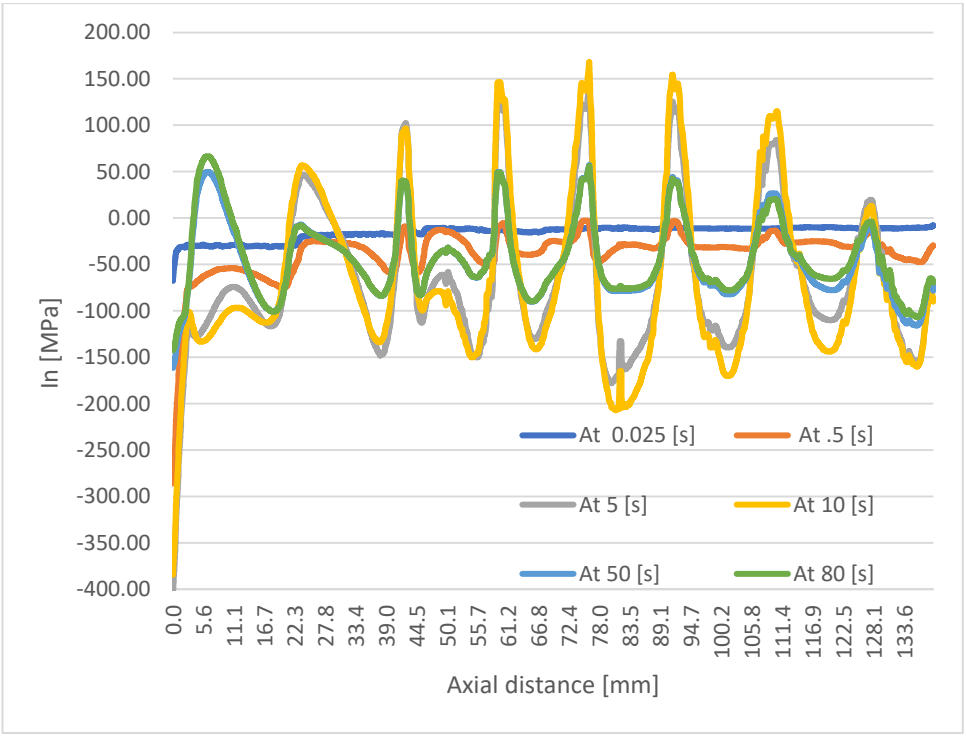

Figure 5.18 Azimuthal stress along the axial direction in the 2D nozzle extension.

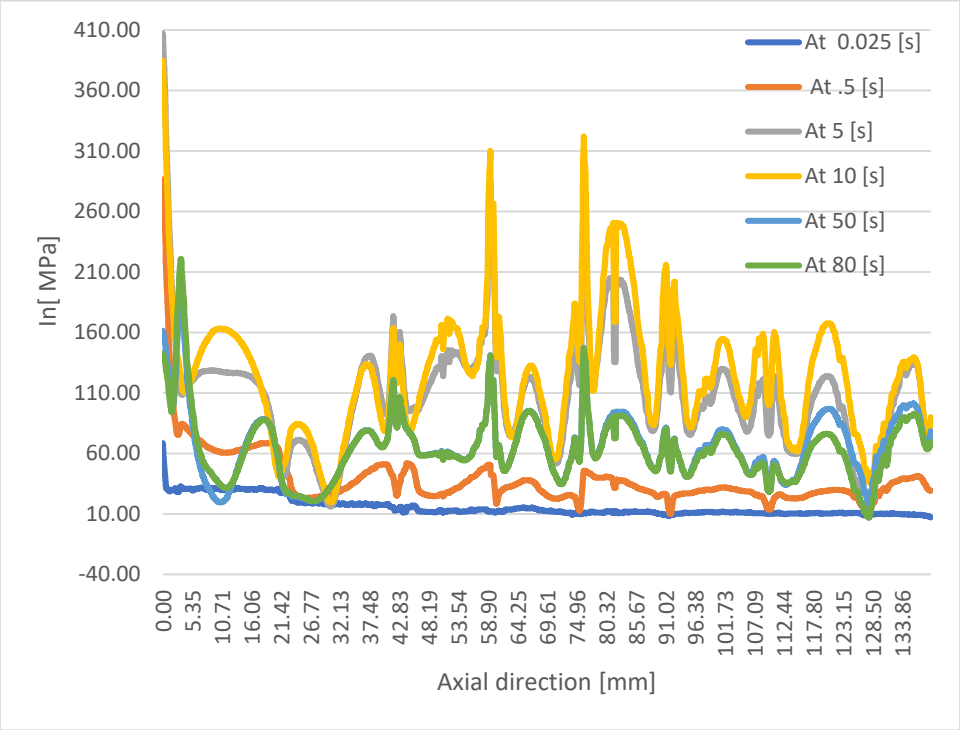

Figure 5.19 Von-Mises stress along the axial direction in the 2D nozzle extension.

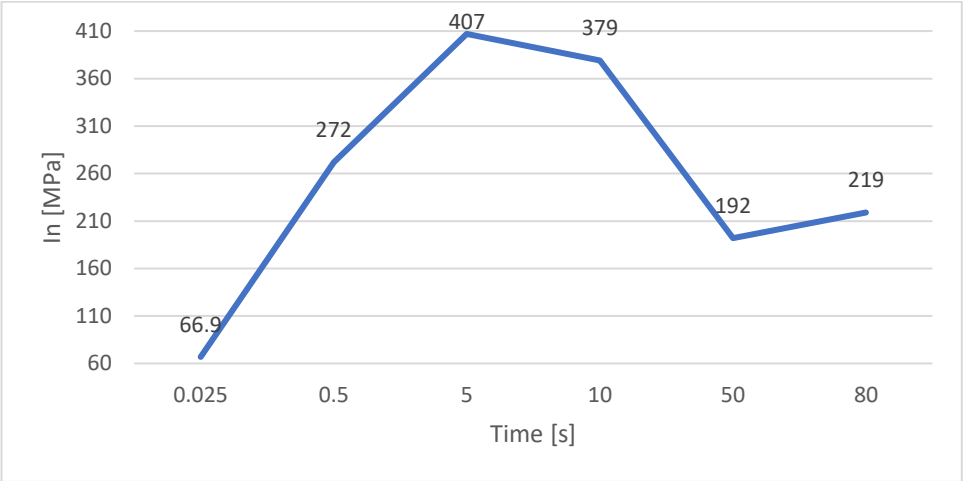

Figure 5.20 Von-Mises stress as a function of time from engine ignition.

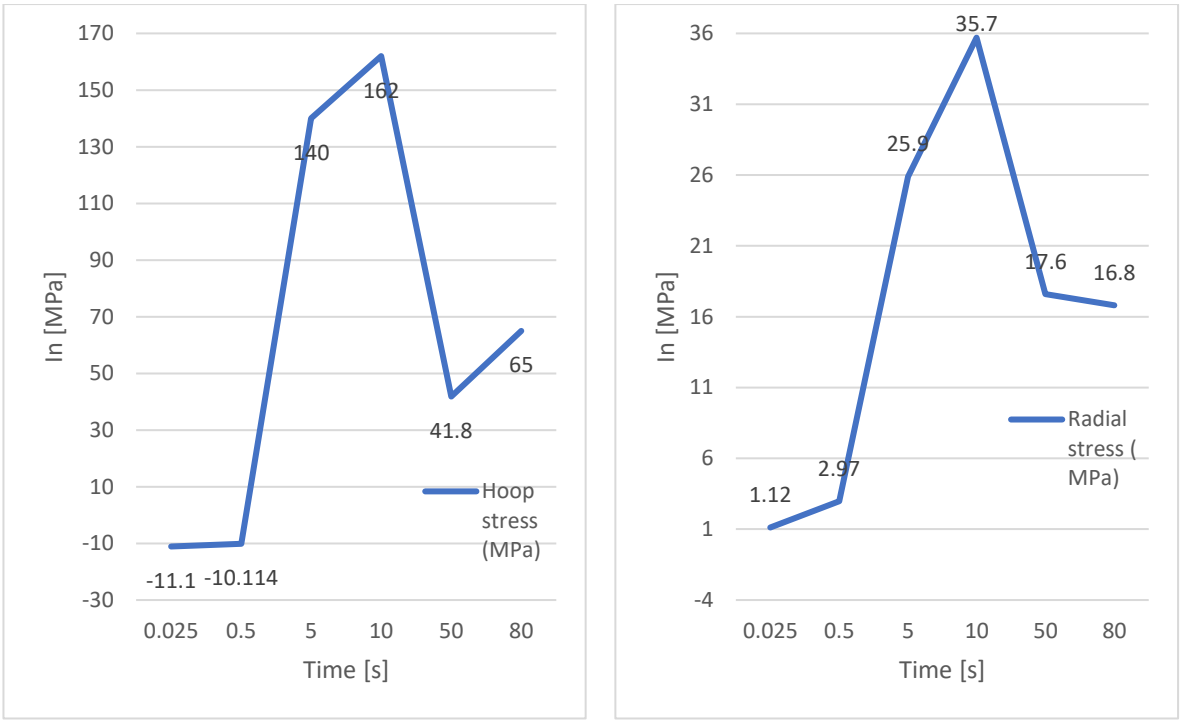

Figure 5.21 Azimuthal stress (left) and radial stress (right) as a function of time after engine ignition.

The geometry of the nozzle extension and its BCs are axisymmetric. The radial, azimuth and Von Mises stresses acting on the structure are shown in Figure 5.22 to Figure 5.28 as functions of the radial position.

The results of the thermo-structural analysis for the nozzle extension show that

- The pressure and temperature of the gas are greater at the initial point of the nozzle extension.
- The gas continues to expand in the nozzle extension.
- The design of the nozzle extension near its initial section must be modified.

The maximum radial stress due to the effect of the thermal field T = 978.39 K is equal to 228 MPa at the time t = 10 s after engine ignition.

The corresponding maximum azimuthal stress in the wall of the nozzle extension is 136 MPa at its initial point, as shown in Figure 5.18. The maximum azimuthal stress as a function of the radial position is 407 MPa.

The Von-Mises stress shown in Figure 5.26 makes it possible to evaluate whether or not the component will fail due to the thermal and mechanical loads imposed at its boundaries. The maximum Von Mises stress as a function of the radial position changes reaches 494 MPa where the material temperature is equal to 1800 K. Therefore, its value is higher than the yield stress of the cobalt alloy L-605 (466 MPa), but nevertheless lower than its ultimate stress (994 MPa). The analysis then shows that the component will undergo permanent deformations under the action of its thermal and mechanical loads, but failure will not necessarily occur.

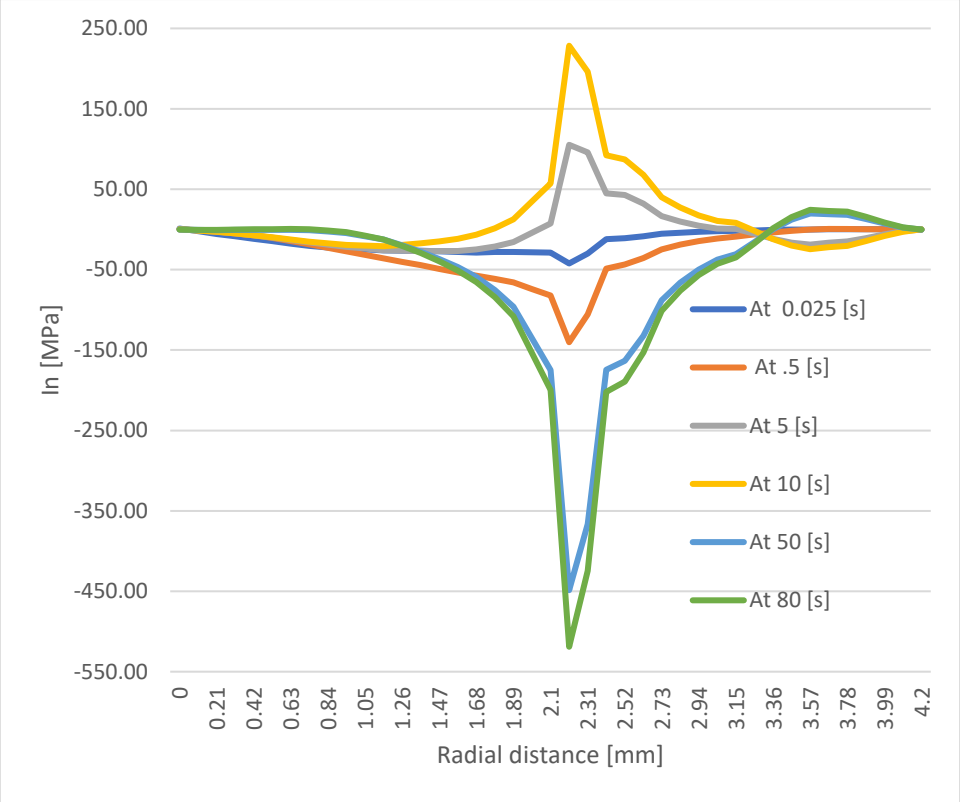

Figure 5.22 Radial stress in the 2D nozzle extension along the radial direction

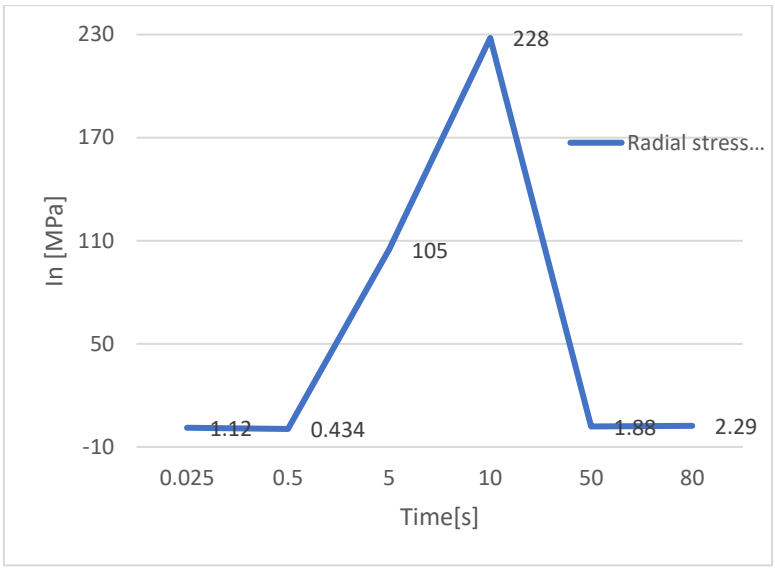

Figure 5.23 Radial stress in the 2D nozzle extension as a function of time.

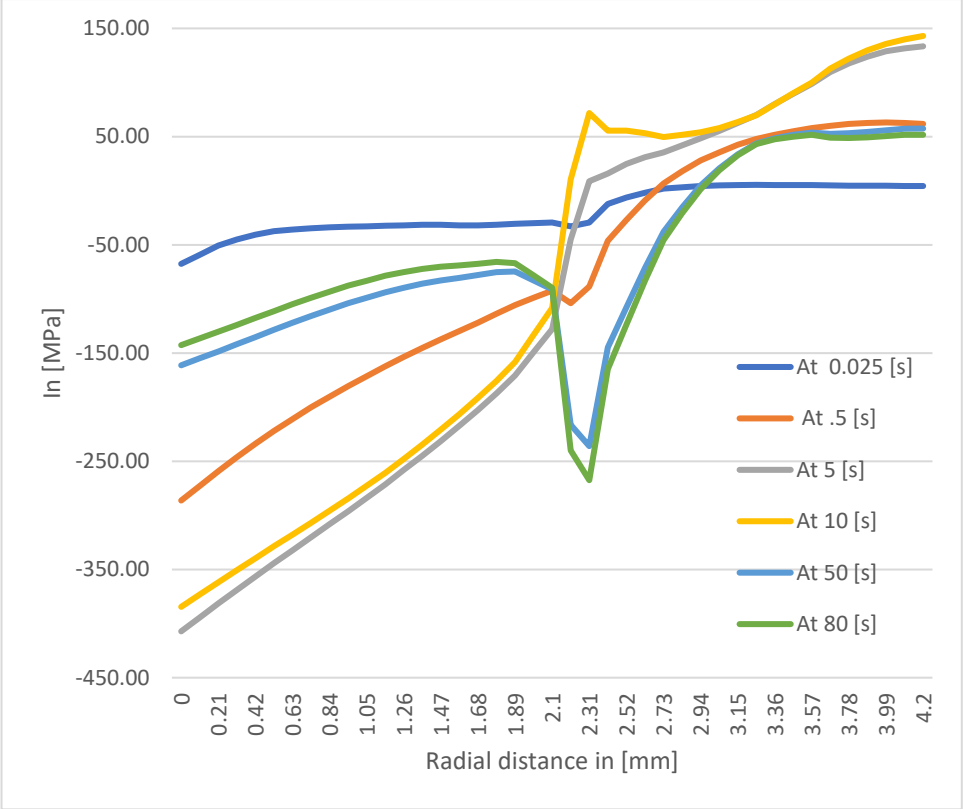

Figure 5.24 Azimuthal stress in the 2D nozzle extension as a function of the radial position.

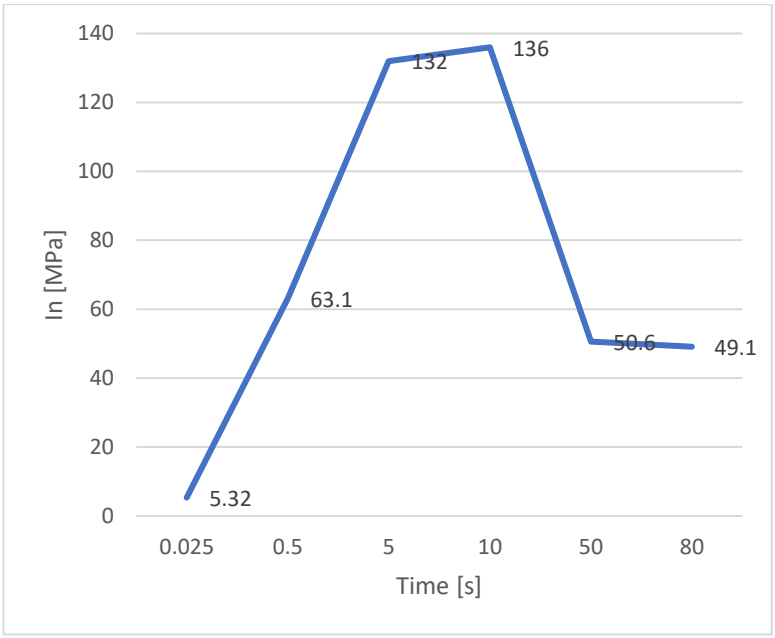

Figure 5.25 Azimuthal stress in the 2D nozzle extension as a function of time.

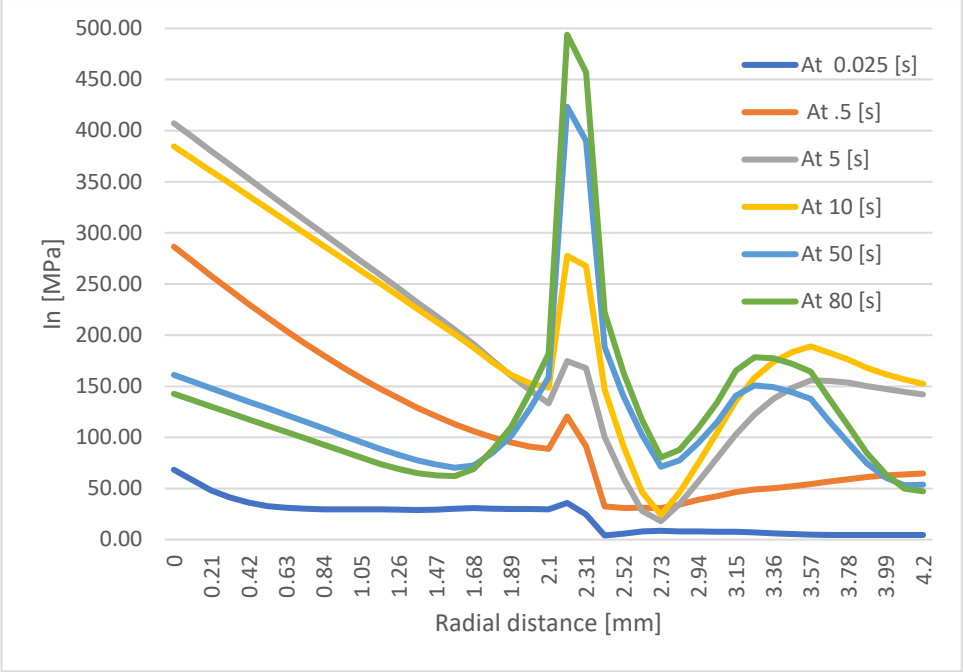

Figure 5.26 Von-Mises stress of the 2D nozzle extension in the radial direction.

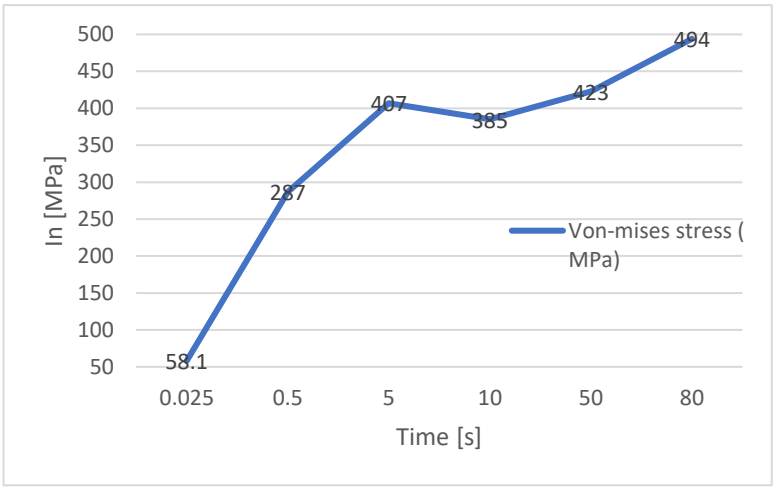

Figure 5.27 Von-mises stress of the 2D nozzle extension as a function of time.

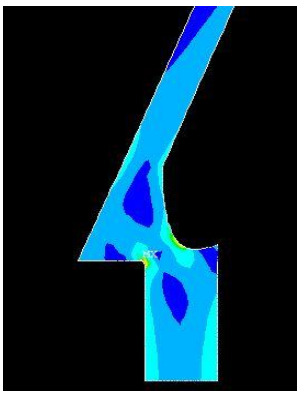

Figure 5.28 Maximum Von-Mises stress acting in the 2D nozzle extension along the radial direction

6 Conclusion and Future work

From the present research the following conclusions can be drawn:

- Thermal and structural loads acting on the thrust chamber of a typical nitrogen tetroxide/hydrazine bipropellant rocket engine have been studied using the ANSYS code. The analysis has been performed on three components of the engine thrust chamber: the cylinder, the combustion chamber and the nozzle extension.

- Thermal loads due to combustion act on the whole chamber. The axisymmetric 2D analysis is a fast and reliable method for analyzing the structure of the combustion chamber under all conditions. The steady-state and transient analyses showed that for a combustion temperature equal to 2229 K and pressure equal to 6.5 bar the structure is stressed below the yield limit of the material used (molybdenum).

- The 2D axisymmetric analysis in steady state of the 2D combustion chamber shows the non-uniform pressure distribution axial position does not affect the structure, since the stresses it induces are within the yield limit of molybdenum. The transient thermal analysis shows that the temperature reaches equilibrium at 60 s from the motor's ignition with a maximum of 2058 K. The temperature profile of the combustion chamber is not constant since its shape is not uniform.

- The analysis performed for thermal and structural load on 2D combustion chamber shows that the maximum Von Mises stress is 156.8 MPa near MPa close to the throat. At the time t = 5 s from engine ignition the maximum temperature is 1228.5 K and gives rise to the maximum Von Mises stress.

- Steady state analysis of 2D nozzle extension show that, the stresses produced due to the non-uniform internal pressure distribution fall within the limits of the yield strength for the L-605 Co alloy. The transient thermal analysis of the nozzle extension shows that the temperature reaches steady-state at 80 s after engine ignition, with a maximum value of 1800 K at the initial point of the nozzle extension. This thermal field creates a maximum Von Mises stress of 494 MPa, about 10% higher than the yield limit of the material.

6.1 Recommendations

The analysis performed in this thesis was based on the use of the radiation cooling of the chamber. The results show that it is necessary to perform a further refinement of the thermo-structural analysis, possibly introducing the fluid film cooling, which would reduce the heat flow to the inner wall. For the nozzle extension, it is necessary to refine its design by adding a bevel to the corner, since the maximum Von Mises stress has been observed at that location.

6.2 Future work

- In this thermo-structural analysis, the material has been considered as linear and elastic. A more realistic and accurate analysis might take into consideration the plastic and visco-elastic behavior of the structure.
- The effects of creep have been neglected in this analysis but might be incorporated into future studies.
- As the rocket engine gives rise to dynamic effects, to improve the accuracy of the analysis it may be appropriate to consider the effects of vibrations.

BIBLIGRAPHY

[1] L. Denies, “Regenerative cooling analysis of oxygen/methane rocket engines,” Space Engineering, Delft, Netherlands Jul. 2018.

[2] “Rocket Thrust Equations.” [Online]. Available: https://www.grc.nasa.gov/WWW/K-12/rocket/rktthsum.html. [Accessed: 03-Sep-2018].

[3] G. P. Sutton and O. Biblarz, *Rocket Propulsion Elements Ninth Edition*, Ninth. California,U.S.A: John Wiley & Sons, Inc., Hoboken, New Jersey, 2017.

[4] B.Nufer, “HYPERGOLIC PROPELLANTS : THE HANDLING HAZARDS AND LESSONS LEARNED FROM USE,” 2018.

[5] A. G.Accettura, *Green Propellants*, Volume 223. France: American Institute of Aeronautics and Astronautics, Inc. 1801 Alexander Bell Drive, Reston, Virginia 20191-4344, 2008.

[6] G. Pace, A. Pasini, and L. Torre, “PulCheR-Pulsed Chemical Rocket with Green High Performance Propellants: Second Year Project Overview,” in *51st AIAA/SAE/ASEE Joint Propulsion Conference*, 2015, pp. 1–17.

[7] D. Valentian and A. Souchier, “Green Propellant Implementation for Space Missions and Upper Stage Propulsion,” *43rd AIAA/ASME/SAE/ASEE Jt. Propuls. Conf. Exhib.*, no. July, pp. 1–9, 2007.

[8] D. Haeseler, V. Bombelli, … P. V.-E. S., and U. 2004, “Green Propellant Propulsion Concepts for Space Transportation and Technology Development Needs,” *Proc. 2nd Int. Conf. Green Propellants Sp. Propuls.*, 2004.

[9] B. Nufer, “HYPERGOLIC PROPELLANTS : THE HANDLING HAZARDS AND LESSONS LEARNED FROM USE,” 2018.

[10] H. Burkhadt, M. Sippel, A. Herbertz, and J. Klevanski, “Space Launcher Liquid Propulsion,” in *Comparative Study of Kerosene and Methane Propellant Engines for Reusable Liquid Booster Stages*, 2002, no. December, p. 10.

[11] “RD-58MF.” [Online]. Available: http://www.astronautix.com/r/rd-58mf.html.[Accessed: 03-Sep-2018]

[12] “Proton-M, Propulsion.” [Online]. Available: http://www.b14643.de/Spacerockets_1/East_Europe_2/Proton-M/Propulsion/engines.htm. [Accessed: 25-Sep-2018].

[13] “HM7-B.” [Online]. Available: http://www.astronautix.com/h/hm7-b.html. [Accessed: 10-Sep-2018].

[14] A. A. and Defence, “HM-7 and HM-7B Rocket Engine - Thrust Chamber.” [Online]. Available: http://cs.astrium.eads.net/sp/launcher-propulsion/rocket-engines/hm7b-rocket-engine.html. [Accessed: 04-Oct-2018].

[15] D. H. Huang and D. K. Huzel, *Modern Engineering for Design of Liquid-Propellant Rocket Engines*. Boulder: American Institute of Aeronautics and Astronautics 370 L’Enfant Promenade, SW, Washington DC, 20024-2518,

1992.

[16] G. Schulte, “High performance 400N MMH/NTO bipropellant engine for apogee boost maneuvers,” in *35th Joint Propulsion Conference and Exhibit*, 1999, no. June.

[17] Y. Matsuura, S. Iihara, and Y. Tashiro, “Hypergolic Propellant Ignition Phenomenon with Oxidizer Two-Phase Flow Injection,” *49th AIAA/ASME/SAE/ASEE Jt. Propuls. Conf.*, vol. 30, no. 5, p. 4154, 2013.

[18] Ariane Group, “400N bi-propellant apogee motor,” *Chem. bi-propellant thruster Fam.*, vol. 49, no. 0.

[19] Ariane Group, “Customer Reference – Aerospace Ariane 6 propulsion module : Simplified by additive manufacturing Components.” .

[20] L. R. Bell, “APOLLOSM-LM RCS ENGINE DEVELOPMENT PROGRAM SUMMARY REPORT VOLUME 3,” 1995.

[21] “CEARUN.” [Online]. Available: https://cearun.grc.nasa.gov/. [Accessed: 25-Sep-2018].

[22] “Finite Element Method – What Is It? FEM and FEA Explained.” [Online]. Available: https://www.simscale.com/blog/2016/10/what-is-finite-element-method/. [Accessed: 14-Sep-2018].

[23] N. preferred reliability Practices, “STRUCTURAL STRESS ANALYSIS,” *Practice*, no. April. pp. 1–10, 1996.

[24] L.R.Bell, “Apollo SM-LM RCS ENGINE DEVELOPMENT PROGRAM SUMMARY REPORT,” 2017.

[25] R. Article, V. S. Kulkarni, K. C. Deshmukh, and P. H. Munjankar, “Thermal stress analysis due to surface heat source,” *Int. J. ofAdvances AppliedMathematics Andm. Therm.*, vol. 2, no. 2, pp. 139–149.

[26] J. E. Akin, “Thermal Stress Analysis.” J.E. Akin, Texas, pp. 270–287, 2009.

[27] “NASA Chemical Equilibrium with Applications (CEA).” [Online]. Available: https://www.grc.nasa.gov/www/CEAWeb/. [Accessed: 14-Sep-2018].

[28] R. Sarwade, “Life Prediction Analysis of a Subscale Rocket Engine Combustor using a Fluid-Thermal-Structural Model,”Auburn, Alabama, 2006.

[29] T. Analysis, “6. Thermal-Stress Analysis.” Iinternational Journal of Advances in Applied Mathematics and Mechanics Thermal, Maharashtra, India,2014

[30] J. M. Seitzman, “Rocket Propulsion Thrust Coefficient , Characteristic Velocity and Ideal Nozzle Expansion,”Atlanta, 2006, pp. 1–5.

[31] M. Martinez-Sanchez, “Convective Heat Transfer: Reynolds Analogy Heat,” in *Rocket Propulsion*, no. 3, M. Martinez-Sanchez, Ed. Cambridge: Massachusetts Institute of Technology, 2005, pp. 1–16.

[32] G. Leccese, D. Bianchi, B. Betti, D. Lentini, and F. Nasuti, “Convective and Radiative Wall Heat Transfer in Liquid Rocket Thrust Chambers,” *J. Propuls. Power*, vol. 34, no. 2, pp. 318–326, 2018.

[33] L. D'Agostino, "Liquid Propellants," in *Liquid Propellant Rockets*, L. D'Agostino, Ed. Pisa: Università di Pisa, 2008/09, 2008, p. 198.

[34] "isentropic Flow Equations." [Online]. Available: https://www.grc.nasa.gov/www/BGH/isentrop.html. [Accessed: 18-Sep-2018].

[35] S.K.SOM, *INTRODUCTION TO HEAT TRANSFER*, Eastern Ec. Karagpur: Asoke K. Ghosh, PHI Learning Private Limited, M-97, Connaught Circus, New Delhi-110001 and Printed by Baba Barkha Nath Printers, Bahadurgarh, Haryana-124507., 2008.

[36] X. Dai and A. Ray, "Life prediction of the thrust chamber wall of a reusable rocket engine," *J. Propuls. Power*, vol. 11, no. 6, pp. 1279–1287, Nov. 1995.

[37] R. Stark, C. Génin, C. Mader, D. Maier, D. Schneider, and M. Wohlhüter, "Design of a Film Cooled Dual-Bell Nozzle," 2017, no. 178, p. 74239.

[38] C. N. Scott, R. W. Nordlie, W. W. Sowa, and G. C. Marshall, "INVESTIGATION OF EXTENDABLE NOZZLE CONCEPTS," 1972.

[39] K. Davis, E. Fortner, M. Heard, H. McCallum, and H. Putzke, "Experimental and Computational Investigation of a Dual-Bell Nozzle," 2015.

[40] Shankar Shiva, Babu Shailesh, Kumar Sai, and Rao TBS, "Thermo-Structure of Dual-Bell Nozzle," *Int. J. Eng. Innov. Technol.*, vol. 4, no. 11, pp. 292–299, 2015.

[41] "r1e.jpg(685×510)."[Online].Available: http://www.astronautix.com/graphics/r/r1e.jpg. [Accessed: 28-Sep-2018].

[42] "Bipropellant Rocket Engines | Aerojet Rocketdyne." [Online]. Available: http://www.rocket.com/propulsion-systems/bipropellant-rockets. [Accessed: 25-Sep-2018].

[43] S. Loff, "About the H-II Transfer Vehicle (HTV)," 2018. [Online]. Available: https://www.nasa.gov/mission_pages/station/structure/elements/htv_about.html. [Accessed: 04-Oct-2018].

[44] "In-Space Transfer Vehicle Primary Propulsion | Aerojet Rocketdyne." [Online]. Available: http://www.rocket.com/inspace_xferprop. [Accessed: 10-Sep-2018].

[45] Aerojet, "Aerojet Operations," *Aerojet A gen Company Redmond Operations.*, no. October, Redmond, WA, p. 93, Oct-2011.

[46] *ESA – Human Spaceflight and Exploration – Advanced Reentry Vehicle activities begin with contract signature*. ESA, 2009.

[47] "Aerojet Propulsion Maneuvers Second ATV Vehicle to ISS | Aerojet Rocketdyne." [Online]. Available: http://www.rocket.com/article/aerojet-propulsion-maneuvers-second-atv-vehicle-iss. [Accessed: 28-Sep-2018].

[48] J. L. Cannon, "Liquid Propulsion: Propellant Feed System Design," *Encycl. Aerosp. Eng.*, vol. 2, p. chapter 2.3.11, 2010.

[49] R. Ballard, *Liquid Propulsion Systems – Evolution & Advancements Launch Vehicle Propulsion & Systems*. 2015.

Appendix A. R-4D LPRE

R-4D liquid propellant rocket engine.

The R-4D was first manufactured by Marquardt (Aerojet Rocketdyne) company in 1962, it is a bipropellant rocket engine of 445N nominal thrust that has successfully flown in Apollo mission and a Lunar module for reaction control system like attitude control and for orbit maneuvering, orbital injection and several other applications (see Figure A. 5). The engine is design good in the sense that it withstands structural stress imposed by outer atmosphere and stress due to their operation. The cooling system for R-4D is based, on one side, on radiation cooling method which is mounted on the exterior surface of the engine, so that heat can be radiated out into the space vacuum and other side film cooling method is used as an additional cooling method. The engine sense vibrational loads due to launch system and in space when other engine starts to operate vibration stress is observed on other engine parts. The R-4D has of course tested before (vibrational test and heat soaking test) to make sure the structural strength of the material is satisfactory, and to confirm that the thermal stress of the materials within the yield strength and do not create any damage [20].

Figure A. 1 R-4D 490 N attitude control thruster by Marquardt.

The engine in above Figure is designed to work under various environmental conditions and operating loads, as well as vibration stresses from boosters when the engine is exposed to aerodynamic forces. As it reaches the space, the engine will be affected by vibration stress from different thrusters. These parameters are crucial while designing major components of the R-4D engine, like the combustion chamber, nozzle extension, and hardware associated with the combustion chamber like propellant valves and combustion chamber assembly. The vibrational stress due to the rocket boosters is more dangerous than the vibrations experienced in space [20].

Several tests were made to make sure about material can withstand structural loads, for instance during the test was conducted for quality process five engines successfully

completed boost vibration test. Major components of the R-4D engine are bell joint, combustion chamber. Combustion chamber attaches hardware, propellant valves and injector assembly [20].

The R-4D family of thrusters has shown to be 100% successful: 1000 engines have been delivered so far, of which 695 have flown, which is considered an achievement. R-4D, which is designed and machined by Marquardt, looks like simple hardware. This engine consists of only four moving parts: two valves in the combined armature-seat pin, and the spring used to bring back the armature to the failsafe closed position. The engine is designed to operate in outer space, which imposed severe and stringent requirements on the parts of engines, and finally on the material selected for each application. The main objective of the engines is to convert chemical energy into thrust thanks to the combustion process in the combustion chamber and to accelerating the of the combustion products in a convergent-divergent (Laval) nozzle [20].

The present R-4D engines combustion chamber operates with a throat temperature above 1366.4 K. Including thermal resistance and mechanical property requirements, other factors also need to be matched, like the fact that valves and injectors must be compatible with liquid propellants, the combustion chamber and injector face need to be suitable with the combustion products, etc. In addition, the strength to weight ratio of the used materials at different temperatures is important. Repeated cyclic type operation and narrow tolerance of valves parts require the using high wear resistance materials as well as anti-galling characteristics [20].

It is very important to have very good knowledge of the thermal expansion and thermal conduction characteristics of the materials used, to avoid relaxation of attached hardware from pre-stresses and overstressing of other parts of the engine. This helps the engine while in operating condition reaching extreme temperature profiles [20].

R-4D has a solenoid valve body, which is used still today as maneuvering thrusters and in the design of different rocket engines. It has been proved to be efficient and reliable. This component is a chief structural part of the valve assembly and it is machined in the shape of a spool. The valve is surrounded by magnetic coils. The inlet end of the valve includes thread fitting to connect with the propellant pipes with a gap for flow control orifice and strainer. The outlet spool is also threaded to connect valve seat assembly. The manufacturing technique of spool shaped valve has been improved currently. Earlier valve was manufactured in two parts and welded together with lynco 92 weld rod. This manufacturing method was stopped due to defective welding some problems were encountered. Currently, the valve is shaped and machined in one piece. [20].

Evolution of R-4D engine

As soon as the R-4D engine was successful, it started to grow up in space industries. Many engines with different names but the similar configuration of R-4D was machined. R-4D was started by a company called Marquardt but now it is acquired by Aerojet Rocketdyne. The evolution of earth storable bi-propellant rocket engine was started in 1962 by Marquardt company and now the R-4D family has many branches and applications are evolving. The updated version of engines which are manufactured these days are especially concerning on the material point of view.

In 1950-60, Marquardt company developed the first bi-propellant rocket engine called R-1E engine, the function of this engine is to control attitude, and as reaction control system. Later, due to the rise of mono-propellants, the demand for R-1E engines decreased, but still they are used in few missions. After the successful mission of Gemini and Apollo, earth storable bi-propellants were seriously considered for use on spacecraft and satellites. R-4D was developed and became a starting point for future developments. Namely, the evolution of earth storable bi-propellant rocket engine was started in 1962 by Marquardt company and now the R-4D family has many branches and their applications are evolving. From a pre-shuttle era that is from 1960-1970, a new version of the R-4D engine were studied, like versions using different mixtures ratios and nozzle exit dimensions, Materials like niobium alloy C-103 from machining the combustion chamber, etc. The updated versions of the engine that are manufactured these days are especially concerned about issues relating to materials [41][42].

Over the last 50 years, the performance of this family of engines has improved. The main reason is to use better material system and thermal management approaches. The specific impulse has increased from 312 s to 335 s and operating time also increased up to 40,000 s, nearly 11 hours.

Figure A. 2 Evolution of R-4D Family (Image courtesy of Aerojet Rocketdyne [41][42])

Models and missions

R-1E Engine

The H-II Transfer Vehicle (HTV), is a space vehicle for the international space station (ISS), built by the Japan Aerospace Exploration Agency (JAXA) . HTV is an unmanned cargo vehicle used to transport supplies needed for the ISS. HTV carries more than 5443.1 kg of needed materials as payload [43]. HTV takes a position a few meters away from ISS, and then one crew member uses the ISS arm to connect with HTV and place it on the bottom surface of the space station [43]. HTV has two main part: one is known as Pressurized Logistics Carrier (PLC), which transports experiment racks, food and clothes for use onboard. The internal pressure of 1atm is maintained. The second portion is Unpressurized Logistic Carrier (ULC), which carries exterior experimental setup or spare parts which are used in ISS [43]. R-1E is used in (HTV) mission, thus Aerojet supports space missions by providing a suitable rocket engine. For HTV Aerojet produced 28 R-1E engines which produce110 N of thrust. They are used as reaction control engines and for attitude control during docking[44]. Technical specifications of R-1E are shown in Table A. 1 [45].

Sl.no	Technical Specifications	
1	Propellant	MMH and NTO
2	Thrust at steady state	111 N
3	Chamber pressure	7.3 bar
4	Expansion Ratio	100:1
5	Specific impulse	280 s
6	Mass	2 kg
7	Valve	R-4D-Solenoid type

Table A. 1 Technical specifications of R-1E

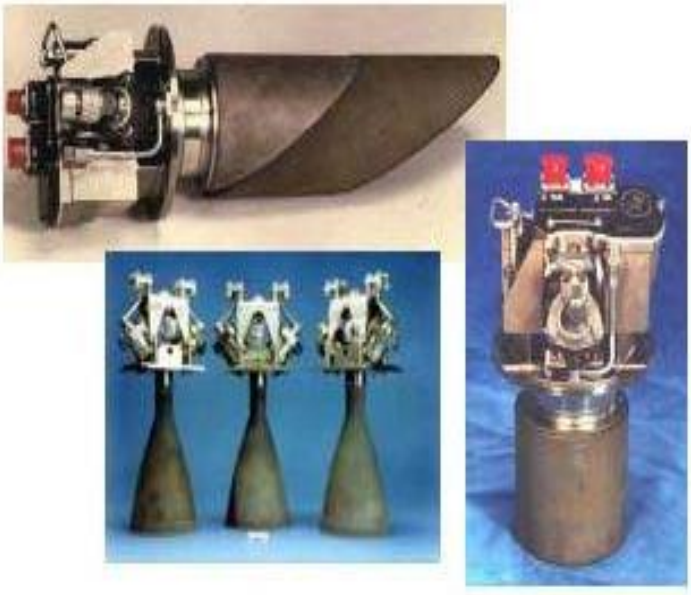

Figure A. 3 R-1E rocket engine (Image courtesy Aerojet Rocketdyne)

HiPAT Engine

High-Performance Apogee Thruster (HiPAT), is also known as R-4D-15. The R-4D-15 has served to space for five decades and all missions were successful. The HiPAT is a premier apogee rocket engine of best choice; it helps large spacecraft and satellites get into Geostationary orbit (GEO), also helping in orbital maneuvering for many communication satellites [45]. Eurostar 3000 (E3000), is a general satellite used in commercial and military communication satellite. R-4D-15 rocket engine is used in this satellite for maneuvering purpose. Boeing space system 720HP was another mission which uses R-4D-15 thruster. Boeing 720HP was introduced in 1997 and launched in 1999 with payload mass ranging from 600 to 1620 kg and mass at launch ranging from 5400 to 5900 kg [46]. Technical specification of HiPAT are shown in Table A. 2[45].

Sl.no	Technical Specification	
1	Propellant	Hydrazine and NTO
2	Thrust at steady state	445 N
3	Chamber pressure	9.4 bar
4	Expansion Ratio	300:1
5	Specific impulse	326 s
6	Mass	5.2 kg
7	Valve	Solenoid Valve

Table A. 2 Technical specification of HIPAT.

Figure A. 4 HiPAT rocket engine

R-4D-11 Rocket Engine

Automated Transfer Vehicle (ATV) or Ariane Transfer Vehicle (ATV), was developed by the European space agency (ESA). It is a spacecraft used to transport cargo from earth to ISS. This vehicle has been launched into orbit five times using an Ariane-5 launch vehicle and a few times with different launch vehicles [47].

The five (ATV) are named Jules Verne, Johannes Kepler, Edoardo Amaldi, Albert Einstein and George Lemaitre. These five ATV were loaded with propellant, water, air, food, scientific equipment's, exterior experiment usage materials and all onboard usage. R-4D-11 is used in ATV mission, Aerojet manufactured four models of R-4D-11 that produce 490 N of thrust [47]. R-4D-11 is a bipropellant rocket engine which is used in circularization maneuvers. It also helps in approaching near to ISS or taking position near to ISS. After the preliminary orbit is achieved, the R-4D engine operates and helps the ATV to place into an elliptical orbit, after that R-4D-11 engine helps ATV to circularize the vehicle's orbit [47].

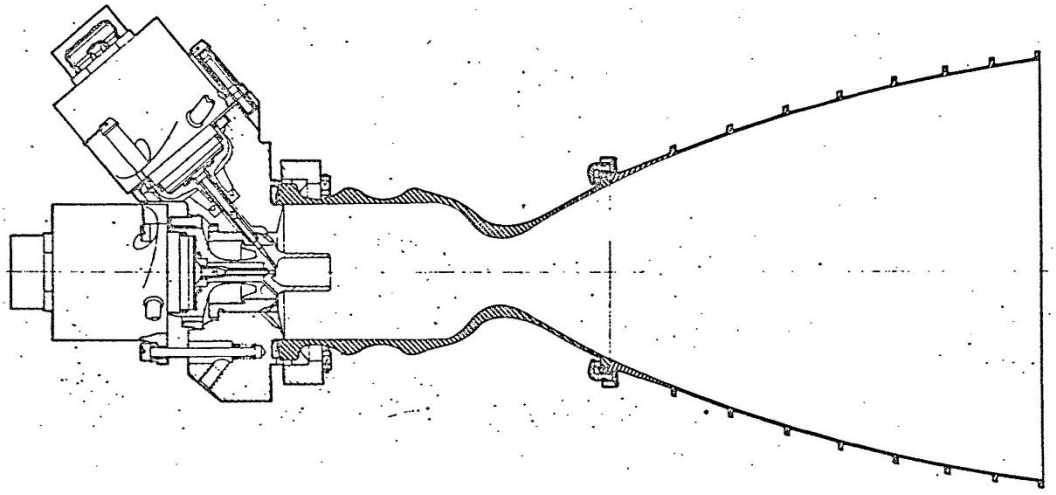

Figure A. 5 Draft R-4D by Marquardt [24].

Appendix B. LPRE Design

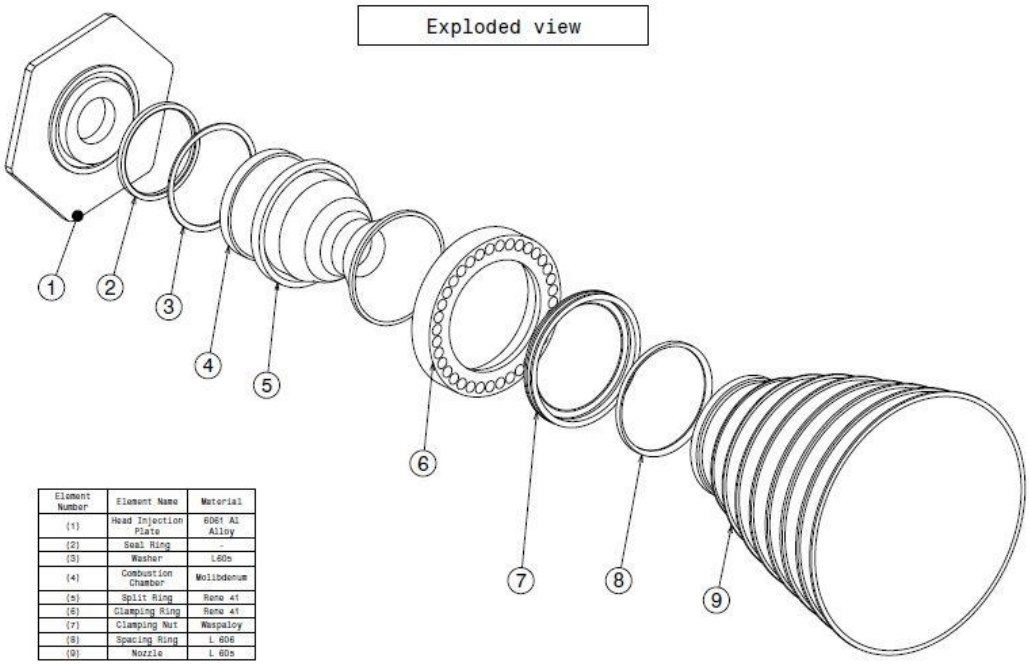

Element Number	Element Name	Material
(1)	Head Injection Plate	6061 Al Alloy
(2)	Seal Ring	-
(3)	Washer	L605
(4)	Combustion Chamber	Molibdenum
(5)	Split Ring	Rene 41
(6)	Clamping Ring	Rene 41
(7)	Clamping Nut	Waspaloy
(8)	Spacing Ring	L 606
(9)	Nozzle	L 605

Figure B. 1 Exploded view of rocket engine designed by Solid Works

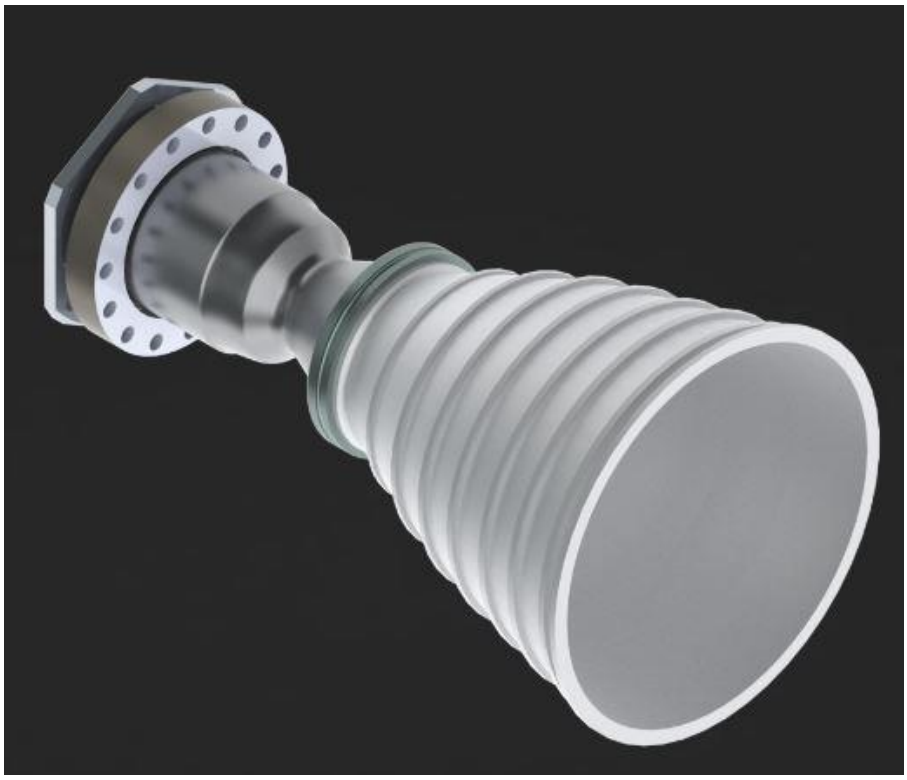

Figure B. 2 Rendering of rocket engine using Solid Works

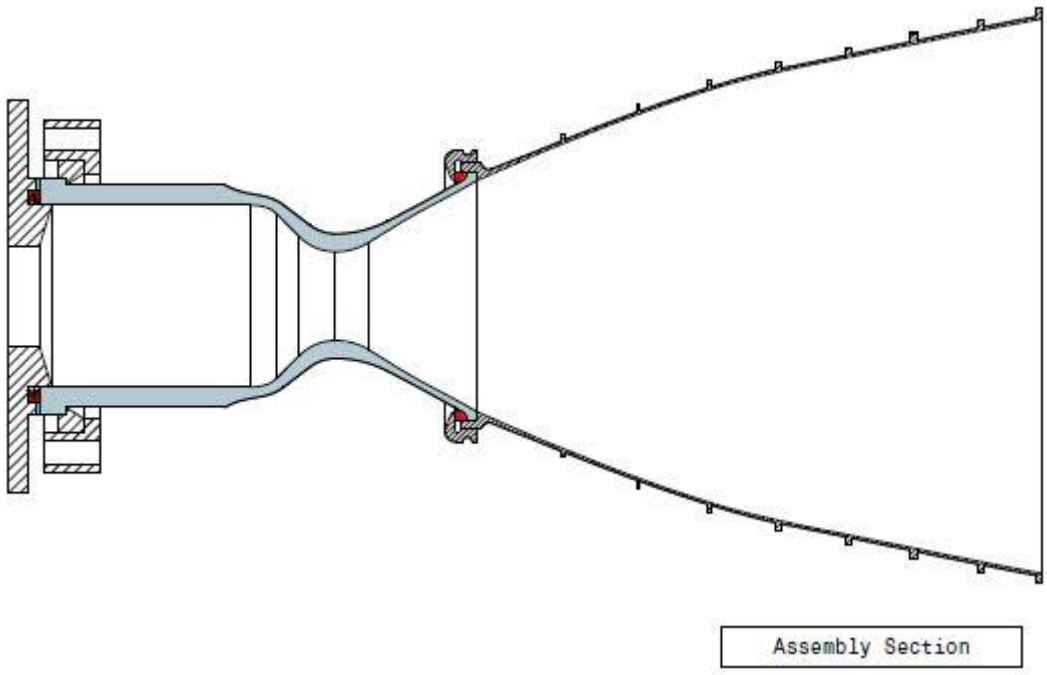

Figure B. 3 Assembly of rocket engine by Solid Works

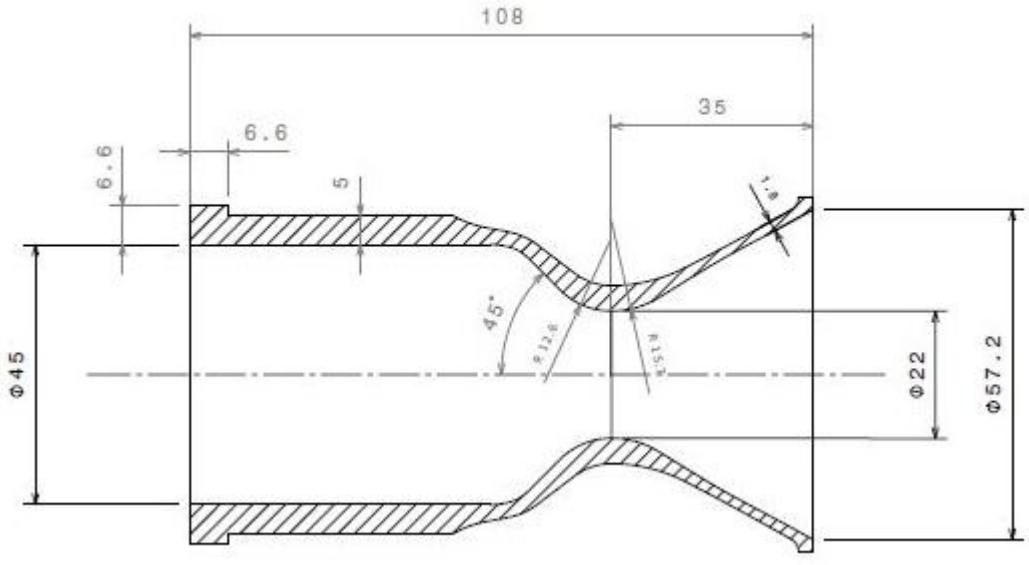

Figure B. 4 Combustion chamber by Solid Works

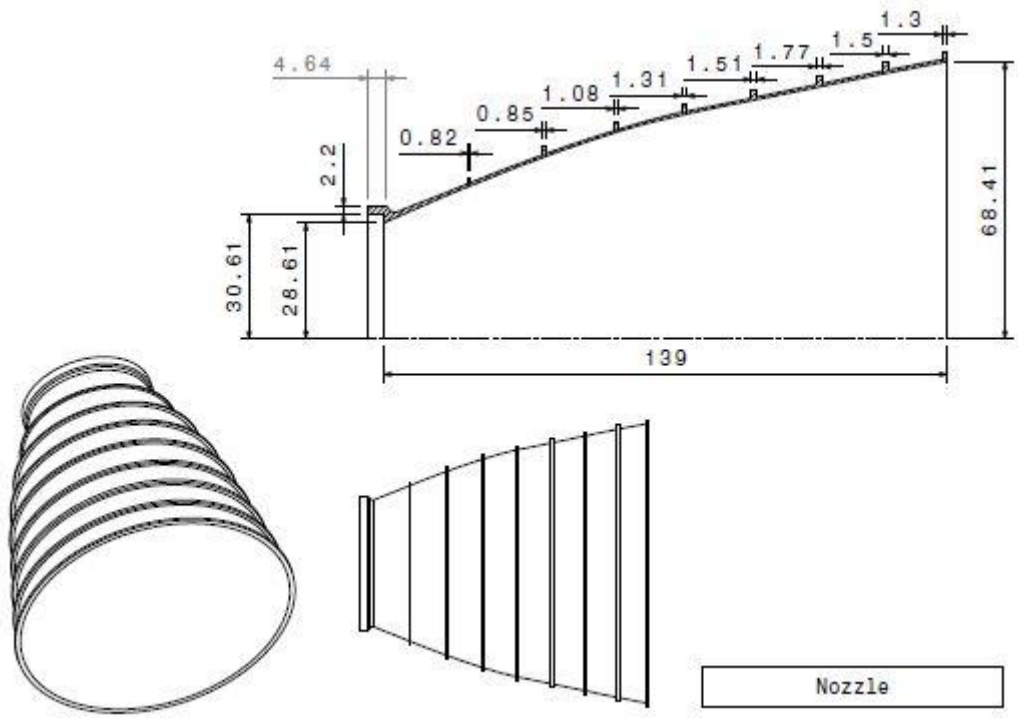

Figure B. 5 Nozzle extension using Solid Works

Appendix C. Feed system

All feed system is equipped with valves and pipes for filling and usually also for removing the liquid propellant. According to many researchers or experts, gas pressure feed system gives an admirable performance to turbopump systems when the total impulse is low, the chamber pressure is low, engine thrust to weight ratio is low. In turbopump feed mechanism, tank pressure of propellant is much lower, hence tank masses are bit lower. Turbopump feed system usually gives good performance when the vehicle total impulse is relatively large, the chamber pressure is high and the mission velocity is high [1][48].

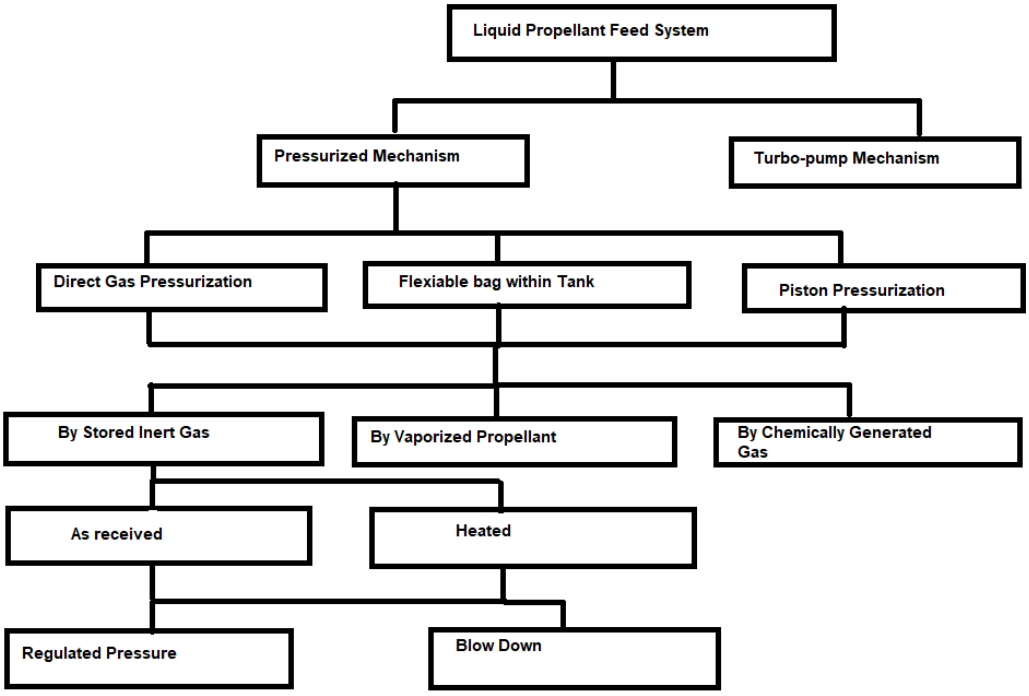

Figure C. 1 Flowchart of the feed system.

The pressure feed mechanism mostly includes,

- Pressurized tanks to store propellants.
- Pressuring gas to provide energy for the feed system.
- Valves to control the pressure and flow.
- Ducting to transfer fluids.
- One or more thrust chamber to generate thrust.

Pressure feed mechanism is broadly categorized according to the pressuring source, which shows how the propellant drive out from the tank [48].

This mechanism is simple and low-cost design, which balances engine performance. The system will be bit heavy because of the pressurized tanks and can be reliable with few parts. The pressure feed system is most commonly used in orbit maneuvering, orbit insertion, attitude control, reaction control and small upper stage propulsion. The operational factors which are influencing pressuring requirements are propellant

vaporization, tank wall temp, vapour condensation, the solubility of the pressurization gas, chemical reaction [48][1]. There are many liquid propellant engines which are equipped with pressure feed mechanism in rocket engine series, but these are the two liquid propellant rocket engines manufactured from the same company known as Aerojet Rocketdyne and features and engine characteristics are listed below [48].

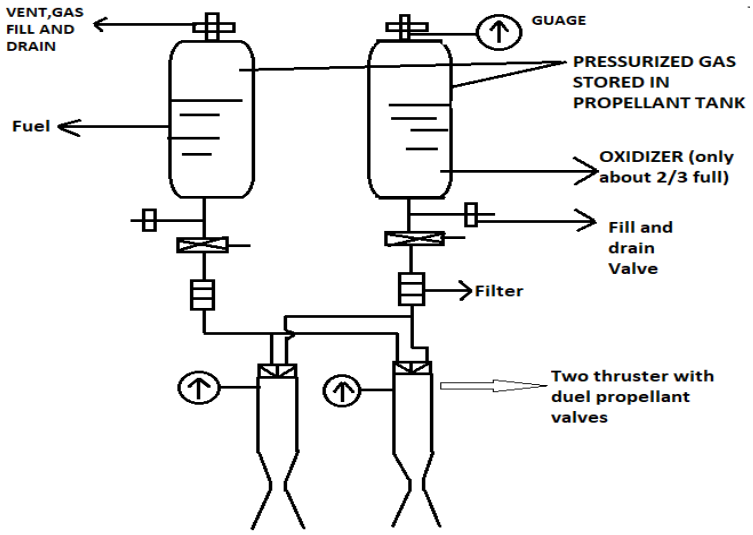

Figure C. 2 Schematic diagram of pressure fed engines

AJ10-137

AJ10-137 is a pressure fed liquid propellant rocket engine, AJ10-137 is used for orbital maneuvering engine (OME). AJ10-137 was designed based on vehicle mass and operational condition, long life and aids in achieving multiple starts. AJ10-137 is a radiatively cooled engine which was manufactured by Aerojet company. AJ10-137 rocket engine uses Aerojet N_2O_4 / Aerozine-50 as a propellant. AJ10-137 was used in Apollo SPS, Apollo CSM. The chamber pressure of AJ10-137 pressure fed engine is 6.90bar and oxidizer to fuel ratio is 1:6. The thrust produced by this engine is 97.50 kN and a specific impulse of 312 s and burn time was 585 s. Currently, this engine is out of production, but it served many missions with good success rate [49].

Kestrel

Kestrel is a liquid propellant rocket engine with pressure fed system designed by Space X. Kestrel uses LOX-RP-1 as a propellant which is used in the upper stage, Kestrel produces 30.70 kN of thrust and a specific impulse of 320 s. Space X built the high-efficiency kestrel, low-pressure vacuum rocket engine. Kestrel does not have a turbopump, but it is fed by tank pressure. Kestrel is equipped with ablatively cooling method near the chamber and throat and the nozzle is equipped with a radiation cooling method. The chamber is constructed with niobium alloy. Kestrel was provided by roll controller and torch ignitor which are tested in vacuum to make sure that engine start. Igniters are capable of many starts as they use similar propellants as the main engine. Image courtesy by Space X.